4-21-2015 12:00 AM

The Role of Hydroxyl Surface Groups on the Dechlorination Activity of Iron Bearing Nanoparticles

Jorge Gabayet
The University of Western Ontario

Supervisor
Jose Herrera
The University of Western Ontario

Graduate Program in Civil and Environmental Engineering
A thesis submitted in partial fulfillment of the requirements for the degree in Master of Engineering Science

THE ROLE OF HYDROXYL SURFACE GROUPS ON THE DECHLORINATION ACTIVITY OF IRON BEARING NANOPARTICLES

(Thesis format: Integrated Article)

by

Jorge Luis Gabayet Dominguez

Graduate Program in
Civil and Environmental Engineering

A thesis submitted in partial fulfillment
of the requirements for the degree of
Master of Engineering Science

The School of Graduate and Postdoctoral Studies
The University of Western Ontario
London, Ontario, Canada

Abstract

Dechlorination of groundwater contaminants by nano zero valent iron (nZVI) has been successfully utilized for a wide range of halogenated hydrocarbons. At the same time incorporation of noble metals such as Pd to nZVI has shown to result in a catalytic effect in the dechlorination reaction. Despite the extensive research to improve nZVI reactivity, 1,2-DCA remains recalcitrant to dechlorination by nZVI. These dechlorination processes are known to occur as a surface mediated reactions. However, a complete understanding of the surface composition and the role of the species present on the nZVI surface in the dechlorination adsorption/reaction mechanisms still needs to be achieved. α-FeOOH, α-Fe_2O_3, γFe_2O_3 are the most frequently observed species present in the surface of the nZVI particles. In this thesis, the mechanisms through which 1,2-DCA and TCE interact with these iron species are studied by means of in situ spectroscopic techniques. Experimental results demonstrate that surface hydroxyl groups play a critical role in the adsorption processes and that interaction of both 1,2 DCA and TCE with these hydroxyl groups results in the formation of an ethoxide surface complex. From temperature program experiments it was found that surface morphology, crystalline structure and surface speciation can lead to the existence of non-equivalent adsorption sites, with different chemical environments. This surface heterogeneity has a direct effect in the adsorption/reaction mechanisms, resulting in the formation of different observed desorption products. A reaction mechanism is proposed to rationalize all these observations.

Keywords

nZVI, trichloroethylene, 1,2-dichloroethylene, FTIR, UV-Vis, TPD, TPR hydroxyl groups, adsorption, reaction mechanism, γ-Fe_2O_3, FeOOH, α-Fe_2O_3.

Co-Authorship Statement

All the experiments were performed by the candidate under the guidance of Dr. Jose Herrera and Dr. Denis O'Carroll.

The candidate wrote the draft manuscripts in the following chapters:

Chapter 3: The relevance of hydroxyl surface groups on the dechlorination activity of iron oxide bearing species

By Jorge Luis Gabayet Dominguez, Jose Herrera, and Denis O'Carroll.

Contribution:

Jorge Gabayet: performed all the experiments, collected, analyzed, and interpreted all the data and wrote the draft of the manuscript.

J. Herrera and Denis O'Carroll: initiated the research topics, provided guidance on the experiments, assisted in data interpretation, and reviewed/revised the draft chapters.

Dongmin Yun: Assisted in the development of the initial experimental protocol, experimental troubleshooting, and provided suggestions for data interpretation.

Acknowledgments

As I look back and think about these years that I spend in graduate school, an overwhelming sense of gratitude and accomplishment fills me. I am grateful because all these triumphs, defeats, learning experiences, frustrations and joyful moments that involve graduate school, I had the opportunity to share them with great people. People that has make this life learning experience more meaningful, enriching and of course fun. Because graduate school for me has not been only about mastering scientific knowledge and overcoming practical problems, for me it has been a complete life changing experience, where learning goes beyond the class rooms and penetrates every moment of your life.

Because of this and much more I will always be grateful to my supervisors Dr. Jose Herrera and Dr. Denis O'Carroll, which gave me the opportunity to demonstrate myself that I could learn and accomplish more that I could ever belief, also for not giving up on me during all the hard moments and for all the encouragement and mostly for the great change of working with you.

I also want to thank to all my friends, especially to Dongmin Yun, for not only being patient enough to teach and help me during my master, but for always been a great friend when I needed one. Also to all the RESTORE, LDAN and London friends for letting me find in London a second home, and to my best friends that words will never be enough to thank them for being always there for me no matter what.

I want to express also a special thanks to my parents and siblings who during all my life have encourage me and supported me to follow my dreams. For their never ending love and kindness. And for sacrificing themselves to give me all the opportunities that have lead me to where I am.

Table of Content

List of Tables, Figures and Schemes

List of Tables

List of Figures

List of Schemes

List of Abbreviations

1,1-DCE	: 1,1-Dichloroethene
1,2-cis-DCE	: 1,2-cis-Dichloroethene
1,2-DCA	: 1,2-Dichloroethane
1,2-DCE	: 1,2-Dichloroethene
ATR	: Attenuated total reflectance
BET	: Brunauer, Emmett, Teller isotherm equation
Cl-VOC	: Chlorinated volatile organic compounds
CMC	: Carboxymethyl cellulose
DFT	: Density functional theory
DRIFTS	: Diffuse reflectance infrared Fourier transform spectroscopy
DR-UV-VIS	: Diffuse reflectance ultraviolet visible spectroscopy
ECD	: Electron capture detector
EPC	: Electronic pneumatic control
ETC	: Electron transfer coefficient
FID	: Flame ionization detector
FTIR	: Fourier transform infrared
GC	: Gas chromatographer
IR	: Infrared

MCT	: Mercury cadmium telluride
MS	: Mass spectrometer
MZVI	: Micro zero valent iron
NAPL	: Non aqueous phase liquid
NZVI	: Nano zero valent iron
ORP	: Oxidation reduction potential
PCE	: Tetrachloroethylene
PRBs	: Permeable reactive barriers
SEM	: Scanning electron microscopy
STM	: Scanning tunneling microscopy
TCD	: Thermal conductivity detector
TCE	: Trichloroethylene
TPD	: Temperature programed desorption
TPR	: Temperature programed reaction
UHV	: Ultra high vacuum
US EPA	: United States Environmental Protection Agency
VC	: Vinyl Chloride
XPS	: X-ray photoelectron spectroscopy
XRD	: X-ray diffraction

Chapter 1

1. Introduction

1.1 Ground water contamination

Groundwater is an important source of water for industrial, irrigation, domestic and drinking purposes. In the U.S. in 2005, 20% of the water withdrawals came from groundwater.[1] In Canada 30.3% of the population uses groundwater as drinking water source and for domestic use.[2] Groundwater systems are in danger of pollution by industrial, agricultural or commercial activities.[3] Among the most harmful pollutants, chlorinated hydrocarbons pose the highest risks to groundwater sources.[4] In North America industrial production of chlorinated solvents started in the early 1900s with a main production of carbon tetrachloride followed by trichloroethylene (TCE) and tetrachloroethylene (PCE). [4] These solvents were widely used in the metallurgic industry as part of the metal degreasing process. Because of the industrial demand for these solvents by 1986 the U.S. alone produced approximately 23, 1 and 0.2 million drums of 1,2-dichloroethane (1,2-DCA), trichloroethane and TCE, respectively. Because of the lack of regulations for the handling, transportation and disposal of these solvents, inappropriate disposal of solvent waste was by waste burial, evaporation lagoons and underground injection. These common practices led to vast contamination of groundwater systems. It was not until 1974 when the scientific and social concerns about the contamination of the drinking water sources triggered the passing by the U.S. government of the Safe Drinking Water Act followed by the Toxic Substances Control Act and the Resources Conservation and Recovery act in 1976. This set of legislation resulted in the development of standard methods and regulations for the disposal and monitoring of contaminants in the environment. Another event that triggered the development of methodologies and techniques for monitoring the drinking water contamination was the recognition of the existence of the non-aqueous phase liquids (NAPLs) in groundwater that resulted from a case study in West Germany in the late 1960s, a study that regrettably remained greatly unknown until the early 1980's.[4]

NAPLs pose a threat to groundwater systems due to their physicochemical properties. Because of their low liquid viscosity, water interfacial tension and partitioning in to the soil, NAPLs are able

to mobilize in to the subsurface and invade rock fractures. Their low aqueous solubility allows them to form long term sources of contamination to the incoming groundwater. In addition most of these NAPLs have a low degradability and significant toxicological health and environmental effects.[4]

From the common groundwater contaminants, chlorinated volatile organic compounds (Cl-VOCs), more specifically TCE and 1,2-DCA are categorized as probable carcinogens and pose a hazard to the environment .[5] 1,2-DCA is used in vinyl chloride monomer and polyvinyl chloride manufacture.[6] TCE is mainly used in vapor degreasing and cold cleaning of metal parts; it is also used in the dry cleaning industry and for cleaning electronic components. Entry to the groundwater arises from anthropogenic activities such as discharges from dry cleaning facilities, sewage treatment plants, leaking from landfills, storage tanks, and improper disposal or dumping of residues. [7]

A promising groundwater remediation technology for these sites is nano zero valent iron (nZVI) [3]. ZVI particles were first shown to degrade TCE and other chlorinated hydrocarbons by Gillham and collaborators.[8] ZVI has been used since then in permeable reactive barriers (PRBs) for in situ remediation. Regardless of the effectiveness of PRBs for degrading contaminants from the contaminated plume, PRBs are incapable of remediating the source zone, and therefore are a long term clean up technology, requiring constant monitoring and adjustment. On the other hand, nZVI has been shown to be promising for the remediation of source zone contaminants.[9] Although nZVI can successfully dehalogenate most C1 and C2 chlorinated hydrocarbons, to this date 1,2-DCA has shown to be highly recalcitrant to reduction by nZVI. The inability of nZVI to reduce 1,2-DCA has been tentatively linked to the structural stability and relative low reduction potential of 1,2 DCA. [10]

Reaction between ZVI and chlorinated hydrocarbons is known to be a surface mediated reaction.[3, 11] Therefore the surface composition and structure of the zero valent iron particles has a direct effect on the effectiveness of the adsorption and reaction mechanisms of dechlorination. Thus, an in depth understanding of the surface mechanisms that take place between nZVI and the chlorinated compounds will facilitate optimization of the surface composition of nZVI with enhancement in dechlorination activity. Hematite (α-Fe_2O_3), maghemite (γ-Fe_2O_3), magnetite

(Fe_3O_4), and goethite (α-FeOOH) have been identified as phases present on nZVI surfaces. Since dechlorination by nZVI requires adsorption of the chlorinated hydrocarbons over the nZVI surface, the interaction and adsorption mechanisms of these iron oxides and oxyhydroxides can have a great effect in the dechlorination reactivity. Hence a comprehensive understanding of the adsorption and reaction mechanisms between the chlorinated hydrocarbons and these iron oxide species, could potentially provide insightful information of the dechlorination mechanisms between nZVI particles and TCE and 1,2-DCA.

1.2 Research Objectives

This research work forms part of the INTEGRATE interuniversity project, for the research and development of remediation technologies for subsurface contamination. The objective of this work is to establish the interaction mechanisms between the iron species hematite (α-Fe_2O_3), maghemite (γ-Fe_2O_3), magnetite (Fe_3O_4), and goethite (α-FeOOH), observed on the nZVI surface, [12,13] and the groundwater contaminants 1,2-DCA and TCE. The comparison of the adsorption phenomena between TCE and 1,2-DCA will enable an explanation of the recalcitrance of 1,2-DCA towards dechlorination with nZVI. Specific objectives of this thesis include:

1. Identify the adsorption sites and interaction mechanisms between ground water contaminants TCE and 1,2-DCA and the surface of nanozero valent iron as well as iron oxide species maghemite, hematite, magnetite and goethite.
2. Identify and quantify the products resulting from the desorption of the surface adsorbed contaminants 1,2-DCA and TCE over the aforementioned iron oxide species.
3. Evaluate the electron donor capacity and contribution to reduction of these different species in the context of the dechlorination mechanism.

1.3 Project Novelty

A general agreement exists on the importance of the surface area and surface composition of nZVI, and its effect in the dechlorination rate of groundwater contaminants.[14,14b] Also dechlorination pathways have been proposed for the dehalogenation of different chlorinated hydrocarbons with nZVI[15]. In spite of these efforts, it is not well understood the different role iron oxides species present in the nZVI surface played in the proposed reaction pathways and overall dechlorination kinetics. In situ spectroscopy analysis is a powerful technique that can allow us to study surfaces and catalytic systems under working conditions, permitting to assess adsorption and reaction products. In situ describes simultaneous spectroscopy and gas phase measurement on the same sample at the same time, providing insightful information on the adsorption modes of surface intermediaries and the contribution of different surface moieties to the reaction mechanism. This projects aims to tackle the gap in the understanding of this surface phenomena by using in situ diffuse reflectance Fourier transform infrared (DRIFT), in situ diffuse reflectance UV-visible DR-UV-vis as probing techniques to monitor the interaction of nZVI with 1,2 DCA and TCE. The identification of desorption products by temperature program desorption (TPD) coupled to a gas chromatograph (GC), flame ionization detector (FID) and electron capture detector (ECD) are also integral part of this study.

1.4 Thesis Outline

Chapter 1: Project background and research objectives.

Chapter 2: Literature review of previous work on the reaction mechanism, rate limiting steps, surface composition and effects in zero valent iron morphology on dechlorination reactions.

Chapter 3: Is dedicated to frame the experimental methodology, and the discussion of the results of the present research work.

Chapter 4: Summarizes the most important findings of this study and provides recommendations for further work.

1.5 References

1. Kenny, J.F., Barber, N.L., Hutson, S.S., Linsey, K.S., Lovelace, J.K., and Maupin, M.A., 2009, Estimated use of water in the United States in 2005: U.S. Geological Survey Circular 1344, 52 p.

2. Environment Canada. Water, Water Sources. Groundwater. www.ec.gc.ca

3. Zhang, W. X.; Wang, C. B.; Lien, H. L., Treatment of chlorinated organic contaminants with nanoscale bimetallic particles. *Catalysis Today* **1998,** *40* (4), 387-395.

4. James F. Pankow, John A. Cherry, Dense chlorinated solvents and other DNAPLs in groundwater: history, behavior, and remediation. Waterloo Press.1996,Chapter1, 3-46.

5. Miranda, B.; Diaz, E.; Ordonez, S.; Vega, A.; Diez, F. V., Oxidation of trichloroethene over metal oxide catalysts: kinetic studies and correlation with adsorption properties. *Chemosphere* **2007,** *66* (9), 1706-15.

6. Huang, C. C.; Lo, S. L.; Tsai, S. M.; Lien, H. L., Catalytic hydrodechlorination of 1,2-dichloroethane using copper nanoparticles under reduction conditions of sodium borohydride. *Journal of environmental monitoring : JEM* **2011,** *13* (9), 2406-12.

7. Environment Canada. Trichloroethylene, Priority Substance List, Assesment Report. Canadian Environmental Protection Act.1993

8. Gillham, R. W.; Ohannesin, S. F., Enhanced Degradation of Halogenated Aliphatics by Zero-Valent Iron. *Ground Water* **1994,** *32* (6), 958-967.

9. Bennett, P.; He, F.; Zhao, D.; Aiken, B.; Feldman, L., In situ testing of metallic iron nanoparticle mobility and reactivity in a shallow granular aquifer. *Journal of contaminant hydrology* **2010,** *116* (1-4), 35-46.

10. Song, H.; Carraway, E. R., Reduction of Chlorinated Ethanes by Nanosized Zero-Valent Iron: Kinetics, Pathways, and Effects of Reaction Conditions. *Environmental Science & Technology* **2005,** *39* (16), 6237-6245.

11. Lien, H.-L.; Zhang, W.-X., Nanoscale Pd/Fe bimetallic particles: Catalytic effects of palladium on hydrodechlorination. *Applied Catalysis B: Environmental* **2007,** *77* (1–2), 110-116.

12. Li, X.-q.; Zhang, W.-x., Iron Nanoparticles: the Core−Shell Structure and Unique Properties for Ni(II) Sequestration. *Langmuir* **2006,** *22* (10), 4638-4642.

13. Liu, C.-C.; Tseng, D.-H.; Wang, C.-Y., Effects of ferrous ions on the reductive dechlorination of trichloroethylene by zero-valent iron. *Journal of hazardous materials* **2006,** *136* (3), 706-713.

14. (a) Yan, W.; Lien, H.-L.; Koel, B. E.; Zhang, W.-x., Iron nanoparticles for environmental clean-up: recent developments and future outlook. *Environmental Science-Processes & Impacts* **2013,** *15* (1), 63-77; (b) O'Carroll, D.; Sleep, B.; Krol, M.; Boparai, H.; Kocur, C., Nanoscale zero valent iron and bimetallic particles for contaminated site remediation. *Advances in Water Resources* **2013,** *51*, 104-122.

15. Liu, Y. Q.; Majetich, S. A.; Tilton, R. D.; Sholl, D. S.; Lowry, G. V., TCE dechlorination rates, pathways, and efficiency of nanoscale iron particles with different properties. *Environmental Science & Technology* **2005,** *39* (5), 1338-1345.

Chapter 2

2 Literature Review

2.1 Introduction

Contamination of groundwater systems by chlorinated volatile organic compounds (Cl-VOCs) poses a serious threat to the environment. The toxicity of Cl-VOCs and their physicochemical properties makes them a long term source of groundwater contamination, with potential treat to drinking water sources. The complex mixture of compounds found in contaminated sites makes remediation of these sites difficult. Nano zero valent iron (nZVI) has been proven to be effective in the attenuation of a vast range of contaminants[1]. The incorporation of an additional metal functionality such as Pt or Pd has been proposed as a way to increase nZVI dechlorination activity. The bimetallic systems have shown an increase in dechlorination rates and a depletion of more toxic reaction intermediates[2]. Unfortunately 1,2-DCA has remained recalcitrant to degradation by bimetallic nZVI systems.[3] In general, reduction of Cl-VOCs by nZVI and bimetallic systems are suggested to be surface mediated reactions that are highly affected by the surface composition of the nanoparticles[2]. Despite large efforts to understand the reaction mechanisms and role of surface morphology in the reaction, a clear understanding of the contribution to the dechlorination reaction of the different surface species found in the nZVI particles, and the surface reaction intermediaries has yet to be achieved. Therefore a comprehensive study of the impact of the different iron species in the adsorption/reaction mechanisms is essential for a re-engineering of the surface composition of the nanoparticles with the aim to enhance dechlorination of groundwater pollutants. In this chapter a comprehensive review of studies that have addressed the surface composition, dechlorination reaction rates over nZVI, and bimetallic nanoparticles as well as the physicochemical properties of different iron oxides is presented.

2.2 Zero valent iron nano particles

The necessity of remediating the environmental hazards that chlorinated hydrocarbons pose to ecosystems and public health, and the inefficiency of remediation methods such as pump and treat or bio degradation used in the early 1990s have generated the need for novel remediation technologies. During this time researchers were also studying the use of metals to function as electron donors for reduction of chlorinated hydrocarbons.[4] The use of zero valent metals for dehalogenation reactions was first investigated by Reynolds and collaborators followed by Gillham and collaborators.[5] In the study of Gillham, dechlorination of various Cl-VOCs was achieved in the presence of zero valent iron (ZVI). [6]

Thereafter the implementation of ZVI as a remediation tool spread widely through the construction of permeable reactive barriers (PRBs). These PRBs worked in the remediation of the contaminant plume, and were implemented for the remediation of contaminated soil, with several remediation field scale experiments.[169] However, ZVI presented some drawbacks that limited its application, such as the accumulation of more toxic byproducts due to the lower reactivity of ZVI for mono and dichlorinated aliphatic compounds. Also the inability to treat deep aquifers due to the technical difficulties for the construction of the PRBs, and the incapability of treating the contaminant source zone were additional ZVI limitations. [10] Because of these limitations and the development of methodologies for nanoparticle synthesis, Zhang and collaborators successfully synthesized nanoparticles of ZVI, which showed an increase of reactivity towards some polychlorinated biphenyls and chlorinated aliphatic compounds 10 to 100 times higher compared to their micro sized equivalent.[2] The discovery of the improved reactivity of these nanoparticles opened the possibility for the use of this technology for in situ remediation of the source zone by a direct injection of these particles in the subsurface.

2.2.1 Synthesis of zero valent iron nano particles

nZVI particles are characterized for having a core-shell structure and a diameter smaller than 100 nm.[11] The most common laboratory synthesis method is by sodium borohydride ($NaBH_4$) reduction of iron salts in anoxic conditions.[1] This synthesis is carried in aqueous solutions, commonly using iron chloride or iron sulphate as precursors for the nanoparticles. Sodium borohydride is used in a stoichiometric excess, the excess of borohydride is suggested to help in the formation of highly uniform iron nanoparticles.[12]

Where the general reaction for iron (III) chloride reduction can be written as: [12]

$$4Fe^{3+} + 3BH_4^- + 9H_2O \rightarrow 4Fe^0(s) + 3H_2BO_3^- + 12H^+ + 6H_2\,(g)$$

And for iron(II) sulphate:[13]

$$2Fe^{2+} + BH_4^- + 3H_2O \rightarrow 2Fe^0(s) + H_2BO_3^- + 4H^+ + 2H_2\,(g)$$

The resulting particles by this method show an amorphous structure, where the core of the nZVI particles consists in α-Fe with a diameter of <1.5 nm [11] surrounded by an oxide layer which has a range in thickness of 2 to 5 nm,[1,60,61] as it forms during the synthesis as a result of the reaction between oxygen or water with the nZVI surface. This oxide layer is usually composed by iron (hydr)oxides and iron oxides. This thin layer can play a role in the electron transfer between the core of the nZVI particle to the contaminant species.[11]

The reaction capacity of nZVI can be affected by several factors ranging from particle agglomeration, pH, surface area, nZVI aging, and addition of a catalyst. Agglomeration of the nZVI particles results from Van der Waals and electromagnetic forces acting in the nZVI colloid; these forces trigger the formation of nZVI aggregates which precipitate out of solution. [11] The use of surface coating techniques by means of anionic polymers have been investigated as a way to prevent agglomeration, and polymers such as Carboxymethyl Cellulose (CMC), Polyacrylic acid (PAA), and guar gum have been proposed and investigated as stabilizers.[14] Nowadays the most successful nZVI formulations are obtained in the presence of a hydrophilic polymer to prevent agglomeration.

2.2.2 Surface composition

Since the dechlorination reaction between the Fe^0 and the chlorinated compounds is mediated by the surface of the iron particles, the surface area has been found to affect the reaction rate. Therefore the use of nano scale iron particles was the logical step to take from the micro size particles since the surface area increases due to the reduction of the particle size. When comparing nZVI with micro scale zero valent iron a surface area of 15-34 m^2/g and <1 m^2/g respectively can be measured.[11] The increase of surface area of the iron particles results in a higher reactive sites density, which can explain the larger reaction rates observed towards dechlorination.[11] This indicates that to understand the interaction mechanisms and effects of the ZVI surface species, a comprehensive characterization of the nZVI surface is necessary. Indeed, it has been shown that the passivation film formed on the iron particles is influenced by the formation mechanism and the pre-treatment and synthesis of the iron particles.[15] Liu and collaborators reported x-ray photoelectron spectroscopy (XPS) analysis for purchased micro iron, which yielded a surface composition of 85% goethite (α -FeOOH) and 12% of maghemite (γ-Fe_2O_3). After applying an acid wash pre-treatment with H_2SO_4, an increase in the goethite phase in the surface was observed (95%), together with a decrease in maghemite (from 12% to 1.8%) and the formation of magnetite (3%).[15] Li and collaborators studied the surface composition of dried nZVI particles, synthesized by $NaBH_4$ reduction, using high resolution-XPS they reported that iron is likely present in the form of FeOOH .[16] Lien and collaborators reported surface characterization results obtained by X-ray diffraction (XRD) of dried bimetallic Pd-nZVI observing maghemite/magnetite, lepidocrocite (γ -FeOOH) and hematite (α -Fe2O3) species. Also XRD studies were conducted for Pd-nZVI after 48 hrs of reaction with TCE and the formation of lepidocrocite was reported.[17]

Most of the surface studies of the ZVI and nZVI surface rely on XPS and XRD for the identification of the surface species, nevertheless this requires the experiments to be performed in ex situ conditions, i.e. using dried samples. The necessity of studying the surface composition within the aqueous system is mandatory in order to comprehend the reaction phenomena taking place in groundwater systems.

In order to address the limitation of an ex situ characterization with an un-avoidable exposure of the nZVI particles to oxygen, Filip and collaborators studied the nZVI oxidation by water in

anaerobic conditions, utilizing a Mössbauer spectroscopy experimental set up. Freshly synthesized and oxidized nZVI particles were frozen in liquid nitrogen to avoid further oxidation, and Mössbauer spectra were obtained. In addition density functional theory (DFT) calculations were performed for the construction of an atomic model for quantum chemical calculations. The Mössbauer experiments revealed the formation of a single iron phase: the formation of $Fe(OH)_2$ when nZVI reacted anaerobically with water, simulating ground water conditions. The presence of $Fe(OH)_2$ was also confirmed by XRD analysis. Fig.2.1, retrieved from Filip and collaborators, illustrates this result. It can be observed the formation of $Fe(OH)_2$ as nZVI is being depleted by oxidation in oxygen free water.[18]

A similar experiment but with an exposure of approximately 1 hour to air, showed a fast oxidation of the iron (II) hydroxide to the more stable Fe_3O_4 (magnetite) phase,[18] proving the sensitivity of the nanoparticles to fast oxidation under aerobic conditions, and illustrates the challenges associated with nZVI characterization after exposure to air even at short periods of time. The theoretical calculations are in accordance with the observations of the Mössbauer and XRD experiments and pointed to the formation of a reaction intermediary: HFeOH, that would limit the reaction rate for the formation of the $Fe(OH)_2$. The suggested formation of the HFeOH intermediary was proposed as:

$$Fe^0 + H_2O \rightarrow HFe^{I}OH \qquad \text{Reaction (1)}$$

$$HFe^{I}OH + H_2O \rightarrow Fe^{II}(OH)_2 + H_2 \qquad \text{Reaction (2)}$$

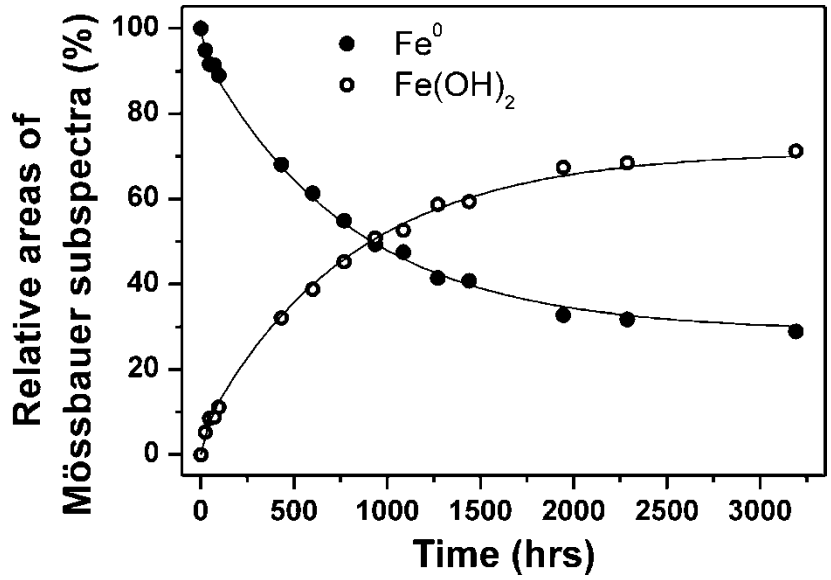

Figure 2.1. Time evolution of the integrated spectral area for nZVI and $Fe(OH)_2$ in the anaerobic reaction of nZVI with water at 25ºC. **Reprinted with permission from Filip, J.; Karlický, F.; Marušák, Z.; Lazar, P.; Černík, M.; Otyepka, M.; Zbořil, R., Anaerobic Reaction of Nanoscale Zerovalent Iron with Water: Mechanism and Kinetics.** ***The Journal of Physical Chemistry C*** 2014, ***118*** **(25), 13817-13825. Copyright (2015) American Chemical Society.**

Since the equilibrium of the surface species have been shown to be susceptible to the environmental conditions that surround the nanoparticles, research efforts have focused on the investigation of the effect of water chemistry parameters that could alter the shell composition of the ZVI particles. Factors such as the oxidation reduction potential (ORP), pH, temperature, and dissolved ions have been investigated for the passivation or enhancement of the reduction rate for chlorinated hydrocarbons by zero valent iron. Ritter and collaborators conducted in situ Raman spectroscopy experiments where exposure of micro zero valent iron (mZVI) to air was avoided to prevent further oxidation. Raman spectroscopy allowed them to identify hematite and magnetite as the principal phases on the surface with some maghemite present as well. After in situ column experiments where water, in the first experiment, and a TCE solution, in the second experiment, were injected in to the column, the removal of maghemite and hematite from the surface of the particles was observed. In situ potential measurements showed values of -470 mV at a pH of 7.5 and -525 mV at a pH of 9 for water and TCE solution experiments, respectively.[19] As shown in Fig.2.2 The Pourbaix diagram suggests a thermodynamically stable phase of magnetite.[20]

Since the potential and pH measurements for the TCE solution in situ experiment do not support TCE as an oxidizer for mZVI, the removal of the hematite, maghemite surface layer has been attributed to a comproportionation reaction:

$$Fe_2O_3 + Fe^0 + 6H^+ \rightarrow 3\,Fe^{2+} + 3H_2O$$

The ORP and pH conditions in the experiment will determine whether the newly form Fe^{2+} precipitates to a more stable phase such as magnetite or an iron hydroxide.[19]

As seen, factors that can affect the reaction rate, such as the pH, could promote the formation of a range of iron species at different water quality conditions. An increase in the pH to values close to a pH of 9 can produce the precipitation of iron hydroxide ($FeOH_{(s)}$). This iron hydroxide is unstable at pH values of 6-7 favoring the formation of magnetite (Fe_3O_4), also this iron hydroxide at neutral pH values can also suffer a phase transformation to maghemite after an aging period.[15] Aging of the nZVI can occur in anoxic or in aerobic solutions, thus ORP can also play a role on these transformations.

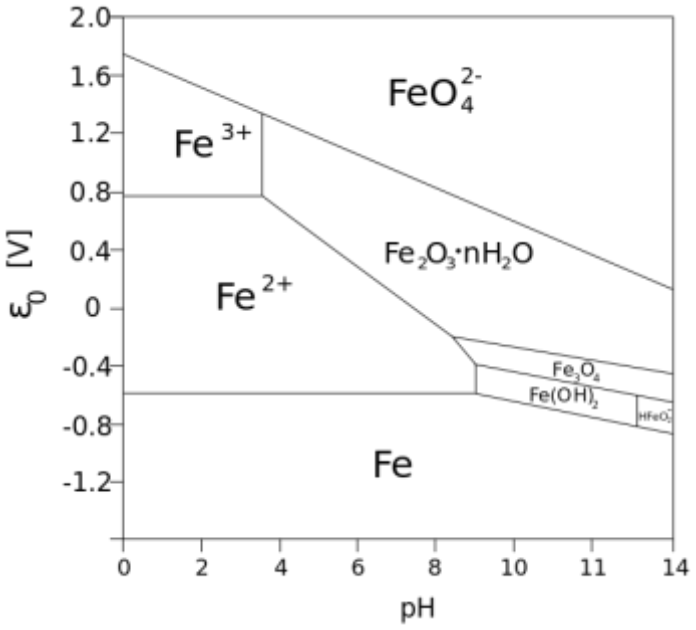

Figure 2.2. Pourbaix diagram of Iron.

Reprinted from *Corros Sci*, 38/12, Beverskog, B.; Puigdomenech, I., Revised Pourbaix diagrams for iron at 25-300 degrees C / 2121-2135., Copyright (2015), with permission from Elsevier

For instance, in anoxic solutions the oxidation takes place as a two steps process, a fast oxidation (approximate 2 days) followed by a slower oxidation reaction. The oxide layer that is formed in anaerobic solutions is composed of magnetite, as opposed to maghemite or hematite layer that is observed in aerobic solutions. Also it has been observed that the aging process affects the iron reductive capacity by consequence of the phase transformation of the core from an amorphous Fe^0 core to a highly crystalline iron.[1]

The importance of understanding the composition of the shell covering the Fe^0 core is also emphasized by the electronic conduction capacity of the different iron species and their adsorption capacity. For instance, magnetite is considered as an electron conductor and hematite and maghemite hinder electron transfer.

The effect of water in the reaction mechanism was also studied by Uludag and Bowers, where they observed a threshold in activity linked to moisture content in the gas phase dechlorination of TCE by mZVI. They observed a relative humidity threshold of 72% and 92% for the TCE removal mechanism to shift from adsorption to reduction by acid washed ZVI and partially oxidized ZVI respectively. The importance of water as a proton donor was noticeable. They also suggested that in the gas phase the reaction with Fe^0 required the adsorption in to the zero valent surface or into the iron oxide surface, this TCE adsorption could be in competition with water adsorption when a low concentration of protons is present. They also noticed that dechlorination took place only when sufficient protons were available[21] Regardless of these observations direct evidence of the proposed adsorption mechanisms between the ZVI surface, TCE and water were not provided. In additional studies Uludag and Bowers further evaluated the role of water in the dechlorination of TCE by zero valent iron in the gas phase under batch reactors conditions, resulting in similar observations where a low relative humidity results in preferential adsorption removal mechanisms in comparison to dechlorination reactions that take place at higher relative humidity values.[22] In a later study, the same group concluded that the decrease in the reaction rate of TCE dechlorination by ZVI is due to the increase of the nonreactive sites attributed to the iron (III) oxides that are formed in the oxidation reaction of the zero valent surface with water and dissolved oxygen, another reason that they suggested for the decrease in the reaction rate was due to possible mass transfer limitations generated by the oxide layer. They also acknowledged the lack of a comprehensive understanding of the effects of water and the oxide layer due to the un availability

of techniques that would allow them identify the reactive and nonreactive sites and establish the role of each compound.[23]

Other parameters such as anions in the groundwater system have shown to affect the dechlorination rate over ZVI. This effect is linked to three different mechanisms: a) adsorption-precipitation of species that passivate the surface, such as phosphate and carbonate ions. b) catalyst poisoning species such as sulfide and sulfite for the case of bimetallic nZVI formulations. c) redox species that compete for reactive sites with the halogenated hydrocarbon, such as perchlorate, nitrite, and nitrates.[24]

2.2.3 Structural and surface differences in iron oxide surfaces

The structure of iron oxides and oxyhydroxides has been widely investigated because of the ferromagnetic properties and the natural availability of this material. The use of hematite has been exploited in heterogeneous catalysis and environmental applications for contaminant adsorption, and mitigation of halogenated compounds. Also hematite is widely used in Fisher-Tropsch synthesis and oxidation of alcohols to ketones and aldehydes.[25,26] Because of the high stability and availability of hematite, its reactivity has been studied in comparison with other iron oxide and hydroxide phases. Chemisorption and physisorption of different organic molecules over these surfaces has been reported, as well as chemical reactions between the surface hydroxyl groups present in these iron oxides and chemisorbed probe molecules.[27] Magnetite has been utilized in the preparation of magnetic recording media because of its magnetic capacity.[28] Goethite, as part of the oxyhydroxide iron species with high natural occurrence and its important role in aquatic, atmospheric and terrestrial systems has also been studied.[29, 62]

Hematite is the most stable phase of the iron oxide and is the product of natural aging of maghemite and magnetite. [30] Thermal annealing is proven to enhance this phase transformation, and a difference in the transformation pathway and conversion temperature between micro and nano size crystals has been reported. Li and collaborators observed a conversion of magnetite to maghmite at 109 ^{o}C with a further transformation to hematite at temperatures above 500 ^{o}C. This result was

compared with the observed conversion of micro size magnetite that converted directly to hematite at a starting temperature of 300 ºC only.[31]

2.2.3.1 Cristal structure and surface termination of iron oxides

Hematite (α-Fe_eO_3)

It is conformed of fully oxidized iron, Fe (III) in a rhombohedral centred hexagonal structure, with Fe^{+3} ions located in 2/3 of the octahedral sites which are surrounded by six oxygen atoms,[32] as observed in Figure 2.3.[33]

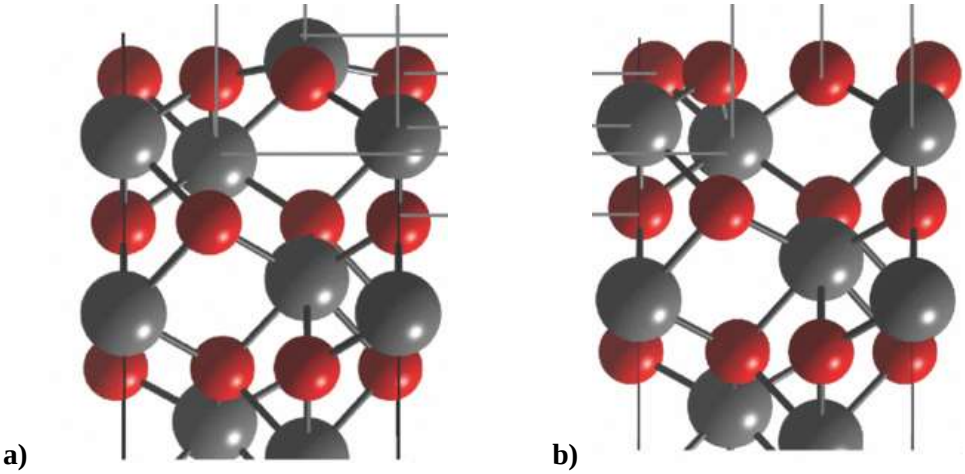

Figure 2.3. Side view of hematite unites cells a) Iron surface termination b) oxygen surface termination. Gray and red spheres represent Fe and O atoms respectively. **Adapted with permission from Pabisiak, T.; Kiejna, A., Fe adsorption on hematite (alpha-Fe2O3) (0001) and magnetite (Fe3O4) (111) surfaces. *The Journal of chemical physics* 2014, *141* (13), 134707. Copyright [2015], AIP Publishing LLC.**

Maghemite (γ -Fe_2O_3)

Similar to hematite the crystal is composed of fully oxidized iron. It possess 2 and 1/3 iron vacancies sites in the unit cell.[34] The lattice vacancies have been shown to be located in the octahedral sites, as observed in Figure 2.4. [35]

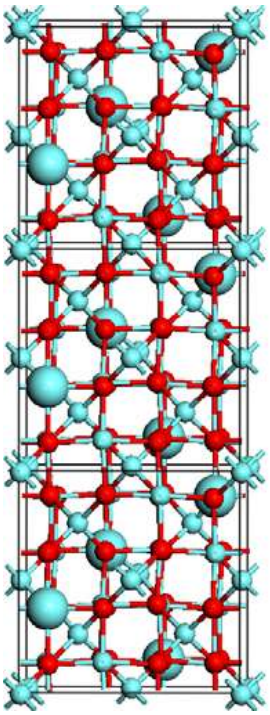

Figure 2.4. Maghemite crystalline structure, green spheres represents iron and red spheres oxygen. Large spheres represent possible positions for the iron vacancies. **Modified with permission from Grau-Crespo, R.; Al-Baitai, A. Y.; Saadoune, I.; De Leeuw, N. H., Vacancy ordering and electronic structure of gamma-Fe2O3 (maghemite): a theoretical investigation. *J. Phys.-Condes. Matter* 2010, *22* (25). DOI: doi:10.1088/0953-8984/22/25/255401 Copyright (2015) IOP publishing.**

Goethite (α-FeOOH)

It is characterized for having an orthorhombic structure that contains Fe (III) atoms coordinated in an octahedral configuration,[36] as observed in Figure 2.5.[37] In ambient and aquatic conditions, the surface termination of goethite can consist of single, double or triple coordinated hydroxyl groups with underlying Fe atoms. [29]

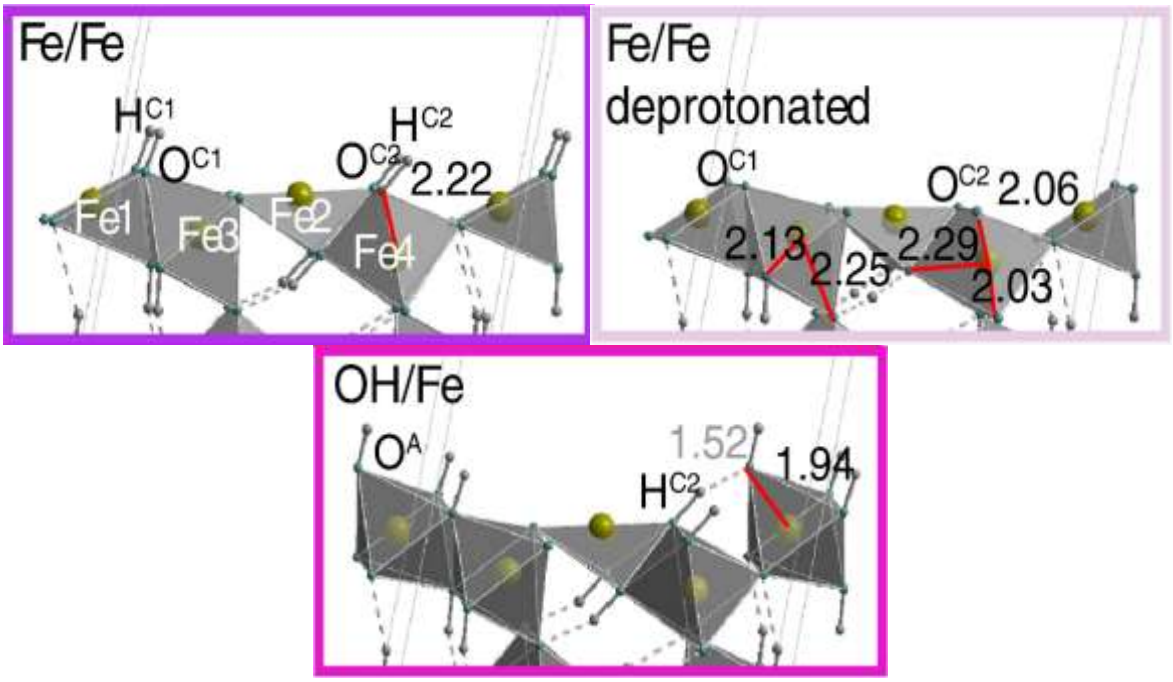

Figure 2.5. Goethite's most stable surface terminations. Iron termination (Fe/Fe), Deprotonated Iron surface (Fe/Fe deprotonated), and OH terminated (OH/Fe). Iron is represented by the yellow spheres; oxygen and hydrogen are represented by the green and white spheres respectively. Reprinted from *Surface Science*, 606 /(21-22), Otte, K.; Schmahl, W. W.; Pentcheva, R., Density functional theory study of water adsorption on FeOOH surfaces, 1623-1632. Copyright (2015), with permission from Elsevier

Magnetite (Fe_3O_4)

In contrast to the other iron species, magnetite contains iron in the +2 and +3 oxidation states. These iron ions are enclosed in a cubic inverse spinel, in which the Fe^{+3} are coordinated tetrahedrically and Fe^{+2} is located in the octahedral sites.[38] This iron species have important magnetic and electronic properties due to the electronic transfer between the Fe^{+2} and Fe^{+3} ions.

Differences in the chemical interaction between the 1,2-DCA and TCE towards the previously discussed iron species can be potentially explained by a combination of the difference in the surface termination, crystalline structure and oxidation state of the iron species present in these different oxides.

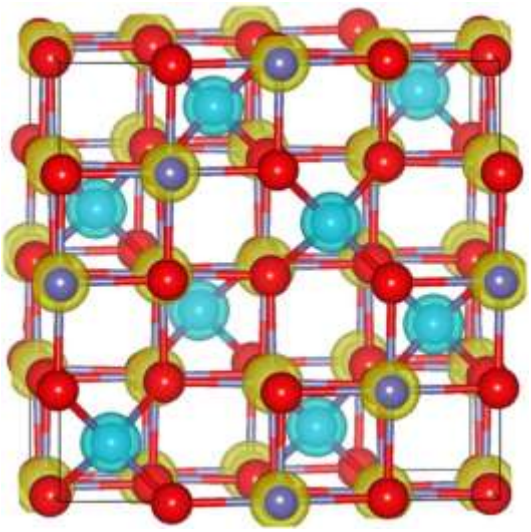

Figure 2.6. Magnetite crystalline structure representation, red, yellow shell with blue and light blue shell with blue sphere represent O, Octahedral Fe and Tetrahedral Fe respectively. Reprinted from *Surface Science*, 606 /(9-10), Yu, X. H.; Huo, C. F.; Li, Y. W.; Wang, J. G.; Jiao, Fe3O4 surface electronic structures and stability from GGA plus U, 872-879.,Copyright (2015), with permission from Elsevier

For instance, in their study of hematite surface termination reactivity towards carbon tetrachloride (CCl_4), Camillone and collaborators observed a rapid adsorption of CCl_4 on the magnetite terminated surface, while on fully oxidized hematite adsorption was negligible. They attributed this result to the difference in the surface termination between both oxides. Indeed, under their experimental conditions, they observed an iron surface termination and oxygen atoms with vertically oriented dangling bonds in magnetite that allowed the interaction with the CCl_4 molecule. These were not present for hematite [26]

Experimental comparative reactivity studies between phases with similar oxidation structure such as hematite and maghemite are scarce. In an attempt to tackle these differences Al-Baitai and collaborators carried computational simulations of adsorption of formic acid and hydroxyethanal over dehydrated and hydrated surfaces of hematite and goethite. In their results they observed a higher reactivity of the dehydrated iron oxides surfaces towards adsorption of both probe sorbate compounds. This was explained by means of a decrease of the surface energy as the dissociative adsorption of water in the surface occurs leading to an increase of the coordination of the iron-oxygen on the surface. This interaction was observed to take place through the oxygen water atom with the surface iron ion, and a hydrogen bond with the surface oxygen. Another interesting

observation was the higher tendency of maghemite to adsorb formic acid in comparison with hematite, and was explained in terms of the higher stability of the hematite surface, and the instability of the maghemite surface.[34]

Contributions of the surface termination have been observed not only between different iron species. For instance, Kubicki and collaborators using DFT simulations investigated the adsorption of phosphate on different goethite crystal phases such as (100), (010), (001), and (101). From their observations they concluded that adsorption of phosphates is selective towards certain crystalline phases, due to the variability in the surface termination that each plane contains. Additional experiments indicated a difference in the adsorption modes of phosphates into the goethite surface as the size of the particles changed from micro to nano size.[63]

Additional research has shown that the ability of the adsorption site to form a surface complex is not the only necessary requirement, but also the existence of neighboring species that can contribute to the stabilization of the adsorbed molecule. This was reported by Loring and collaborators when studying the coordination of arsenate to goethite surfaces. Where arsenate was hypothesized to adsorb to a single coordinated oxygen site in the surface, and the resulting complex was stabilized by hydrogen bonding to neighboring hydroxyl groups or adsorbed water.[64]

The previously discussed investigations demonstrate the importance of the iron oxide surface termination in the capacity to interact and react with adsorbed molecules. The role of the hydroxyl groups in the stabilization of the surface and the interaction towards compounds is also clear. Also the availability and distribution of the oxygen and iron atoms in the surface seems to have a large effect on the success of these interactions. All these observations give us a further understanding of the importance of investigating the surface interaction between the different iron species that can be found on the nZVI surface and our target contaminants.

2.3 nZVI reduction of chlorinated hydrocarbons

Dechlorination of zero valent iron was first studied by Gillham and collaborators where they observed that dechlorination was achieved for most of the halogenated hydrocarbons in the

presence of ZVI. It was also observed that the available surface area is important in the reaction rate and suggested that a smaller particle size would allow an increase in the reaction rate.[5] One of the limitations of dechlorination of TCE and tetrachloroethane by ZVI was the production of more toxic by-products such as cis 1,2-dichloroethene and vinyl chloride. Zhang and collaborators took one step forward and reported a novel method for synthesising nano particles of zero valent iron and bimetallic nZVI particles which had a higher surface area and resulted in increased reaction rates in comparison with the micro size ZVI. Also, no chlorinated by-products (hydrocarbons) were observed.[10]

On the other hand because of its structural stability and relative low reduction potential 1,2-DCA has shown to be highly recalcitrant to reduction to nZVI,[39] Also it has been suggested that as the bond strength between the C-Cl atoms increases, the capacity of the nZVI to reduce the chlorinated hydrocarbon diminishes.[40] This is consistent with the observations by Gillham and collaborators where they reported that highly chlorinated hydrocarbons are reduce at a higher reaction rate.[2]

2.3.1 Reaction mechanisms

Reductive dechlorination for TCE has been suggested to occur by two possible mechanisms; β-elimination and hydrogenolysis. The reaction pathway preference has been observed to be influenced by the particle size. ZVI has shown a preferential dechlorination pathway by β-elimination.[2b, 41] This is in contrast to nZVI synthesised by sodium borohydride, which shows a preferential pathway by hydrogenolysis, and commercially available nZVI that reacted primarily by β-elimination for TCE dechlorination. [11, 42] Fig.2.7 depicts the proposed dechlorination pathways as reported by Arnold and collaborators.[43]

The dechlorination mechanism for chlorinated ethanes has been observed to be influenced by the degree of chlorination and the position of the chlorine atoms in the molecule. β -elimination is favored in compounds with chlorine atoms located in the α,β position. On the other hand compounds that pose only α chlorine atoms have a preferential reaction mechanism via hydrogenolysis. Other mechanisms such as dehydrohalogenation can be activated under high pH conditions. [39] Song and collaborators reported the effect of pH in the reaction mechanism

selectivity of 1,1,2,2-tetrachloroethane showing a decrease in reactivity as the pH increased. This phenomena was rationalized in terms of effects of pH in the surface composition of the nZVI where low pH promotes a corrosion of the shell layer and higher pH allows the precipitation of iron species that passivates nZVI. Also the effect of pH was observed as predicted in the selectivity of the reaction mechanism; where at higher pH values the dehydrohalogenation pathway was favored.[39]

In the investigation done by Arnold and collaborators the proposed reaction mechanisms is highly dependent of the surface composition of the nZVI particles where first step is given by the formation of a surface adsorbed species. Here the chlorinated hydrocarbon is bonded to the surface through a π bond. Where the surface iron in the surface oxide would function as a Lewis acid site, and the alkynes and alkenes are presented as Lewis bases. They also suggest that this mechanism would explain the increased reactivity to highly chlorinated ethylenes since the increase in the number of chlorine atoms would augment the electron density withdraw from the π system due to chlorines higher capacity to attract the bonding pair of electrons . This results in a decrease of the energy of the π^* orbitals of the double bond, inversely affecting the Lewis basicity, therefore increasing the capacity for the formation of a surface complex intermediary through the π system. The second proposed step suggests the formation of the di-σ-bonded surface intermediate; this di-σ-bonded system can go through two fast consecutive halide ion eliminations by forming a mono-σ-bonded vinyl surface intermediary and then acetylene. Depending on the availability of hydrogen, an alternative reaction with surface adsorbed hydrogen will follow a fast ion elimination of the halide resulting in hydrogenolysis products.[43] Unfortunately only indirect evidence of the formation of the di-σ-bonded system has been provided to date.

From this suggested mechanism and previously discussed research the importance of the role of the surface composition is undoubtable, and the need of a comprehensive understanding of the surface role in the adsorption/reaction mechanism is clear. This will allow us to prove the formation of surface intermediaries, distinguish reactive sites, and further explain the recalcitrance that lower chlorinated compounds like 1,2-DCA show towards dechlorination by nZVI.

In this regard, 1,2-DCA dechlorination in the presence of zero valent nanoparticles has been reported by Chang and collaborators. By using zero valent copper nano particles with sodium

borohydride as the reducing agent, 85% 1,2-DCA dechlorination was achieved within a 5 hours period. A degradation pathway via two main mechanisms: A single step reductive dihaloelimination that resulted in ethylene production and two consecutive steps of hydrogenolysis that resulted in the formation of chloroethane and ethane was proposed. Since product analysis showed a 79% ethane and only a 1.1% ethylene, a hydrogenolysis path is suggested as the major reaction pathway followed by dihaloelimination as a minor contributor. [40] 1,2-DCA has also been observed to degrade under catalysed hydrogen assisted dechlorination conditions.[44,45,46,47]

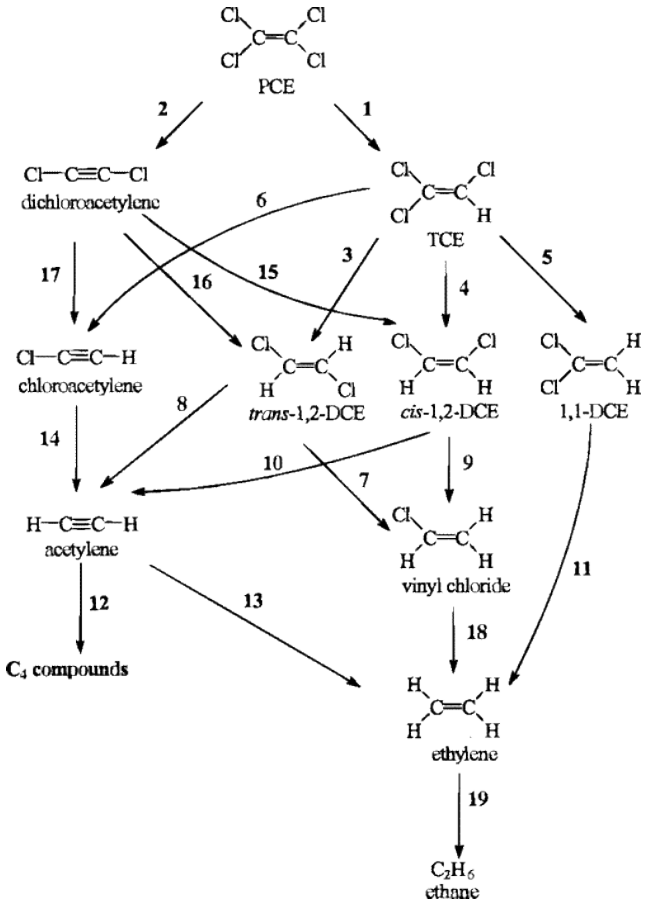

Figure 2.7. Proposed reaction mechanism for PCE dechlorination by Fe^0; where reaction 1,3,4,5,7,9,14,17 and 18 correspond to hydrogenolysis, reactions 2,6,8 and 10 are reductive β-elimination, reaction 11 corresponds to α-elimination and reactions 13,15,16 and 19 are hydrogenation reactions.[43] Adapted with permission from Arnold, W. A.; Roberts, A. L., Pathways and kinetics of chlorinated ethylene and chlorinated acetylene reaction with Fe(O) particles. *Environmental Science & Technology* 2000, *34* (9), 1794-1805.. Copyright (2015) American Chemical Society.

2.3.2 Proposed rate limiting steps in dechlorination reactions

Understanding the rate limiting step of TCE and 1,2-DCA dechlorination can provide insights into the difficulties associated with dechlorination of 1,2-DCA with zero valent metals. Several studies have been done to understand the rate limiting step in the TCE-ZVI system; nevertheless experimental setups cannot always take into account all the conditions that are required to resemble dechlorination under groundwater environments. Bylaska and collaborators used theoretical calculations to determine the electron transfer mechanisms in the reductive dechlorination of TCE in gas and aqueous systems, where the rate limiting step was found to be the first electron transfer.[48] Li and collaborators used an electrochemical setup to determine if the rate limiting mechanisms for TCE dechlorination in presence of an iron electrode was due to electron transfer mechanisms or chemical dependent factors such as the rate of bond breaking, molecular rearrangement or chemisorption. They reported that TCE dechlorination rate was limited by chemical dependent factors rather than limited by electron transfer, and suggested that chemisorption may be the step that controls the overall reaction rate. For this study they investigated the dependence of the electron transfer coefficient (ETC) on temperature, where the ETC is known to be dependent only on the amount of electrons that are transferred before and after the rate limiting step and a symmetry factor. Evaluating the ETC of their proposed experimental set up at different temperatures allowed them to assess if the rate limiting step for TCE reduction was indeed electron transfer. In their investigation they found a temperature dependence of the ETC for TCE, which results in the reaction rate to be limited by chemical dependent factors such as chemisorption, rates of bond breaking or molecular rearrangement that can be influenced by the change in temperature and therefore a change in the activation energy. [2b] In another investigation Su and collaborators found the activation energy of the TCE dechlorination reaction with ZVI in aqueous solution to be in the range of 32.9 and 39.4 kJ mol^{-1} which is higher than the required activation energy for a diffusion limited processes, suggesting the system is limited by a surface chemical reaction.[41]

2.3.3 Surface adsorption and reaction processes

As previously discussed the effect of different surface composition can have a great influence on the reaction mechanisms via different effects; (1) The incompatibility between the surface and the adsorbate to allow the formation of a surface intermediary necessary for the surface mediated reaction to take place, (2) the formation of a surface compound that is thermodynamically more stable than the desired reaction product and (3) the formation of a surface intermediary that is weakly adsorbed and would not allow the reaction to take place.

In situ spectroscopic analytical techniques are powerful tools that have been widely used in the study of these types of surface phenomena. The use of in situ spectroscopy present several advantages compared to ex situ analysis since physicochemical or structural changes on the surfaces can take place when they are exposed to ambient conditions for ex situ analysis. The use of these in situ techniques has slowly grown in environmental engineering as the development of new technologies has required the understanding of surface phenomena at a more fundamental level in order to improve these technologies.[49]

Among these, in situ diffuse reflectance Fourier transform infrared spectroscopy (DRIFTS), Attenuated total reflectance (ATR)-FTIR and diffuse reflectance UV-visible spectroscopy can be utilized to identify and semi-quantify different iron oxides and oxyhydroxides species.[50] These spectroscopic techniques can be performed under operando conditions. In situ UV-vis can enable probing of the electronic changes in the bulk composition of the iron species while operando FTIR can provide valuable information about the surface interaction between these iron oxide surfaces and the target contaminants. As previously discussed the chemisorption of the contaminants to the surface of the iron nanoparticles, represent an important step in the dechlorination mechanism. Thus a clear understanding of these surface interactions can provide useful information to improve contaminant degradation reactions.

For instance, Jeurissen and collaborators by means of Fourier transform infrared (FTIR) studied the catalytic dechlorination mechanisms of 1,2-DCA and TCE over Pd and Cr supported over different aluminum oxides. When 1,2-DCA interacted with γ-alumina at 300^{o}C, infrared vibration bands associated to vinyl chloride (VC) were observed. These were attributed to dehydrochlorination processes in the presence of Lewis acid sites in the alumina surface. The

authors suggested a second adsorption species formed from the coordination to a Lewis acid site, resulting in an acetaldehyde-like bonded R-C^{H}=O--Al^{+3}species (Fig. 2.8). Another process by which VC dechlorination can occur more easily is by a protonation by an acid catalyst in the presence of moisture or OH surface groups. This protonation process will result in the formation of a carbocation stabilized by resonance. The instability of the carbocation due to its electron deficiency will allow it to undergo a nucleophilic attack by a surface oxygen or adsorbed water. Another mechanism that was suggested for the formation of the carbocation is through an OH surface group simultaneously attacking the two carbons of the vinyl chloride. Regarding the adsorption of TCE into the alumina surface, the authors reported that during the initial steps in the oxidation of TCE, adsorption over CrO_x/Al_2O_e lead to the formation of monochloroacetyl chloride as CH_2Cl-C^{Cl}=O--Al^{3+} (Fig.2.9).[51]

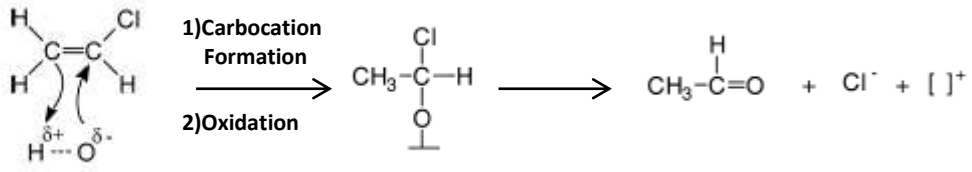

Figure 2.8.Vinyl chloride dechlornation to acetaldehyde by nucleophilic attack of surface oxygen to the carbocation. Modified from. Reprinted from *Catalysis Today*, *54* (1), Feijen-Jeurissen, M. M. R.; Jorna, J. J.; Nieuwenhuys, B. E.; Sinquin, G.; Petit, C.; Hindermann, J.-P., Mechanism of catalytic destruction of 1,2-dichloroethane and trichloroethylene over γ-Al2O3 and γ-Al2O3 supported chromium and palladium catalysts. 65-79., Copyright (2015), with permission from Elsevier

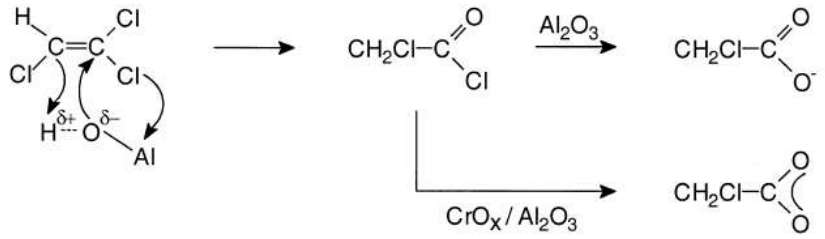

Figure 2.9. Formation of the surface monochloracetyl chloride in the presence of the alumina surface, and the propose mechanism of TCE oxidation. Modified from. Reprinted from *Catalysis Today*, *54* (1), Feijen-Jeurissen, M. M. R.; Jorna, J. J.; Nieuwenhuys, B. E.; Sinquin, G.; Petit, C.; Hindermann, J.-P., e 65-79., Copyright (2015), with permission from Elsevier

In another investigation by the same group, carried by means of FTIR and temperature program desorption (TPD), the adsorption of TCE over aluminosilcates was evaluated. The authors observed that as the SiO/Al_2O_3 ratio increased the amount of physisorbed TCE increases due to the increase in the hydrophobicity of the sorbent/catalyst. The use of FTIR allowed them to identify the role of the hydroxylated surface of the aluminum oxide in the adsorption process.[52]

Additional adsorption studies have been conducted by Scaranto and Giorgiani where the adsorption of different halocarbons over titanium dioxide was followed by means of FTIR and complemented by the use of computational modeling. Scaranto and collaborators used difluoromethane as an adsorbant which allowed them to make spectroscopic observations of the adsorbed species. They observed the formation of negative bands in the region of 3700 cm^{-1} when the titanium dioxide was used as a background and it is allowed to interact with the difluoromethane, these bands can be easily assigned to the loss of isolated OH surface groups, and the appearance of a broad band in the region of 3500- 3700 cm^{-1} linked to H bonded hydroxyls. Another observation reported was the formation of 2 different C-F stretching vibrations. The authors rationalized these results in terms of an acid-base interaction between the surface and the adsorbate where one of the F atoms interacts with one of the Lewis acid sites on the surface (Ti^{4+}), the other interaction mechanism was suggested to be in the form of a H bond between the surface Lewis basic site (OH, O^{2-}) and any of the two hydrogen atoms originally present in the difluoromethane molecule. In order to further probe this phenomenon the authors carried DFT (density functional theory) calculations and obtained from all the possible adsorption mechanisms a required interaction between the surface Ti^{+4} and the F atoms, while adsorption due to the interaction of the surface O^{-2} and OH differed between each simulation in the degree of involvement of these sites.[53]

In a further study, Scaranto and collaborators studied by similar means the interaction of vinyl halides such as vinyl chloride and vinyl fluoride on the surface of titanium dioxide. Since their previous work showed the interaction between the surface Lewis acid sites and the halide atom, and because of the heterogeneity that characterizes oxide surfaces, lead them to understand the distribution and strength of the available surface Lewis sites that results for the different local chemical environments. For this they perform adsorption experiments with probe molecules, this probe molecules help to distinguish the strength between the existing surface Lewis acid sites. In

this case CO was used as probe molecule. The formation of two stretching bands for the C-O vibration with a blue shift allowed them to differentiate between two different Ti^{+4} Lewis acid sites that interact differently because of the chemical environment in which they are located. When the interaction of the vinyl halides with titanium dioxide surface was probed, the adsorption phenomenon showed the formation of H-bonds through the appearance of a negative peak in the IR spectrum corresponding to the surface OH species and the interaction of the halogen species with the surface Lewis acid sites. In their spectra the differentiation of the adsorption between the two different Lewis acid sites was not possible, and this was attributed to the electrophilic properties of the halogen atom that would make the difference in the vibrational modes between the two sites too small to be experimentally resolved. Ab initio DFT calculations performed to simulate the adsorption process agreed with the experimental observation for the elongation of the C-X (halogen) bond due to the interaction with surface Lewis acid sites and the elongation C-H due to H bond formation.[54,54b] When chlorodifluoromethane was utilized as a probe molecule similar interactions were observed as in the DFT calculation, most noticeable the possibility of interaction by any of the halogenated atoms in the chlorodifluoromethane molecule with the surface Lewis acid sites. This resulted in an increase in the bond length from the atom interacting directly with the Lewis acid site. A similar formation of an H bond between coordinated unsaturated oxygen or hydroxyl groups with the C-H of the halogenated compound was also observed.[55]

The use of ATR-FTIR has been utilized as a spectroscopic technique as an alternative approach for the understanding of these type of surface interactions. The study of attenuation mechanisms of water contamination by adsorption on iron oxides and oxyhydroxides has provided significant insights in this field.[62,63,64] Abadleh and collaborators investigated the adsorption mechanisms of arsenic bearing organic contaminants such as dimethylarsinic acid, p-Arsanilic acid, and arsenate on α -FeOOH and α -Fe_2O_3. In their experimental set up the investigated iron surface was exposed to a flow of the contaminant under controlled pH conditions. Limitations due to the inclusion of water in the spectroscopic system and the high response of water to infrared adsorption required monitoring of adsorption through the stretching bands of As-O in the 950-750 cm^{-1} region. Experimental results along with DFT calculations demonstrated that the adsorption complex of these organoarsenical compounds forms by a ligand exchange mechanisms, where adsorbed water

acts as a leaving group.[67] The interaction can occur in a mono or bidentate manner with the surface iron. [65, 66] These adsorption mechanisms are highly sensitive to the degree of protonation of the arsenic-bearing molecule and the surface sites of the (oxyhydr)oxides which are in turn controlled by the pH conditions of the system.[65, 66]

Because of the challenge in understanding surface phenomena in complex surfaces such as the iron oxides, the use of single crystals allows a simplification of the phenomena occurring and therefore a fundamental understanding of the surface mechanisms that could take place between the substrate and the adsorbate. Indeed, as previously discussed, interactions between the surface and the chlorinated contaminants can be highly dependent on the surface characteristics (e.g. amount of available Lewis acid sites and/or amount of under coordinated oxygen or hydroxyl groups). Because of this, the importance of the crystalline structure becomes apparent since the presence of these available sites will be dictated by the crystal surface termination of the different iron oxides/oxyhydroxides in nZVI.

In order to understand the surface interaction between iron oxides and simple chlorinated compounds Abid and collaborators studied the surface reactions of magnetite (Fe_3O_4) surface grown over a hematite single crystal and CCl_4 by means of temperature program reaction/desorption. It is worth noting the difference in their experimental conditions to make a proper comparison with actual environmental systems which are obviously more complex. The use of ultra-high vacuum (UHV) conditions and temperature starting from 100 K to 1200 K were utilized. The use of UHV conditions ensures the cleanliness of the iron oxide surface removing most of the hydroxyl surface species; this makes the comparison with normally hydroxylated surfaces present at ambient conditions more complicated. From their experiments they observed desorption of CCl_4 species by means of recombinative desorption, the authors also observed the formation of C_2Cl_4 and attributed this to an associative desorption mechanism. At last they observed the formation of $OCCl_2$ by an extraction of a lattice oxygen atom from the iron oxide surface. Because of the experimental condition differences a direct comparison to our system can result unfeasible.[56,57]

In a similar experimental set up Garet and collaborators studied the reactivity of Fe^0 deposited on a multilayer of FeO crystal, and observed a difference in the reactivity and mechanism of Fe^0

towards CCl_4 as the size of the Fe^0 cluster increased. In their experiments they also observed the formation of C_2Cl_4 and $OCCl_2$ species, where the oxygen that is present in the $OCCl_2$ species is similarly abstracted from the FeO substrate. Interestingly for their proposed reaction mechanism they suggested the interaction of the CCl_4 to form intermediate species that contain C, Fe and Cl atoms. [58]

Rim and collaborators also studied the reactivity of CCl_4 towards Fe_3O_4 by means of scanning tunneling microscopy (STM) and DFT calculations. In previous studies where the interaction was performed at room temperature, the adsorption takes place via a dissociative adsorption, two surface chlorine surface species were observed, one in the iron located in the top of the lattice and another one at a 3-fold oxygen vacancy site, with a selectivity of 90% towards the 3-fold oxygen vacancy sites.[59] In this experiment adsorption was performed at 224 K and desorption ramping slowly to 500 K. The authors reported different observations. When chlorine is bonded only to iron terminated Fe_3O_4, two different chlorine species are observed similarly, one resulting from the interaction on top of the surface terminated iron atom and the second at the 3-fold oxygen vacancy sites, but with an opposite selectivity, where 90% of the adsorbed compounds were observed in the iron top sites. This observation was linked to the effect of temperature in the capacity to form phosgene ($COCl_2$) products, and the capacity to extract surface oxygen atoms from this iron oxide phase.[28]

All these observations lead us to acknowledge the complexity of these surface interactions, and the necessity of a fundamental adsorption phenomena study, capable of explaining the surface processes taking place between groundwater contaminants 1,2-DCA and TCE and the different iron species that can be found in the nZVI surface, together with the need for using in situ spectroscopic techniques to explore and probe the surface phenomena at the time scale associated with these processes.

2.4 References

1. Yan, W.; Lien, H.-L.; Koel, B. E.; Zhang, W.-x., Iron nanoparticles for environmental clean-up: recent developments and future outlook. *Environmental Science-Processes & Impacts* **2013,** *15* (1), 63-77.

2. (a) Zhang, W. X.; Wang, C. B.; Lien, H. L., Treatment of chlorinated organic contaminants with nanoscale bimetallic particles. *Catalysis Today* **1998,** *40* (4), 387-395; (b) Li, T.; Farrell, J., Electrochemical investigation of the rate-limiting mechanisms for trichloroethylene and carbon tetrachloride reduction at iron surfaces. *Environmental Science & Technology* **2001,** *35* (17), 3560-3565.

3. Lien, H. L.; Zhang, W. X., Hydrodechlorination of chlorinated ethanes by nanoscale Pd/Fe bimetallic particles. *J Environ Eng-Asce* **2005,** *131* (1), 4-10.

4. Reynolds, G. W.; Hoff, J. T.; Gillham, R. W., Sampling Bias Caused by Materials Used to Monitor Halocarbons in Groundwater. *Environmental Science & Technology* **1990,** *24* (1), 135-142.

5. Gillham, R. W.; Ohannesin, S. F., Enhanced Degradation of Halogenated Aliphatics by Zero-Valent Iron. *Ground Water* **1994,** *32* (6), 958-967.

6. Scherer, M. M.; Richter, S.; Valentine, R. L.; Alvarez, P. J. J., Chemistry and microbiology of permeable reactive barriers for in situ groundwater clean up. *Critical Reviews in Environmental Science and Technology* **2000,** *30* (3), 363-411.

7. Wilkin, R. T.; Su, C. M.; Ford, R. G.; Paul, C. J., Chromium-removal processes during groundwater remediation by a zerovalent iron permeable reactive barrier. *Environmental Science & Technology* **2005,** *39* (12), 4599-4605.

8. Liang, L. Y.; Korte, N.; Gu, B. H.; Puls, R.; Reeter, C., Geochemical and microbial reactions affecting the long-term performance of in situ 'iron barriers'. *Adv Environ Res* **2000,** *4* (4), 273-286.

9. Gupta, N.; Sass, B. M.; Gavaskar, A. R.; Sminchak, J. R.; Fox, T. C.; Snyder, F. A.; O'Dwyer, D.; Reeter, C., Hydraulic evaluation of a permeable barrier using tracer tests, velocity measurements, and modeling. *First International Conference on Remediation of Chlorinated and Recalcitrant Compounds, Vol 6* **1998**, 157-162.

10. Wang, C.-B.; Zhang, W.-x., Synthesizing Nanoscale Iron Particles for Rapid and Complete Dechlorination of TCE and PCBs. *Environmental Science & Technology* **1997,** *31* (7), 2154-2156.

11. O'Carroll, D.; Sleep, B.; Krol, M.; Boparai, H.; Kocur, C., Nanoscale zero valent iron and bimetallic particles for contaminated site remediation. *Advances in Water Resources* **2013,** *51*, 104-122.

12. Zhang, W. X., Nanoscale iron particles for environmental remediation: An overview. *Journal of Nanoparticle Research* **2003,** *5* (3-4), 323-332.

13. Cao, J. S.; Elliott, D.; Zhang, W. X., Perchlorate reduction by nanoscale iron particles. *Journal of Nanoparticle Research* **2005,** *7* (4-5), 499-506.

14. Sakulchaicharoen, N.; O'Carroll, D. M.; Herrera, J. E., Enhanced stability and dechlorination activity of pre-synthesis stabilized nanoscale FePd particles. *Journal of contaminant hydrology* **2010,** *118* (3–4), 117-127.

15. Liu, C.-C.; Tseng, D.-H.; Wang, C.-Y., Effects of ferrous ions on the reductive dechlorination of trichloroethylene by zero-valent iron. *Journal of hazardous materials* **2006,** *136* (3), 706-713.

16. Li, X.-q.; Zhang, W.-x., Iron Nanoparticles: the Core−Shell Structure and Unique Properties for Ni(II) Sequestration. *Langmuir* **2006,** *22* (10), 4638-4642.

17. Lien, H.-L.; Zhang, W.-X., Nanoscale Pd/Fe bimetallic particles: Catalytic effects of palladium on hydrodechlorination. *Applied Catalysis B: Environmental* **2007,** *77* (1–2), 110-116.

18. Filip, J.; Karlický, F.; Marušák, Z.; Lazar, P.; Černík, M.; Otyepka, M.; Zbořil, R., Anaerobic Reaction of Nanoscale Zerovalent Iron with Water: Mechanism and Kinetics. *The Journal of Physical Chemistry C* **2014,** *118* (25), 13817-13825.

19. Ritter, K.; Odziemkowski, M. S.; Gillham, R. W., An in situ study of the role of surface films on granular iron in the permeable iron wall technology. *Journal of contaminant hydrology* **2002,** *55* (1–2), 87-111.

20. Beverskog, B.; Puigdomenech, I., Revised Pourbaix diagrams for iron at 25-300 degrees C. *Corros Sci* **1996,** *38* (12), 2121-2135.

21. Uludag-Demirer, S.; Bowers, A. R., Adsorption/Reduction Reactions of Trichloroethylene by Elemental Iron in the Gas Phase: The Role of Water. *Environmental Science & Technology* **2000,** *34* (20), 4407-4412.

22. Uludag-Demirer, S.; Bowers, A. R., Gas phase reduction of chlorinated vocs by zero valent iron. *Journal of Environmental Science and Health, Part A* **2001,** *36* (8), 1535-1547.
23. Uludag-Demirer, S.; Bowers, A. R., Effects of Surface Oxidation and Oxygen on the Removal of Trichloroethylene From the Gas Phase Using Elemental Iron. *Water, Air, and Soil Pollution* **2003,** *142* (1/4), 229-242.
24. Lim, T. T.; Zhu, B. W., Effects of anions on the kinetics and reactivity of nanoscale Pd/Fe in trichlorobenzene dechlorination. *Chemosphere* **2008,** *73* (9), 1471-1477.
25. Makie, P.; Westin, G.; Persson, P.; Osterlund, L., Adsorption of Trimethyl Phosphate on Maghemite, Hematite, and Goethite Nanoparticles. *Journal of Physical Chemistry A* **2011,** *115* (32), 8948-8959.
26. Camillone, N.; Adib, K.; Fitts, J. P.; Rim, K. T.; Flynn, G. W.; Joyce, S. A.; Osgood, R. M., Surface termination dependence of the reactivity of single crystal hematite with CCl4. *Surface Science* **2002,** *511* (1-3), 267-282.
27. Lorenzelli, V.; Busca, G.; Sheppard, N., Infrared study of the surface reactivity of hematite. *Journal of Catalysis* **1980,** *66* (1), 28-35.
28. Rim, K. T.; Muller, T.; Fitts, J. P.; Adib, K.; Camillone, N.; Osgood, R. M.; Batista, E. R.; Friesner, R. A.; Joyce, S. A.; Flynn, G. W., Scanning tunneling microscopy and theoretical study of competitive reactions in the dissociative chemisorption of CCl4 on iron oxide surfaces. *J Phys Chem B* **2004,** *108* (43), 16753-16760.
29. Song, X. W.; Boily, J. F., Water Vapor Adsorption on Goethite. *Environmental Science & Technology* **2013,** *47* (13), 7171-7177.
30. Sidhu, P. S., Transformation of trae element-substituted Maghemite to Hematite. *Clays and clay minerals* **1988,** *36* (1), 31-38.
31. Li, Y.-S.; Church, J. S.; Woodhead, A. L., Infrared and Raman spectroscopic studies on iron oxide magnetic nano-particles and their surface modifications. *Journal of Magnetism and Magnetic Materials* **2012,** *324* (8), 1543-1550.
32. Wu, C.; Yin, P.; Zhu, X.; OuYang, C.; Xie, Y., Synthesis of Hematite (α-Fe2O3) Nanorods: Diameter-Size and Shape Effects on Their Applications in Magnetism, Lithium Ion Battery, and Gas Sensors. *The Journal of Physical Chemistry B* **2006,** *110* (36), 17806-17812.
33. Pabisiak, T.; Kiejna, A., Fe adsorption on hematite (alpha-Fe2O3) (0001) and magnetite (Fe3O4) (111) surfaces. *The Journal of chemical physics* **2014,** *141* (13), 134707.

34. Al-Baitai, Asmaa. H. de Leeuw, Nora., Computational Studies of the Interaction of Pollutants with Iron Oxide Surfaces. Thesis submitted for the degree of Doctor of Philosophy, University College London 2011.

35. Grau-Crespo, R.; Al-Baitai, A. Y.; Saadoune, I.; De Leeuw, N. H., Vacancy ordering and electronic structure of gamma-Fe2O3 (maghemite): a theoretical investigation. *J. Phys.-Condes. Matter* **2010,** *22* (25).

36. Martin, G. J.; Cutting, R. S.; Vaughan, D. J.; Warren, M. C., Bulk and key surface structures of hematite, magnetite, and goethite: A density functional theory study. *Am Mineral* **2009,** *94* (10), 1341-1350.

37. Otte, K.; Schmahl, W. W.; Pentcheva, R., Density functional theory study of water adsorption on FeOOH surfaces. *Surface Science* **2012,** *606* (21-22), 1623-1632.

38. Yu, X. H.; Huo, C. F.; Li, Y. W.; Wang, J. G.; Jiao, H. J., Fe3O4 surface electronic structures and stability from GGA plus U. *Surface Science* **2012,** *606* (9-10), 872-879.

39. Song, H.; Carraway, E. R., Reduction of Chlorinated Ethanes by Nanosized Zero-Valent Iron: Kinetics, Pathways, and Effects of Reaction Conditions. *Environmental Science & Technology* **2005,** *39* (16), 6237-6245.

40. Huang, C. C.; Lo, S. L.; Tsai, S. M.; Lien, H. L., Catalytic hydrodechlorination of 1,2-dichloroethane using copper nanoparticles under reduction conditions of sodium borohydride. *Journal of environmental monitoring : JEM* **2011,** *13* (9), 2406-12.

41. Su, C.; Puls, R. W., Kinetics of Trichloroethene Reduction by Zerovalent Iron and Tin: Pretreatment Effect, Apparent Activation Energy, and Intermediate Products. *Environmental Science & Technology* **1999,** *33* (1), 163-168.

42. Liu, Y. Q.; Majetich, S. A.; Tilton, R. D.; Sholl, D. S.; Lowry, G. V., TCE dechlorination rates, pathways, and efficiency of nanoscale iron particles with different properties. *Environmental Science & Technology* **2005,** *39* (5), 1338-1345.

43. Arnold, W. A.; Roberts, A. L., Pathways and kinetics of chlorinated ethylene and chlorinated acetylene reaction with Fe(O) particles. *Environmental Science & Technology* **2000,** *34* (9), 1794-1805.

44. Rhodes, W.; Margitfalvi, J.; Borbath, I.; Lazar, K.; Kovalchuk, V.; Ditri, J., Hydrogen-assisted 1,2-dichloroethane dechlorination catalyzed by Pt–Sn/SiO2 catalysts of different preparations. *Journal of Catalysis* **2005,** *230* (1), 86-97.

45. Rhodes, W.; Lazar, K.; Kovalchuk, V.; Ditri, J., Hydrogen-Assisted 1,2-Dichloroethane Dechlorination Catalyzed by Pt–Sn/SiO: Effect of the Pt/Sn Atomic Ratio. *Journal of Catalysis* **2002,** *211* (1), 173-182.

46. Śrębowata, A.; Juszczyk, W.; Kaszkur, Z.; Sobczak, J. W.; Kępiński, L.; Karpiński, Z., Hydrodechlorination of 1,2-dichloroethane and dichlorodifluoromethane over Ni/C catalysts: The effect of catalyst carbiding. *Applied Catalysis A: General* **2007,** *319*, 181-192.

47. Juszczyk, W.; Colmenares, J. C.; Śrębowata, A.; Karpiński, Z., The effect of copper and gold on the catalytic behavior of nickel/alumina catalysts in hydrogen-assisted dechlorination of 1,2-dichloroethane. *Catalysis Today* **2011,** *169* (1), 186-191.

48. Bylaska, E. J.; Dupuis, M.; Tratnyek, P. G., One-electron-transfer reactions of polychlorinated ethylenes: concerted and stepwise cleavages. *The Journal of Physical Chemistry. A* **2008,** *112* (16), 3712-21.

49. Weckhuysen, B. M., Determining the active site in a catalytic process: Operando spectroscopy is more than a buzzword. *Phys Chem Chem Phys* **2003,** *5* (20), 4351-4360.

50. Namduri, H.; Nasrazadani, S., Quantitative analysis of iron oxides using Fourier transform infrared spectrophotometry. *Corros Sci* **2008,** *50* (9), 2493-2497.

51. Feijen-Jeurissen, M. M. R.; Jorna, J. J.; Nieuwenhuys, B. E.; Sinquin, G.; Petit, C.; Hindermann, J.-P., Mechanism of catalytic destruction of 1,2-dichloroethane and trichloroethylene over γ-Al2O3 and γ-Al2O3 supported chromium and palladium catalysts. *Catalysis Today* **1999,** *54* (1), 65-79.

52. Chintawar, P. S.; Greene, H. L., Adsorption and catalytic destruction of trichloroethylene in hydrophobic zeolites. *Applied Catalysis B: Environmental* **1997,** *14* (1-2), 37-47.

53. Scaranto, J.; Giorgianni, S., Adsorption of difluoromethane on titanium dioxide: Investigation of the FTIR spectra and quantum-mechanical studies of the adsorbate–substrate structures. *Spectrochimica Acta Part A: Molecular and Biomolecular Spectroscopy* **2009,** *74* (5), 1072-1076.

54. (a) Scaranto, J.; Charmet, A. P.; Stoppa, P.; Giorgianni, S., Vinyl halides adsorbed on TiO2 surface: FTIR spectroscopy studies and ab initio calculations. *Journal of Molecular Structure* **2005,** *741* (1-3), 213-219; (b) Scaranto, J.; Mallia, G.; Giorgianni, S.; Zicovich-Wilson, C. M.; Civalleri, B.; Harrison, N. M., A quantum-mechanical study of the vinyl fluoride adsorbed on the rutile TiO2 surface. *Surface Science* **2006,** *600* (2), 305-317.

55. Scaranto, J.; Giorgianni, S., Adsorbate–substrate interaction between chlorodifluoromethane and titanium dioxide: Infrared spectroscopy and density functional theory studies. *Vibrational Spectroscopy* **2011,** *56* (2), 161-165.

56. Adib, K.; Camillone, N.; Fitts, J. P.; Rim, K. T.; Flynn, G. W.; Joyce, S. A.; Osgood, R. M., CCl4 chemistry on the magnetite selvedge of single-crystal hematite: competitive surface reactions. *Surface Science* **2002,** *497* (1-3), 127-138.

57. Adib, K.; Mullins, D. R.; Totir, G.; Camillone, N.; Fitts, J. P.; Rim, K. T.; Flynn, G. W.; Osgood, R. M., Dissociative adsorption of CCl4 on the Fe3O4(111)-(2 x 2) selvedge of alpha-Fe2O3(0001). *Surface Science* **2003,** *524* (1-3), 113-128.

58. Parkinson, G. S.; Dohnálek, Z.; Smith, R. S.; Kay, B. D., Reactivity of Fe0 Atoms, Clusters, and Nanoparticles with CCl4 Multilayers on FeO(111). *The Journal of Physical Chemistry C* **2009,** *113* (5), 1818-1829.

59. Rim, K. T.; Muller, T.; Fitts, J. P.; Adib, K.; Camillone, N.; Osgood, R. M.; Batista, E. R.; Friesner, R. A.; Berne, B. J.; Joyce, S. A.; Flynn, G. W., STM study of competitive surface reactions in the dissociative chemisorption of CCl4 on iron oxide surfaces. *Abstr Pap Am Chem S* **2003,** *226*, U381-U381.

60. Kim, H. S.; Ahn, J. Y.; Hwang, K. Y.; Kim, I. K.; Hwang, I., Atmospherically Stable Nanoscale Zero-Valent Iron Particles Formed under Controlled Air Contact: Characteristics and Reactivity. *Environmental Science & Technology* **2010,** *44* (5), 1760-1766.

61. Martin, J. E.; Herzing, A. A.; Yan, W. L.; Li, X. Q.; Koel, B. E.; Kiely, C. J.; Zhang, W. X., Determination of the oxide layer thickness in core-shell zerovalent iron nanoparticles. *Langmuir* **2008,** *24* (8), 4329-4334.

62. Adamescu, A.; Hamilton, I. P.; Al-Abadleh, H. A., Density Functional Theory Calculations on the Complexation of p-Arsanilic Acid with Hydrated Iron Oxide Clusters: Structures, Reaction Energies, and Transition States. *The Journal of Physical Chemistry A* **2014,** *118* (30), 5667-5679.

63. Kubicki, J. D.; Paul, K. W.; Kabalan, L.; Zhu, Q.; Mrozik, M. K.; Aryanpour, M.; Pierre-Louis, A.-M.; Strongin, D. R., ATR–FTIR and Density Functional Theory Study of the Structures, Energetics, and Vibrational Spectra of Phosphate Adsorbed onto Goethite. *Langmuir* **2012,** *28* (41), 14573-14587.

64. Loring, J. S.; Sandstrom, M. H.; Noren, K.; Persson, P., Rethinking Arsenate Coordination at the Surface of Goethite. *Chem-Eur J* **2009,** *15* (20), 5063-5072.

65. Chabot, M.; Hoang, T.; Al-Abadleh, H. A., ATR-FTIR Studies on the Nature of Surface Complexes and Desorption Efficiency of p-Arsanilic Acid on Iron (Oxyhydr)oxides. *Environmental Science & Technology* **2009,** *43* (9), 3142-3147.

66. Adamescu, A.; Hamilton, I. P.; Al-Abadleh, H. A., Thermodynamics of Dimethylarsinic Acid and Arsenate Interactions with Hydrated Iron-(Oxyhydr)oxide Clusters: DFT Calculations. *Environmental Science & Technology* **2011,** *45* (24), 10438-10444.

67. 1. Tofan-Lazar, J.; Al-Abadleh, H. A., Kinetic ATR-FTIR Studies on Phosphate Adsorption on Iron (Oxyhydr)oxides in the Absence and Presence of Surface Arsenic: Molecular-Level Insights into the Ligand Exchange Mechanism. *The Journal of Physical Chemistry A* **2012,** *116* (41), 10143-10149.

Chapter 3

3. Results and discussion

3.1 Introduction

Industrialization has had a heavy impact on the natural environment, including groundwater resources.[1] As an example many groundwater sources are now impacted by chlorinated hydrocarbons, serving as a long term source of contamination.[2] A number of remediation technologies have been developed to clean up chlorinated hydrocarbon impacted sites however they are not typically able to clean up contaminated sites to the desired extent. Nano zero valent iron (nZVI) particles is one promising technology with the ability to degrade a wide range of halogenated hydrocarbons.[1] For example nZVI particles have been proven to successfully dechlorinate contaminants such as tretrachloroethylene (PCE), trichloroethylene (TCE), and other polychlorinated hydrocarbons.[1,4] Given their size, nanoparticles can be injected into the subsurface to target source zone contaminants.[3] Regardless of these promising results, some chlorinated hydrocarbons (e.g., 1,2-Dichloroethane or 1,2-DCA) still remain recalcitrant to dechlorination by nZVI .[5] 1,2-Dichloroethane is categorized as a priority contaminant by the US EPA.

NZVI particles have been doped with noble metals (Pd, Pt) as catalysts to enhance dechlorination rates.[1] These metals not only increase reaction rates but also decrease the amount of lower chlorinated by-products such as vinyl chloride, which can be more toxic that the parent compounds.[1] Despite all the research that has been conducted to comprehend the fundamental mechanisms of the dechlorination process over iron surfaces, there is still a gap in the understanding of these processes at the molecular level. Dechlorination of TCE by nZVI has been proposed to take place through two main reaction mechanisms: hydrogenolysis and β-elimination.[6] Selectivity towards either of these reaction pathways is influenced by the synthesis method,[31,35] and particle size (e.g. micro, nano) of the iron nanoparticles. [34,61] At this point in time it is widely acknowledged that the dechlorination process is a surface mediated reaction.[6] Therefore, the role of the surface layer composition (e.g., iron oxides) on the surface reaction processes that occur during dechlorination over nZVI particles needs to be better understood.

Common techniques utilized for characterization of nZVI nanoparticles include, scanning electron microscopy (SEM), transmission electron microscopy (TEM), X-ray diffraction (XRD), and X-ray photoelectron spectroscopy (XPS).[2] Using some of these techniques, Liu and collaborators reported a surface composition of micro zero valent iron particles of 85% goethite (α-FeOOH) and 12% maghemite (γ-Fe_2O_e).[39] Later, Lien and collaborators observed maghemite (γ-Fe_2O_3), magnetite (Fe_3O_4), hematite (α-Fe_2O_3), and lepidocrocite (γ-FeOOH) by means of XRD in the surface of Pd-nZVI dried nanoparticles.[27] Although the importance of the surface composition and morphology is recognized, the sensitiveness of nZVI particles to oxygen and the inability to conduct some of these characterization experiments in an anoxic environment have prevented the development of a clear model for the surface composition of nZVI. Thus, attempts to understand the role of the surface species in the adsorption/reaction events involved in dechlorination have yet to result in a sound and comprehensive understanding of the governing mechanisms of these dechlorination processes. Reaction mechanisms proposed in the literature are based on batch kinetic experiments. These hypothesize that the reaction of vinyl halides with ZVI takes place through a di-σ- surface bonded intermediary. Nevertheless the same studies acknowledge the lack of direct evidence for this surface intermediary.[6] Hence, a detailed investigation of the surface composition of the nZVI particles, and the elucidation of the role of these surface species in the adsorption/reaction mechanisms of dechlorination is necessary. A complete understanding of these surface mechanisms, and identification of the prevalent surface reaction sites that govern the adsorption/reaction processes will allow the selective surface modification of these nanoparticles, resulting in an enhancement of the dechlorination capacity of the nZVI nanoparticles towards groundwater pollutants.

The work reported in this thesis relies on the use of in situ techniques to address the outlined above challenges that previous researchers have faced when investigating the surface interactions taking place between 1,2-DCA or TCE and the iron bearing surfaces. In situ techniques provide great advantages for the study of ambient sensitive surfaces, such as nZVI. Also, a controlled level of interaction between the solid surface and the chlorinated molecules can be achieved by this experimental set up. Spectroscopic experiments were carried out using in situ diffuse reflectance Fourier transform infrared spectroscopy (DRIFTS) and in situ diffuse reflectance UV-Vis. The use

of DRIFTS provides critical information on the formation, breaking and rearrangement of molecular bonds in both the solid iron surface and the chlorinated molecule, that result from surface interaction phenomena such adsorption or reaction. In situ UV-Vis on the other hand, probes the electronic structure and coordination environment of the atoms in the surface and monitors electronic changes that occur during surface interaction (oxidation, reduction or ligand field rearrangements). The identification of reaction products resulting from this interaction was carried out using temperature program desorption/reaction (TPD, TPR), a technique broadly used for the study of phenomena occurring in the solid/gas interface.[28]. All this information combined provides a distinct depiction of the surface sites active for adsorption and/or dechlorination, their reactivity and selectivity, and offers insights on the possible mechanisms of dechlorination over these iron bearing surfaces.

3.2 Materials

Nano maghemite (α–Fe_2O_3) was purchased from Sigma Aldrich (particle size < 50 nm and surface area between 50 – 254 m^2/g as per manufacturer specifications). For the synthesis of magnetite (Fe_3O_4), Iron (II) chloride tetrahydrate 98% purity, iron (III) hexahydrate ACS 97% purity, and NaOH pearls 97% purity were purchased from Alfa Aesar. For nZVI particle synthesis Sodium Borohydride 98%, K_2PdCl_6 99% (both from ACROS Organics) and $FeSO_4.7H_2O$ 99% (A.C.S. Reagent from Sigma Aldrich) were used. For the Spectroscopic experiments A.C.S. 99.5% purity TCE (Chromasolv for HPLC 99.8%) and Spectrophotometric grade 1,2-DCA (99% purity), both from Sigma Aldrich, were used. KBr (Fluka analytical for IR from Sigma Aldrich) was used as reference for the IR experiments. Anhydrous Sodium Carbonate 99.5% from CALEDON chemicals was utilized in the synthesis of goethite.

For TPR and TPD experiments compressed gases mixtures were purchased, 500 ppm of 1,2-DCA balanced in Helium, and 2000 psi in He together with 204 ppm of TCE balanced in Helium (all from Air liquid). Also ultra-high purity helium, air and nitrogen from Praxair where utilized as gas carrier, for surface clean up and to remove moisture from the FTIR instrument, respectively.

3.3 Preparation of iron oxide surfaces

3.3.1 Magnetite (Fe_3O_4)

Magnetite nanoparticles were synthesized by co-precipitation of 1M $FeCl_2.4H_2O$ and 2M $FeCl_3.6H_2O$ in a basic solution (1M NaOH), as described by the following equation:[7]

$$2Fe^{3+} + Fe^{2+} + 4OH^- \rightarrow Fe_3O_4 + 4H^+$$

The synthesis procedure was performed in anaerobic conditions, utilizing a vinyl anaerobic chamber from COY laboratory products. The required solutions were prepared using deionized water that was purged with N_2. The iron solutions where mixed using a magnetic stirrer and the temperature was raised to 30 ^oC. After the precursor solutions were homogenized and reached a stable temperature, NaOH was added drop wise. The pH was monitored until pH 12 was reached and maintained, this was done using a Hach 160 pH meter, equipped with a non-glass ISFET probe. Once the pH stabilized, the temperature was raised to 70 ^oC and maintained for 2 hours. pH was monitored every 5 minutes during this period. Once the magnetite particles were formed they were removed from solution using a permanent magnet, this step was followed by a thorough wash with deoxygenated water, until pH reached a neutral value. Finally the magnetite nanoparticles were left to dry in a vacuum desiccator.[8]

3.3.2 Hematite (α-Fe_2O_3)

Hematite was prepared by thermal phase transformation of maghemite (γ-Fe_2O_3). The synthesis was performed in a quartz glass tubular reactor with a porous bed quartz frit. Thermal decomposition was achieved at 500 ^oC for 5 hrs under a Helium flow (10 mL/min) with an initial temperature ramp of 10^oC/min.[9]

3.3.3 Goethite (α-FeOOH)

Goethite was produced by double precipitation. A 0.1 M solution of Iron (II) Sulfate in deoxygenated water was placed in a Buchner flask with a continuous bubbling flow of N_2 and stirred at 40 ^oC. This was followed by addition of 0.1 M NaOH to a final Fe:OH ratio of 0.1. A pH of approximately 7.9 is achieved at this step. Immediately after addition of the NaOH solution the

N_2 flow is replaced by air at a 100 ml/min flowrate. The pH is monitored until it stabilizes at a value of ≈ 3.5; this is followed by addition of a 1M $NaCO_3$ to increase the pH to ≈ 9.2. After the desired pH was achieved the reaction was aged for 4 hours with constant stirring and air bubbling. Once the reaction has finished the product was separated by vacuum filtration followed by rinsing in deionized water. The final product was dried under vacuum in a desiccator.[10]

3.3.4 Palladium doping

Pd doped goethite, magnetite, maghemite and hematite nanoparticles were prepared by adding as stabilized K_2PdCl_6 solution in 0.2 g/L NaCl to a deionized water suspension of the solid nanoparticles. The target Pd loading was 0.1% wt.

3.3.5 Characterization

Characterization of the synthesised goethite, hematite and magnetite was carried by means of X-ray diffraction (XRD) and UV-Vis spectroscopy. XRD characterization was carried utilizing a Rigaku rotating-anode X-ray diffractometer with a Co source and measuring Kα (λ = 1.7889 Å) radiation, with a 0.02º step size, in the 2θ range between 10º and 70º, the XRD patterns are depicted in Cu Kα (λ = 1.54059 Å) radiation. UV-vis characterization was carried in a Shimadzu 3600 UV-Vis-NIR spectrophotometer, measurements were performed in diffuse reflectance mode with a Praying Mantis accessory from Harrick Scientific, with a 2 mm slit opening, a scan range from 200 to 800 nm and a background of polytetrafluoroethylene. BET surface areas were measured using a surface area pore analyzer (TriStar II 3020 BET from Micromeritics), samples were pretreated by degassing of the sample at 150 ºC for 6 hours.

3.3.6 Zero valent iron nanoparticles

Bare nanoparticles of zero valent iron were synthesised by reduction of iron sulphate ($FeSO_4.7H_2O$) with sodium borohydride ($NaBH_4$).[11] The synthesis was conducted in an anaerobic chamber. Deionized water was deoxygenated by means of N_2 bubbling for a period of 1 hour. 0.28 M $FeSO_4.7H_2O$ was mixed continuously with a propeller mixer. After the iron salt was completely dissolved 0.56 M $NaBH_4$ was added in a drop wise manner to obtain the reduced iron nanoparticles.

Following $NaBH_4$ addition the synthesised nanoparticles were vigorously mixed for a period of 20 minutes. After mixing, the particles were washed with deoxygenated water to remove excess $NaBH_4$ and sulfates from solution. Separation of the nanoparticles was performed by means of a permanent magnet. The nanoparticles were then dried in a vacuum desiccator that remained inside the anaerobic chamber.

For the formation of Pd doped nZVI particles, the Pd precursor (K_2PdCl_6) was dissolved in 0.2 g/L NaCl. This was performed prior to its addition to the nZVI slurry. The solution was then added to the nZVI solution and mixed for 10 minutes, followed by the previously described rinsing, separation and drying protocol for Pd-free nZVI.

3.4 Spectroscopic experiments

3.4.1 In situ Diffuse Reflectance Fourier Transform Infrared spectroscopy

FTIR spectroscopy was used to probe the surface interaction of the chlorinated compounds with the different iron bearing surfaces. A FTIR spectrophotometer from Bruker (Vertex 70) was used. The system is equipped with a liquid nitrogen cooled MCT detector, and an external Silicon Carbide globar source. In order to perform the in situ experiments a diffuse reflectance accessory was utilized, (Praying Mantis DRIFTS Harrick Scientific, and a Praying Mantis) equipped with a high temperature reaction chamber and KBr windows. Acquisition parameters during the experiments included a spectral resolution of 4 cm^{-1}, a slit aperture of 8 mm, 254 sample scans and a scan range from 4000 to 450 cm^{-1}.

The experimental procedure required the pre-treatment of the surfaces to desorb moisture from the iron bearing surfaces. Pre-treatment was performed in He flow at 45 sccm and at 140 ^oC for 1.5 hrs, with an initial temperature ramp of 10 ^oC/min. Since goethite can undergo a phase transformation at low temperatures (≈180 ^oC),[13] pre-treatment for this phase was carried at 110 ^oC. A spectra was obtained before and after the pre-treatment to confirm the removal of moisture and sample stability (no phase transformation). These measurements were obtained using KBr as a background and with N_2 flow in the DRIFTS chamber to displace ambient moisture and CO_2 that

can interfere with measurements. Fig. 3.1 shows a process flow diagram of the experimental set up for the in situ spectroscopic analysis.

Once the pre-treatment was completed, the clean surface is utilized as spectroscopic background throughout the adsorption experiments. In situ adsorption experiments were performed by injection of the pure liquid contaminant (1,2-DCA or TCE) with a KD scientific infusion syringe pump (model KDS 100) at 1 mL/hr to a 45 sccm He carrier gas flow. The injection port and gas lines were heated to 90 ^{o}C to avoid condensation of the chlorinated hydrocarbons. Injection was performed for approximately 30 minutes, until chamber saturation is observed using the chlorinated hydrocarbon gas phase IR bands. Once saturation was reached, injection of the chlorinated compound was stopped, and the system was flushed with He to remove the gas phase and physisorbed TCE or 1,2-DCA. As the flushing was performed acquisition of IR spectra was performed in 5 minutes intervals until gas phase vibrational frequency bands were no longer observed.

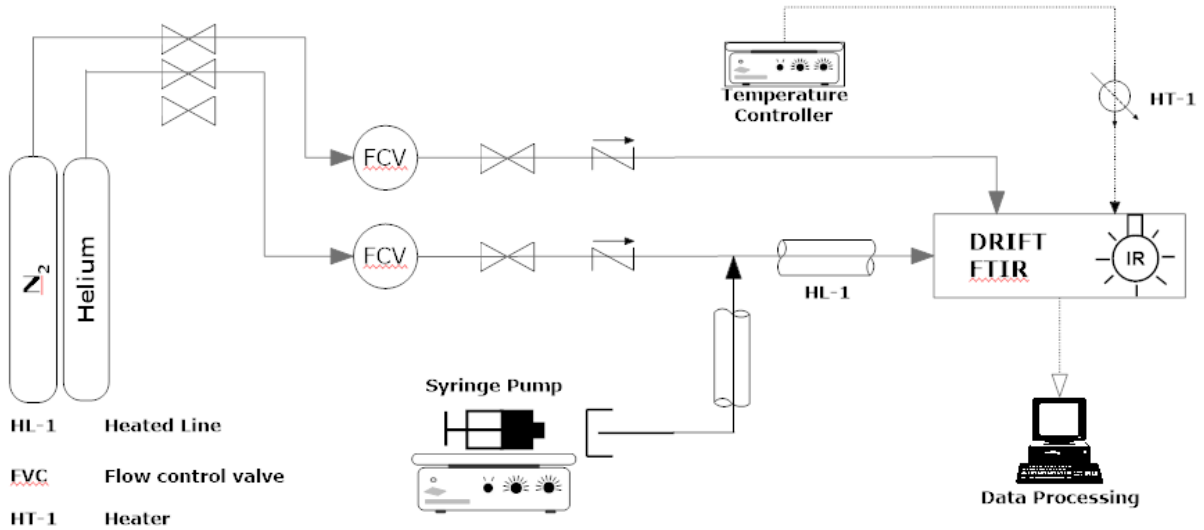

Figure 3.1. Process flow diagram of In-situ Spectroscopy experimental set up.

3.4.2 In situ Diffuse Reflectance UV-Vis spectroscopy

UV-Vis spectroscopy was utilized to monitor possible changes in the electronic structure of the iron-bearing surfaces as they interacted with the target contaminants. For these experiments a Shimadzu 3600 UV-Vis-NIR spectrophotometer was used. The system is equipped with both tungsten and deuterium arc lamp sources. The spectrophotometer contains a photomultiplier tube as well as InGaAs and cooled PbS detectors. To perform the in situ experiments a Praying Mantis DRIFTS accessory from Harrick Scientific, and a Praying Mantis high temperature reaction chamber with quartz windows was utilized. Experiments were conducted at medium scan velocity; with a 2 mm slit opening and a scan range from 200 to 800 nm. Polytetrafluoroethylene was utilized as background in all the measurements.

Sample pre-treatment was performed under similar conditions as in the DRIFTS experiments. A UV-Vis spectrum was obtained before and after the pre-treatment, to ensure no phase transformation occurred during the dehydration of the surface. Injection of the target contaminant was performed under similar conditions as the DRIFTS experiments. Acquisition of UV-Vis spectra was performed in intervals of 5 minutes during TCE or 1,2 DCA injection, as well as during flushing of the contaminant from the reaction chamber using helium.

Spectroscopic experiments were conducted for all iron surfaces, although nZVI and Fe_3O_4 resulted in poor quality spectra due to strong absorption of infrared energy by the sample.

3.5 Temperature Program Experiments

3.5.1 Temperature Program Desorption

Desorption and evolution of surface chemisorbed species was monitored by means of temperature program desorption (TPD). The system consisted of a Temperature control EZ-ZONE PM by Watlow Electronic and a custom made Bluewater Heater furnace and heating system. The desorption products were analyzed using two different systems; an Agilent 7890A GC with Agilent 5975C MS, G3462A flame ionization detector (FID) with an electronic pneumatic control (EPC) and a G3432A thermal conductivity detector (TCD) with EPC. The second system was an Agilent 7890A GC with a G2397AD electron capture detector (μECD) with EPC. Experimental conditions for the pre-treatment of the sample involved the removal of ambient adsorbed moisture by thermal treatment at 140 ^{o}C for a period of 1.5 hours and an initial temperature ramp of 10 ^{o}C/min. Similar to the spectroscopic measurements, goethite samples were pretreated at 110 ^{o}C to avoid phase transformation.

Saturation of the surface was achieved by flowing 45 sccm of 200 ppm TCE with helium as balance. In the case of 1,2-DCA the tank concentration was 500 ppm. Saturation periods of 1 hour and 30 minutes were allowed for TCE and 1,2-DCA respectively. Surface saturation was performed at 100 ^{o}C. After the saturation period the gas flow was switched to pure helium to remove physisorbed contaminant. Desorption was monitored by means of an μECD detector for TCE and with an FID for 1,2-DCA. Once a stable baseline was achieved the temperature program ramp was initiated. The experimental temperature program consisted of a 10 ^{o}C/min ramp from the saturation temperature (100 ^{o}C) to 500 ^{o}C. The stream containing the desorbed gases was sent to the GC with TCE desorption products separated with a 75 m x 450 μm x 2.55 μm BD-624 capillary column with N_2 as carrier gas. Isothermal separation was conducted at 150 ^{o}C for 3.5 min in splitless mode. Samples were collected at 4 minute intervals through the built in six port valve with a 250 μL sampling loop which was kept at 110 ^{o}C. In order to identify unknown peaks observed in the TPD profiles, the TPD experiments were repeated using the EPA extended analyte method 8021.

In the TPD experiments that were conducted with 1,2-DCA a 60 m x 250 µm x 0.25 µm DB-17–MS capillary column was used with Helium as carrier and N_2 as make up gas. The separation method was performed in isothermal conditions at 85 ^oC. Sampling was performed through the GC six port valve with a 500 µL sampling loop. Samples were collected every 1.5 minutes and injected continuously for separation to the ongoing isothermal ramp. Desorption products were analysed through the FID, TCD detectors; desorption products were identified by means of the MS detector.

3.5.2 Temperature Program Reaction

TPR experiments involved a constant flow of 45 sccm of 500 ppm 1,2-DCA gas balanced in helium through the sample while a 10 ^oC/min ramp was applied from 50 ^oC to 500 ^oC. Sample pretreatment was performed following the same protocol used for the TPD experiments. The analytical procedures for analysis of the gas stream are the same as the previously described GC-MS-TCD-FID method for 1,2-DCA TPD experiments. In Fig.3.2 is a process flow diagram for the experimental set up utilized for the TPD and TPR analysis.

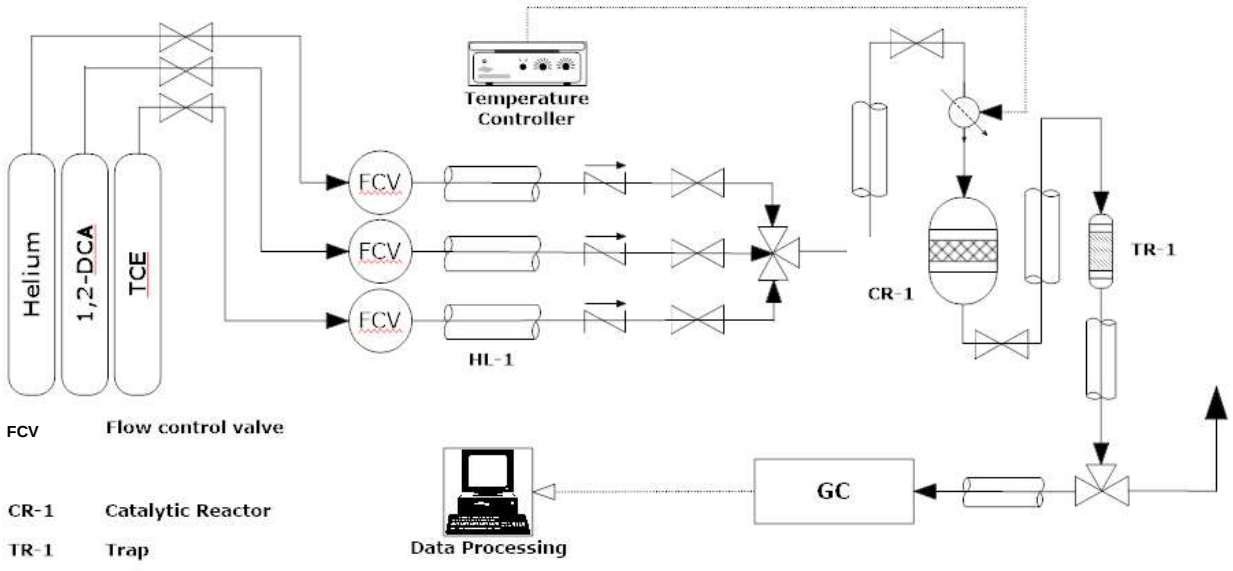

Figure 3.2. TPD -TPR Process Flow Diagram

3.6 Results and discussion

In order to understand the surface mechanisms that govern the interaction between 1,2-DCA, or TCE, and the nZVI surface, it is important to understand the adsorption and reaction mechanisms of these contaminants with different iron species present at the nZVI surface. Figure 3.3 shows the IR spectra of TCE and 1,2-DCA adsorbed on goethite (α-FeOOH). Since the bare surface spectrum is used as background during spectra acquisition, bands appearing as peaks correspond to surface species that are being consumed after adsorption, and bands appearing as valleys correspond to vibrational modes of newly formed surface species. Spectral changes are observed in terms of changes in peak intensity, changes in peak position (shifts), and changes in peak width. Changes in peak intensity are related to changes in concentration of adsorbed species. Interpretation of changes in peak position are linked to variations in the bond strength of specific chemical bonds, and changes in peak widths are related to the distribution of the chemical environment of the adsorbed surface species. Infrared spectra interpretation was carried by analysing the 3800 to 3400 cm^{-1} and 1700 to 1000 cm^{-1} regions. The region from 3800 to 3400 cm^{-1} depicts the area for hydroxyl stretchings (O-H). The negative peaks observed in the higher energy region (3690-3700 cm^{-1}) are attributed to loses of isolated hydroxyl groups that were initially present on the goethite surface (i.e., before TCE or 1,2-DCA adsorption). At the same time that these isolated OH groups are consumed, the appearance of a broader band in the region of 3600-3690 cm^{-1} takes place, and is attributed to H bonded hydroxyl groups[14] between TCE or DCA and the iron oxide surface basic Lewis sites (O^{2-} and/or OH^{-}). The formation of a broader band in this area was also reported by Scaranto and collaborators when adsorption of vinyl halides over TiO_2 was probed by FTIR spectroscopy.[15] The difference in the maximum intensity value for the peaks corresponding to the isolated OH groups in the 3690-3700 cm^{-1} region for TCE and 1,2-DCA suggests that TCE interacts more strongly than 1,2-DCA with the isolated OH groups present on the surface. This difference in the observed interaction phenomenon is summarized in Table.3.1, where the vibrational frequencies observed after adsorption of TCE on most of the tested materials such as γ-Fe_2O_3, α-Fe_2O_3, and α-FeOOH are shown. Disappearance of surface hydroxyl groups suggest that the interaction of both TCE and 1,2-DCA with iron oxide surfaces is strongly linked to the presence of isolated hydroxyl groups present on the iron oxide surfaces.

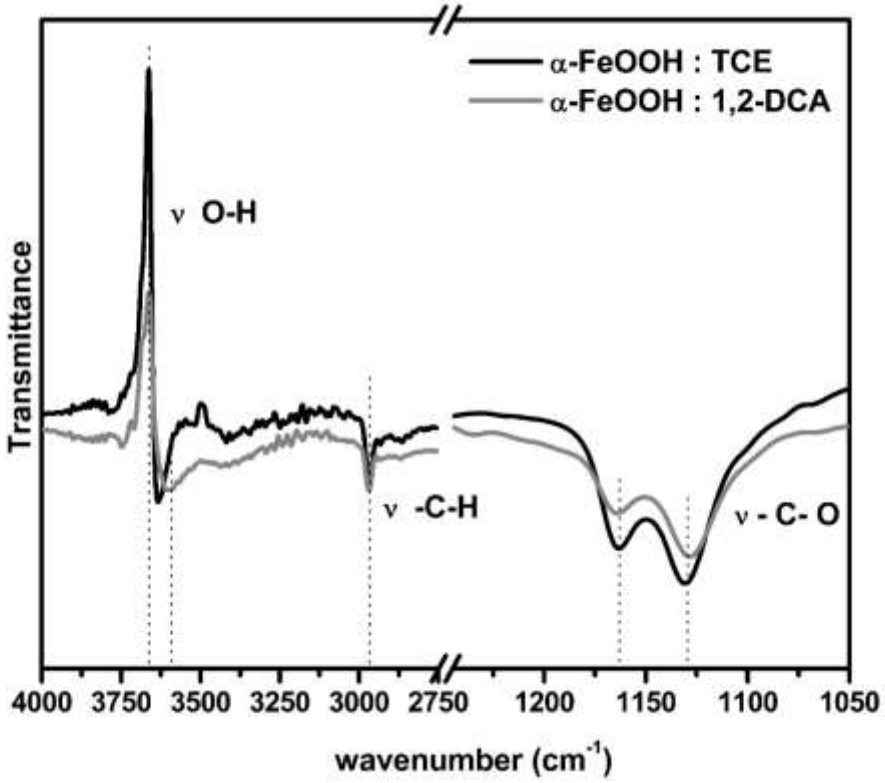

Figure 3.3. Spectra of adsorbed 1,2-DCA (grey) and TCE (black), over α-FeOOH (goethite).

The second peak observed in Fig.3.3 appears in the 1300 to 1000 cm^{-1}range. This is the region of C-O stretching for a single carbon oxygen bond.[18] The presence of a carbon oxygen bond at the surface and the position of the band strongly suggest the formation of surface ethoxide species (Fe^{+} OCH_2CH_3).[19] This type of interaction has been previously reported by Dubicki and collaborators when they studied the structural modification of dichloromethoxy chromium species by means of UV and IR spectroscopy. [18] Kakos and Winter also reported this phenomena for Titanium (IV) ethoxide (TiO CH_2CH_3) when studying its structure.[54] The formation of this ethoxide like species was observed in all iron oxides samples tested for TCE (Fig .3.4, table.3.1) and for 1,2-DCA (results not shown).

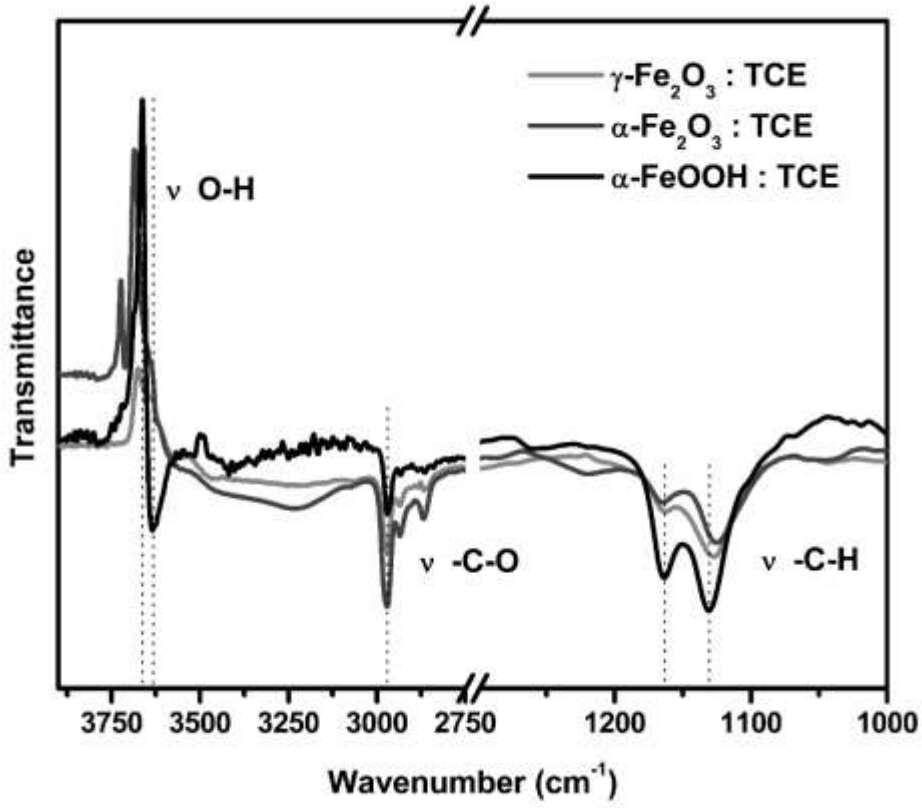

Figure 3.4. Spectra of adsorbed TCE over γ-Fe_2O_3 (light grey), α-Fe_2O_3 (dark grey) and α-FeOOH (black).

For the case of the 3000cm^{-1} region in Fig.3.4, unsaturated hydrocarbons (C=C bearing compounds) have a stretching vibration corresponding to the C-H stretching in the region of 3020-3100 cm^{-1}. This vibration is observed in gaseous TCE at 3100 cm^{-1}.[60] As TCE adsorption takes place over all the iron species tested, a red shift (shift to lower energies) of this peak to 2980-2860 cm^{-1} suggests the formation of a saturated aliphatic C-C bond. This shift in the C-H stretching band is also observed for the case of 1,2-DCA adsorption. The formation of the saturated surface intermediary when TCE is adsorbed is further confirmed by the disappearance of the C=C band at 1595 cm^{-1} (table 3.1). These observations are additional evidence for the formation of a surface ethoxide group during TCE and 1,2-DCA adsorption.

Table3.1 Vibrational frequencies of TCE in gas-phase and adsorbed on γ-Fe_2O_3, α-Fe_2O_3, and α-FeOOH at room temperature.

***TCE ; $ClCH=CCl_2$ (gas)**					**TCE/α-FeOOH**	**TCE/γ-Fe_2O_3**	**TCE/α-Fe_2O_3**
Vibration	Approx. Description	Wavenumber (cm^{-1})	Vibration	Approx. description	Wavenumber (cm^{-1})	Wavenumber (cm^{-1})	Wavenumber (cm^{-1})
ν_1	=C-H	3101	ν_1	-C-H	-2970	-2970	-2969
ν_2	C=C	1595	ν_2	O-H	+3662	+3676	+3723
ν_3	C=C	1586	ν_3	O-H	-3634	-	+3685
δ_1	=C-H	1254	ν_4	C=C	-	-	-
ν_4	C-Cl	944	ν_5	-C-O	-1164	-1163	-1164
δ_1	C-H	848	ν_6	-C-O	-1130	-1126	-1125
			ν_7	C-Cl	inconclusive	-933	-933

* Assignation based from Ref.[63]

\- Bands that appear as valleys

\+ Bands that appear as peaks

Adsorption of TCE and 1,2-DCA thus appears to take place under similar mechanisms, resulting in a common surface intermediary over all the iron oxide/oxyhydroxides. The proposed surface adsorbed intermediary is shown in Scheme 3.1. The bond configuration presented in this scheme summarizes the spectroscopic observations presented on table 3.1. The depicted model proposes adsorption of the chlorinated molecule through the interaction of the surface hydroxyl group and the π (C=C) system. This interaction results in the formation of the C-O bond observed in the FTIR experimental results. The proposed adsorbed intermediary is in agreement with the spectroscopic observations of the elongation of the C-H bond and the C-Cl bond. These results indicate that the adsorption of TCE and 1,2-DCA is strongly linked to interaction of the adsorbate with the surface hydroxyl groups present on iron oxide and the concomitant formation of ethoxide moieties between the chlorinated hydrocarbon and the solid substrate. Thus the surface termination (e.g., distribution of surface hydroxyl groups) which in turn is affected by the crystalline structure of the iron oxides, might play a critical role in the adsorption mechanism. The thermodynamic stability

and surface termination of the different iron species has been in fact widely investigated,[55,56] also its effect in surface reactivity has been previously reported. For instance, reactivity towards carbon tetrachloride is dependent of the iron oxide surface termination: fully oxidized hematite (α-Fe_2O_3) show nearly no reactivity, in contrast magnetite (Fe_3O_4) terminated crystals rapidly adsorb CCl_4. This was explained in terms of surface termination with vertically oriented oxygen atoms readily adsorbing CCl_4. These vertically oriented oxygen moieties are present in magnetite and not in hematite.[20] Reports of differences in reactivity due to differences in crystalline structure of phases with the same oxidation state (e.g., hematite and maghemite) are limited, however an attempt to provide some insight in this regard was done by Al-Baitai and collaborators through computational modeling. Their results suggest a higher surface instability of the maghemite hydrated surface when compared to hydrated hematite. These phenomena were rationalized by means of the difference in the surface energy which decreased as hydration by dissociated water molecules increase the surface iron oxygen coordination. The stability of the hydroxylated surface is greater in the hematite surface when compared to maghemite.[21] These observations provide great insight into the importance and effect that crystalline structure has in adsorption, and the role of surface termination in the reactivity of iron oxide species.

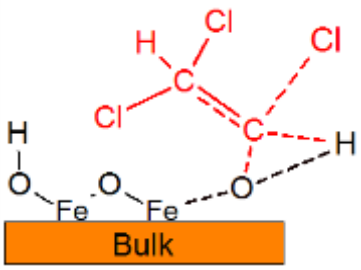

Scheme 3.1. TCE and 1,2-DCA proposed surface adsorbed intermediary formed over iron bearing nanoparticles.

Impact of the crystalline structure in the adsorption process of TCE and 1,2-DCA was investigated by comparing experimental results from α-Fe_2O_3 and γ-Fe_2O_3. Fig. 3.4 shows the FTIR spectra of adsorbed TCE over α-Fe_2O_3 and γ-Fe_2O_3. Bands in the 3400-3800 cm^{-1} region show the interaction of TCE with the surface hydroxyl groups. The adsorption bands for α-Fe_2O_3 and γ-Fe_2O_3 in this region have different intensities. There are also two distinctive peaks at 3724 and 3687 cm^{-1} for α-

Fe_2O_3 and a single band at 3675 cm^{-1} for γ-Fe_2O_3. As discussed in section 2.2.3 α-Fe_2O_3 and γ-Fe_2O_3 are isoelectronic differing mainly in their crystalline structure. Since both materials have similar surface areas (31.4m^2/g for α-Fe_2O_3 and 33.2 m^2/g for γ-Fe_2O_3), the difference in the intensity of the infrared bands in the OH region can be linked to differences in crystalline structure. In contrast, when comparing TCE interaction with α-FeOOH, the spectrum in the OH region shows an intense band suggesting that a stronger interaction takes place in this case, in comparison with α-Fe_2O_3 and γ-Fe_2O_3. This difference in the interaction strength towards OH groups can be hypothesized in terms of the heterogeneity of the surface distribution, accessibility and the quantity of hydroxyl groups that exist within the different iron oxide species.

The surface distribution and strength of OH groups that are able to function as Brønsted acid sites, and other surface active sites available that are suitable for adsorption process, have been previously studied on hematite by means of probe molecules like pyridine, CO and CO_2. These studies have shown a heterogeneous distribution of surface reactive sites. Studies using pyridine and 2,6-dimethyl-pyridine pointed to the presence of sterically unavailable Brønsted acid sites. Adsorption of carbon monoxide demonstrated the existence of non-equivalent Lewis acid sites. Further experiments with CO_2 adsorption indicated the existence of a highly hydroxylated hematite surface.[14] Therefore the degree of hydroxylation, their steric availability and site strength are important factors regulating the surface adsorption/reaction mechanisms. The existence of these non-equivalent adsorption sites, and the heterogeneity in the surface hydroxylation between the different iron species, could explain the difference in adsorption strength of TCE and 1,2-DCA with the different iron bearing surfaces.

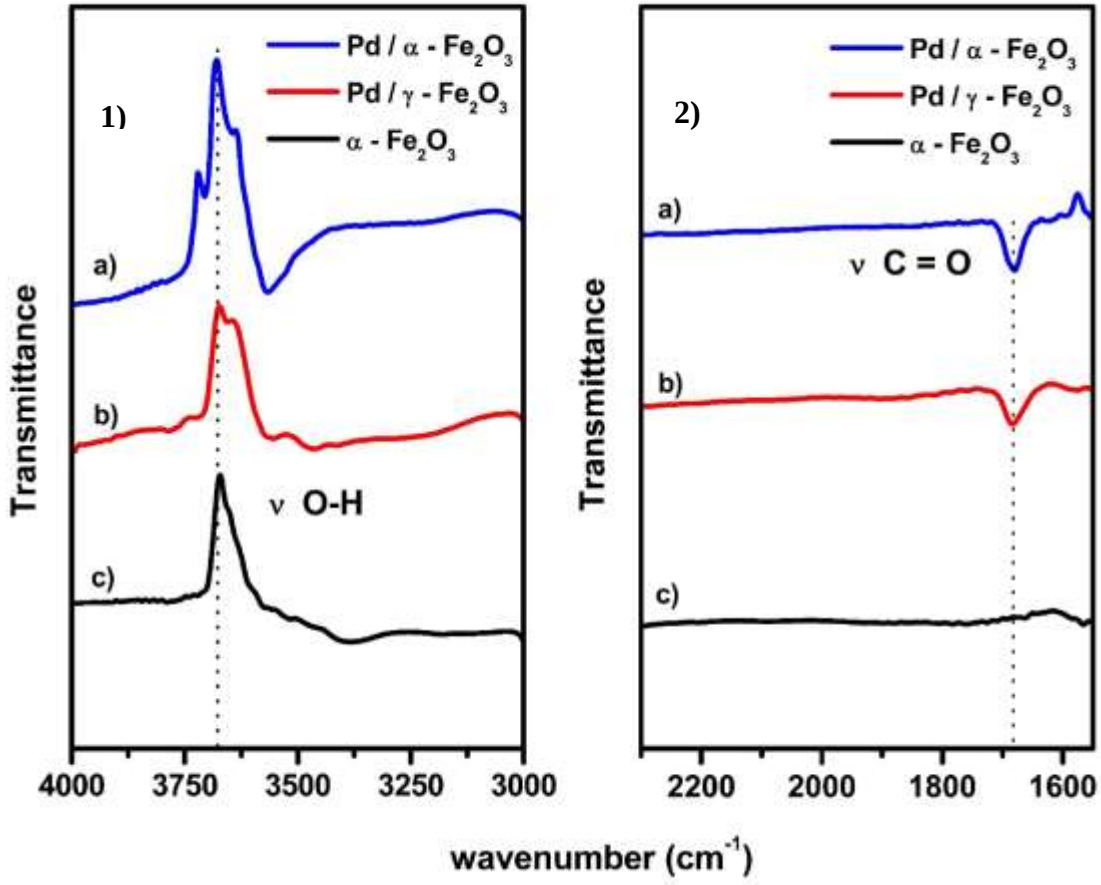

Figure 3.5. Spectra of adsorbed 1,2-DCA over Pd / α-Fe_2O_3 (a), Pd / γ-Fe_2O_3 (b), α-Fe_2O_3 (c).

A further analysis of the hydroxyl infrared region is depicted in Fig. 3.4 and summarized in Table 3.1. As it can be observed in figure 3.4 there are two peaks at 3724 cm^{-1} and 3687 cm^{-1} for α-Fe_2O_3. In the case of goethite (α-FeOOH) a strong band at 3663 cm^{-1} with a shoulder around 3688 cm^{-1} is observed. On the other hand γ-Fe_2O_3 shows a loss in the band at 3674cm^{-1} with a shoulder appearing at 3636 cm^{-1}. As previously mentioned, bands appearing as peaks correspond to surface species that are being consumed after adsorption, and bands appearing as valleys correspond to vibrational modes of newly form surface species. These observed bands in the 3600-3800cm^{-1} range can be assigned to different hydroxyl groups. The bands at 3724 cm^{-1} and 3687 cm^{-1} observed for α-Fe_2O_3 can be assigned to isolated OH groups and H bonded OH groups, both of which are

lost during the adsorption process due to interaction with the probe contaminant, leading to the formation of a new surface species. In comparison the peaks of α-FeOOH correspond to H bonded hydroxyl groups (3663 cm^{-1}) and the shoulder at 3688 cm^{-1} falls in the region of isolated hydroxyl group stretchings. The band observed for γ-Fe_2O_3 at 3674cm^{-1} results from the interaction of TCE with the isolated OH and the second band at 3636cm^{-1} from the loss of the H bonded OH as the molecule adsorbs on the surface.[14] This analysis suggests the existence of diverse chemical environments surrounding the hydroxyl groups present on the different iron surfaces, this difference can be attributed to surface morphology and crystalline structure of these different FeO_x species, as discussed before.

Analysis of the region between 1100 to 1200 cm^{-1} in figure 3.4 shows the formation of two adsorption bands, the first one in the region of 1125-1131 cm^{-1} and a second one at 1163 cm^{-1} for all of the probed surfaces (summarized in Table 3.1). Both of these vibrations, as discussed before, are assigned to the C-O ethoxide stretching frequency.[22] A change in the intensity ratios is observed within the different species. Previous work on α-Fe_2O_3 by Ferretto and collaborators, indicate a heterogeneous distribution of surface sites in α-Fe_2O_3, where both Lewis and Brønsted acid sites can be found. Different Lewis acid sites (Fe^{+3}) with non-equivalent local chemical environment were identified, this non equivalency results in different strength of the Lewis acid sites affecting the strength of the bonds formed after adsorption. [14] Thus the observed change in intensities in the C-O ethoxide region can be rationalized in terms of at least two different non-equivalent available Lewis acid sites which can allow the formation of two different ethoxy groups, where one of the ethoxy groups can be anchored to a single Fe^{+3} in a monodentated fashion or in a bridging configuration as previously observed for dichloromethane adsorption over alumina surfaces.[22]

As discussed before, the addition of a catalytic metal dramatically increases the dechlorination activity of the iron surfaces. Pd has been widely reported to present this catalytic effect, which results in an increase of the reaction selectivity to less toxic, fully dechlorinated products.[1,23] Dechlorination surface mechanisms and the role that Pd plays was investigated by Van den Brink and collaborators and by Jeurissen's research group. Van den Brink studied the catalytic oxidation of dichloromethane on γ-Al_2O_3 by FTIR. They observed the formation of mono and bi-dented methoxy groups together with formates bidentately adsorbed. These surface species were observed to result from the interaction of CH_2Cl_2 with the alumina surface hydroxyl groups. As part of their

experiments they tested the addition of water to the reaction stream and observed an increase in the reaction rate, attributing this result to the increase in the surface availability of hydroxyl groups in the solid surface. [22] Jeurerissen and collaborators also observed the formation of C=O bonds (vibrational frequency in the region of 1684 - 1696 cm^{-1}) in the form of acetaldehyde like adsorbed species when 1,2-DCA was adsorbed onto γ-Al_2O_3.[24]

The effect on the surface intermediaries when Pd is added to our system is depicted in Fig. 3.5. Here the FTIR spectra of adsorbed 1,2-DCA over α-Fe_2O_3, and the Pd modified samples: Pd / α-Fe_2O_3 and Pd / γ-Fe_2O_3 are shown. As previously observed for the case of the Pd-free surfaces, the interaction with the hydroxyl groups and the formation of ethoxide-like surface species is clear. However, when Pd is present in the system, the formation of a new band is observed at 1683 cm^{-1}. This band is observable in α-Fe_2O_3, α-Fe_2O_3, α-FeOOH species when interacting with 1,2-DCA and TCE (data not shown) and is present only for the case of Pd-doped surfaces. The appearance of this band can be rationalized in terms of the formation of a new surface intermediary. As reported by Jeurissen and collaborators, the formation of an acetaldehyde like species is observed as a result of a sequential dehydrodechlorination mechanism where 1,2-DCA first converts to vinyl chloride over γ-Al_2O_3. After this initial step, vinyl chloride is formed and its protonation by surface OH groups results in the formation of a carbocation stabilized by resonance. This carbocation is then stabilized by a surface basic Lewis site (nucleophilic oxygen), leading to the formation of an acetaldehyde like surface species with the concomitant formation of a carbon oxygen double bond.[24]

For this mechanism to be applicable to our system two conditions need to be satisfied. The presence of palladium should increase the formation of vinyl chloride species on the surface, and the presence of Lewis basic sites on the iron oxides surfaces. Indeed in the study of catalytic processes, Pd has been identified as a strong dissociation surface for H_2.[25,26] Moreover, the catalytic capacity of Pd towards dechlorination of halogenated hydrocarbons has been the subject of extensive study in the literature [1,23,27,2]. Specifically TCE has been reported to undergo dechlorination over Pd surfaces yielding vinyl chloride when hydrogen availability limits full dechlorination. [27] To address the possibility of a change on surface hydroxyl groups due to Pd doping and to indirectly test the formation of additional Lewis sites in the presence of palladium, we recorded the infrared spectra of the bare surfaces after dehydration pre-treatment right before

TCE or 1,2-DCA adsorption. Fig.3.6 shows the infrared spectra obtained in this case for both the bare and the Pd doped surfaces.

Analysis of Fig. 3.6 indicates the thermal pre-treatment of the surfaces does not completely remove the broad bands located from 3200 to 3600 cm^{-1} attributed to hydrogen bonded water, and hydroxyls. Also the sharp peak in the region of ~3670 cm^{-1} can be associated to the stretching vibration of isolated hydroxyl groups. However, as palladium is added to the iron surfaces a band change in this region is observed: an evident loss in the sharp peak of the isolated hydroxyl groups and the presence of a broader band in the H bonded hydroxyl region. This phenomenon is also observed on the surface of hematite and maghemite when Pd is added to the surface (not shown). The interaction of Pd with surface hydroxyl groups has been widely reported (e.g., Nyberg and collaborators [25,57]). The decrease on the availability of hydroxyl isolated groups and an increase in the hydrogen bonded OH groups that result from the presence of palladium can be explained in terms of Pd capacity to promote hydrogen bond formation among hydroxyl groups.[57] Moreover, the decrease on the number of isolated hydroxyl groups could also be hypothesized to be the result of condensation reactions between these isolated groups leading to the formation of new Fe-O-Fe, moieties in the surface that can act as Lewis basic sites to yield the surface acetaldehyde-like intermediates observed.

The use of spectroscopic techniques as tools to probe the interaction taking place between the iron oxide surfaces and the chlorinated contaminants indicate that surface hydroxyl groups play a large role in these processes leading to the formation of a C-O bond between 1,2-DCA or TCE and the iron oxide surface. Other observations for the case of TCE point to the disappearance of the C=C bond and a red shift of the C-H stretching mode to frequencies in the region of saturated hydrocarbons. All these phenomena are rationalized in terms of the formation of a surface ethoxide group during adsorption. In contrast the addition of Pd to the surface yields a new band in the region of C=O after TCE or DCA adsorption, this is assigned to the formation of a new surface intermediary that is favored in the presence of Pd and can be linked to an acetaldehyde like moiety previously reported in similar Pd-bearing systems.[24]

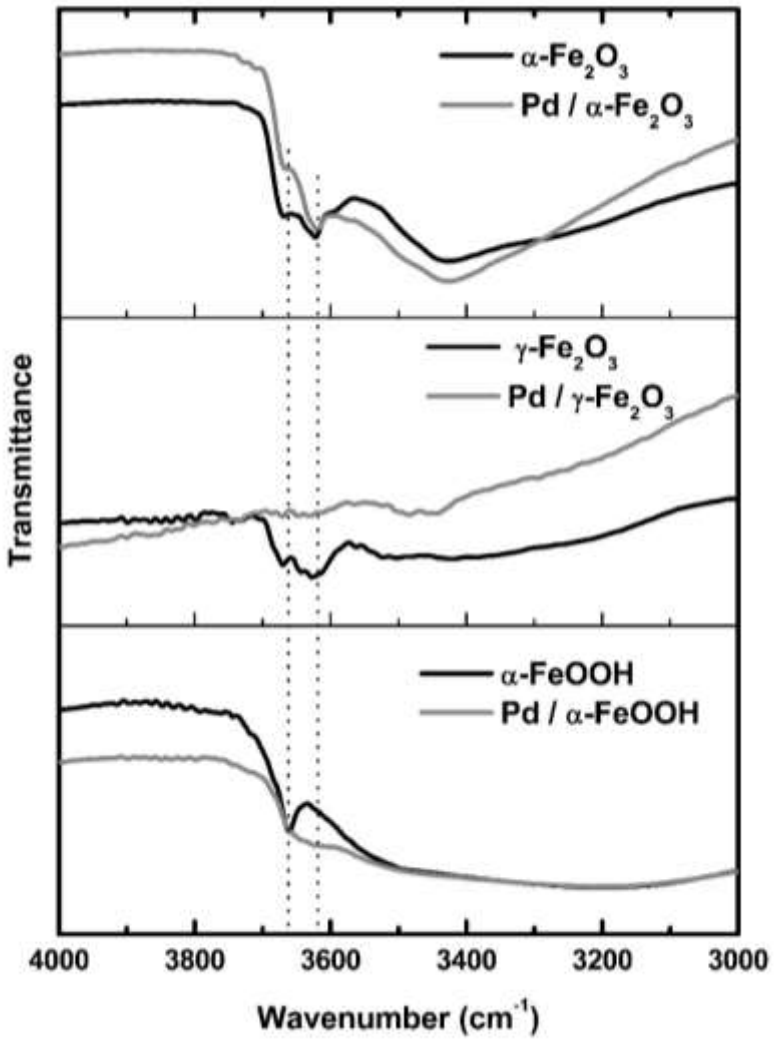

Figure 3.6. Spectra of dehydrated bare (black) α-Fe_2O_3 (top), γ-Fe_2O_3 (middle), α-FeOOH (bottom) and dehydrated Pd doped (grey) α-Fe_2O_3 (top), γ-Fe_2O_3 (middle), α-FeOOH (bottom).

While the use of infrared spectroscopy provides very useful information regarding the chemical bonding of surface interaction taking place between the iron oxide species and the chlorinated molecules, identifying the chemical species formed as a result of these processes is critical to propose a robust surface and reaction mechanism. In this regard, an analytical technique widely used in the study of surface/gas interface processes, temperature program desorption (TPD), is used to provide valuable information related to the reaction pathways taking place over different surfaces. Useful information can be extracted from the TPD profiles that can be related to surface

reactivity, selectivity or to indirectly determine the changes on the surface taking place following reaction.[28] It can also help to distinguish the surface acidity in the case of the surface oxides; this is achieved by the use of probe molecules.[29] TPD has been used to probe adsorption of chlorinated hydrocarbons over iron oxides. For instance, Adib and collaborators proposed reaction pathways resulting from the interaction of CCl_4 with single crystal hematite and magnetite terminated hematite crystals under high vacuum TPD experiments. Their experimental results suggested re-combinative desorption of CCl_4, C_2Cl_4 and $OCCl_2$ species. [20]

For our experimental approach, TPD was used to identify TCE desorption products that could provide evidence of formation of surface adsorbed species containing the chemical moieties observed in the in situ infrared experiments (chloroethoxides for C-C, C-O and C-H single bonds, carbonyl bearing species for C=O bonds, and vinyl chloride for C=C-H bonds). As TCE evolution in TPD experiments were analyzed by means of GC, desorption profiles resolution was limited by the frequency of the sampling intervals of the built in six port valve. Selection of the sampling intervals was carried out as a function of the required time of the GC separation method (4 min. per run).

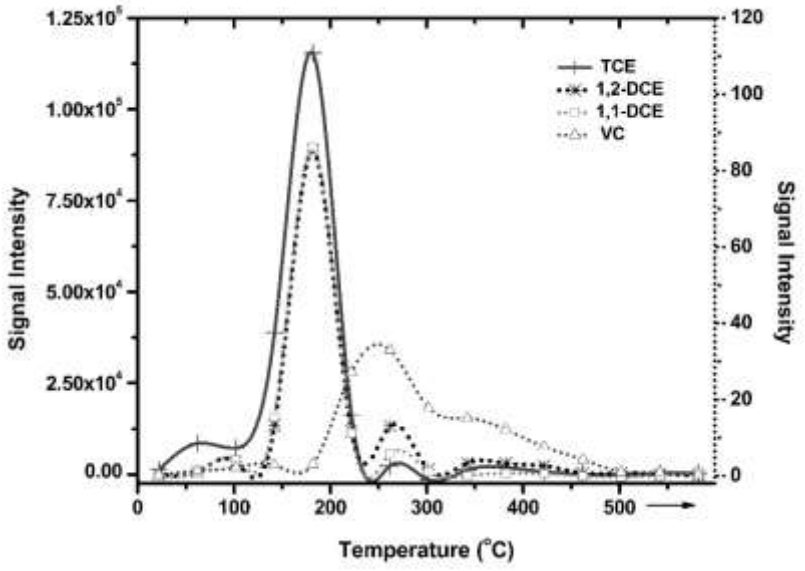

Figure 3.7. Temperature program desorption profile of adsorbed TCE (dark grey) over nZVI, with desorption products: 1,2-DCE (black dots), 1,1-DCE (light grey dots), vinyl chloride (grey dots). Left vertical axis depicts the scale for the signal intensity of TCE desorption (solid line) and the right vertical axis the signal intensity of all other desorption products (dotted line).

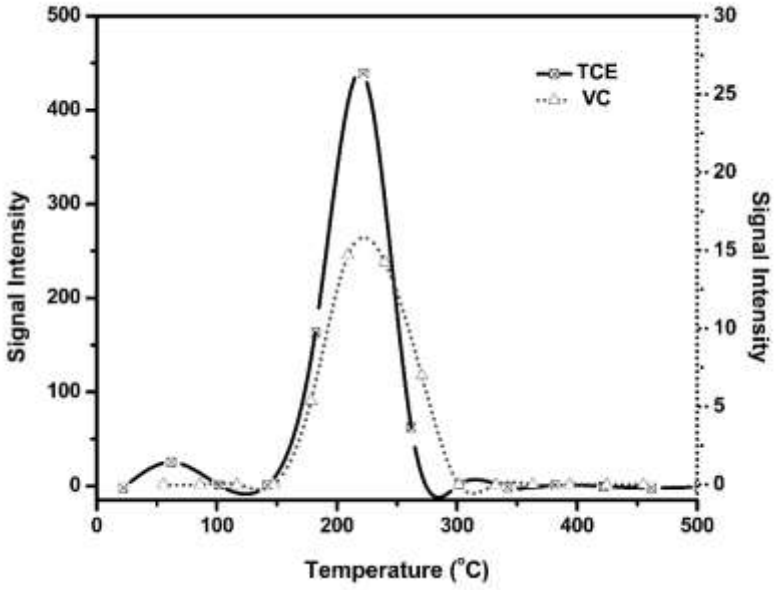

Figure 3.8. Temperature program desorption profile of adsorbed TCE (black) over Pd / nZVI, with desorption product: Vinyl chloride (grey dots). Left vertical axis depicts the scale for the signal intensity of TCE desorption (solid line) and the right vertical axis the signal intensity of vinyl chloride (dotted line).

Temperature program desorption profiles after adsorption of TCE over nZVI and Pd /nZVI are shown in Fig.3.7 and Fig.3.8 respectively. For both figures the left vertical axis depicts the scale for the signal intensity of TCE desorption (solid line) and the right vertical axis the signal intensity of all other desorption products (dashed line). The desorption products of TCE adsorption over Pd-free nZVI are TCE, 1,1-dichloroethene (1,1-DCE), 1,2-dichloroethene (1,2-DCE) and vinyl chloride (VC). These observed desorption species are in agreement with previously reported observations of TCE dechlorination products in both the gas phase or in aqueous conditions.[30,31] For instance, experimental results for TCE dechlorination with nZVI in the gas phase by Uludag and collaborators indicated the presence of 1,2-cis-DCE, 1,1-DCE, VC and ethylene. In their results the relative humidity of the system played an important role, its contribution was adjudicated to the limitation in the availability of surface water which serves as a proton source for the dechlorination via hydrogenolysis.[32] In our experimental results ethylene was not observed due to the low sensitivity of the ECD detector toward hydrocarbons. The presence of the dechlorination products commonly observed due to nZVI dechlorination of TCE in our experiments show not only the surface capability of the nZVI particles to reduce TCE, but more interestingly, suggest a sequential dechlorination process where dechlorinated ethylenes (1,2-cis-

DCE, 1,1-DCE) intermediaries are desorbed at lower temperatures first. This process is followed by the formation of vinyl chloride that results from a further dechlorination step. Though it would be tempting to propose a sequential dechlorination mechanism during desorption, the possibility of two different sites on the nZVI surface, one able to monodechlorinate and another one that didechlorinates needs to be considered as well. Another interesting feature, is the similarity of the desorption profiles of the two dichlorinated species 1,2-cis-DCE, 1,1-DCE. These similarities can indicate the existence of different adsorption sites on the nZVI surface capable of forming the observed dichlorinated intermediaries. These different sites can then lead to the formation of the different desorption products observed during TPD. The presence of dissimilar adsorptions sites can be due to the complexity and heterogeneity of the nZVI shell, where the difference in iron speciation distribution and chemical environment can lead to the formation of non-equivalent reactive sites.[14] The heterogeneity in the surface chemical environment can result in the presence of non-reactive sites that can participate in the adsorption but due to the inaccessibility of the adsorbed complex to other species that are required for dechlorination(i.e. protons, electron transfer) will hinder dechlorination. In this case simple desorption of unreacted TCE occurs when desorption temperature is reached.

It has been proposed that TCE dechlorination over nZVI particles undergoes two possible pathways; β-elimination and hydrogenolysis.[6] In the dechlorination through β-elimination an unsaturated halogenated hydrocarbon is formed. This takes place as a base interacts through its electron pair with a proton of a β carbon. As the removal of this proton takes place, the electrons that were bonding to the proton move towards the adjacent carbon where chlorine is bonded. At the same time, a chloride ion leaves the molecule. The formation of a new π bond between the carbon atoms allows the chlorine to withdraw from the structure with its bonding electrons as chloride.[33] For the case of the hydrogenolysis mechanism, substitution of the halogen atom by hydrogen without disruption of the carbon-carbon bond takes place. Reported results indicate both dechlorination mechanisms taking place over the nZVI surface with a higher selectivity towards a β-elimination pathway. [6,34] The dominant pathways can be found by quantification of the dechlorination by-products. β-elimination of TCE will result in the formation of chloracetylene, which further will decompose to acetylene through a hydrogenolysis substitution and might supplementary transform to ethylene via a hydrogenation mechanism.[35] On the other hand, the

formation of dichlorinated ethylene intermediaries is observed when dechlorination takes place through hydrogenolysis. The formation of trans, cis and 1,1-DCE is the first step of TCE dechlorination via this mechanism. These dichlorinated hydrocarbons can undergo two more hydrogenolysis reactions that will lead to the formation of vinyl chloride that will be further dechlorinated to ethylene.[6] A final hydrogenation reaction can take place after ethylene is formed, yielding ethane as the final product.[35] Our experimental observation of 1,2-DCE, 1,1-DCE and VC suggests reductive dechlorination of TCE via hydrogenolysis in this study.[6]

TPD experiments were also conducted over all iron oxide species tested in our work to compare desorption products and attempt to pinpoint the contribution of each iron oxide species in the adsorption/dechlorination mechanism. In all cases vinyl chloride and TCE were the main desorption products, consistently indicating a hydrogenolysis pathway. This shows all iron oxides surfaces can promote TCE dechlorination. The surface desorption products that were observed in the TPD experiments and formation of similar surface adsorbed species in all probed samples are in agreement with the in-situ FTIR experiments (Fig. 3.3, 3.4). In these experiments spectral evidence highlights the interaction that takes place between TCE or 1,2-DCA and the hydroxyl surface species. Additionally the formation of a C-O band is consistently observed for all probed iron samples species.

From the performed TPD experiments, the formation of dichlorinated and mono chlorinated hydrocarbons is observed as a result of the surface interaction between 1,2-DCA and TCE with the iron oxides / oxyhydroxides or nZVI surface. In order to formulate a comprehensive surface reaction mechanism for the dechlorination process, a pathway that is able to incorporate the spectroscopic and TPD observations is proposed. Scheme 3.2 depicts a generalized dechlorination process for TCE. As adsorption takes place through the interaction of the C=C system and the hydroxyl groups in the nanoparticles surface, the formation of the surface intermediary takes place. This surface adsorbed species leads to the formation of the products observed on the TPD experiments. This adsorption process as it occurs in the surface of the nZVI surface will lead to the formation of dichlorinated ethylenes (1,2-DCE, 1,1-DCE) and consecutive desorption of VC at higher temperatures. In contrast when the adsorption process takes place over the iron oxides / oxyhydroxides surfaces, formation of VC is observed. However a more detailed dechlorination mechanism than the one represented in Scheme 3.2, requires additional spectroscopic evidence to

assess the role of Pd, the bulk iron species, and crystalline structure in the adsorption / dechlorination process.

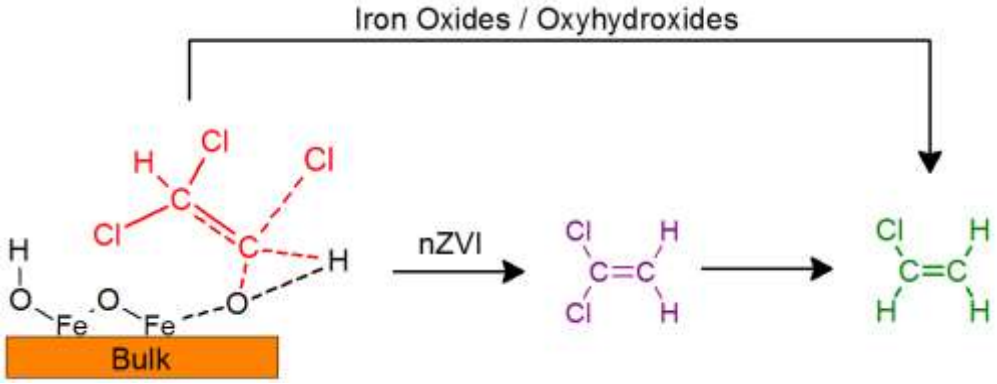

Scheme 3.2. Dechlorination process observed over iron bearing nanoparticles and nZVI surfaces.

It is well established that desorption pathways over reactive surfaces can be altered by the presence of a catalyst. As previously mentioned Pd has been widely used to promote the catalytic dechlorination of halogenated hydrocarbons. [1,23,27] Computational simulations for adsorption of TCE over metal Pd clusters have attempted to address possible dechlorination mechanisms that occurs after adsorption of TCE on the Pd surface. Direct dechlorination and sequential dechlorination were investigated as the two possible pathways. Direct dechlorination of TCE involves the complete removal of the chlorine atoms of TCE at the Pd surface as a preliminary step; after radical-like surface intermediaries are formed addition of hydrogen takes place in order to form the fully dechlorinated hydrocarbon. In contrast, for the sequential dechlorination pathway, a chlorine atom is first withdrawn, followed by hydrogenation, leading to the formation of partially dechlorinated compounds. The newly form partially dechlorinated species undergoes similar cycles until a fully dechlorinated compounds is achieved.[37]

These computational simulations suggest that hydrogen surface coverage and lateral interactions between adsorbed species and dechlorination activation energies affect significantly the rate and

degree of dechlorination of TCE over Pd surfaces. Activation barriers for dechlorination show that the withdrawal of the first two chlorine atoms occurs rapidly and irreversibly. By comparison, the elimination of the last chlorine occurs at a slower rate. In contrast, the activation energy for the hydrogenation process is shown to be higher than that required for the third dechlorination. These calculations thus suggest direct dechlorination to be the main surface process taking place after adsorption. Interestingly, the degree of hydrogen surface coverage does not seem to affect the hydrodechlorination rate for TCE, suggesting a competitive adsorption process. As the coverage of hydrogen is increased dechlorination of TCE decreases because both TCE and hydrogen compete for adsorption sites on the surface. Indeed, hydrogen adsorption is thermodynamically favored over TCE's. At the same time desorption of TCE has a higher activation barrier than that of the first TCE dechlorination step (0.57 eV vs. 0.23 eV respectively), this results in a lack of desorption of pristine TCE. Nevertheless, near TCE surface saturation the effect of Cl-Cl repulsion generated by lateral interactions within adjacently adsorbed TCE molecules decreases the activation barrier for TCE desorption.[37] The effect of lateral interaction between adsorbed species, thus provides further explanation for the observation of unreacted TCE (Fig. 3.7 and 3.8) and 1,2-DCA (data not shown) desorbing from the probed surfaces in the TPD experiments.

In our experimental observations, shown in Fig. 3.8, the addition of Pd to the nZVI surface results in the disappearance of the dichlorinated intermediaries (1,1-DCE, 1,2-DCE). This observation can be rationalized in terms of the previously discussed theoretical study. The addition of Pd to the iron oxide results in the creation of adsorptions sites where TCE adsorption is more favorable, compared to the bare Pd-free iron oxide surface, since the activation energy for adsorption of TCE over Fe^0 and Pd are 49 kJ/mol and 0 kJ/mol respectably.[38,37] As the adsorption of TCE becomes more favorable in the Pd-doped surface, this also leads to the complete dechlorination of TCE over the surface. This is due to the fact that the withdrawal of one or two chlorine atoms takes place rapidly and irreversibly as discussed. Thus a preferential direct dechlorination mechanism takes place when the iron oxide surface is doped with Pd, and dichlorinated compounds are not observed in the TPD experiments (Fig. 3.8). Nevertheless adsorption of TCE does not only occur in the Pd surface, as suggested by our FTIR and TPD observations (Figs. 3.4 and 3.7 respectively). The presence of 1,2-DCE, 1,1-DCE as desorption products for only the case of Pd-undoped iron oxides, but not present for the case of Pd-doped surfaces suggests that either a direct full dechlorination path is available in the presence of palladium or that if dichlorinated intermediaries

are indeed formed they re-adsorb onto the Pd surface where a complete dechlorination takes place. Dechlorination products are observed in the TPD/TPR experiments between the different iron surfaces and 1,2-DCA or TCE (results not shown), suggesting that the surface hydroxide groups present on the iron oxide surface could provide the protons required for the formation of the lower chlorinated vinyl chloride.

In order to understand the effect of Pd in the formation of dechlorinated intermediaries, a comparison of the desorption profiles of VC on nZVI and Pd/nZVI is carried in Fig. 3.9. The overall area of the desorbed VC is similar in both TPD profiles. Moreover, as mentioned above, desorption of dichlorinated intermediaries was not observed for the case of the Pd-doped nZVI sample. A closer inspection of these TPD profiles show that for the case of nZVI there is a shoulder in the region between 250 ^{o}C to 500 ^{o}C. This shoulder can be linked to the existence of two different sites with a distribution of adsorption strengths, likely due to the heterogeneity of the surface. This suggests the existence of adsorption sites where VC can be generated on different chemical environments. In contrast, when Pd is present in the surface, there is no shoulder, suggesting that the presence of Pd decreases the desorption energy of the surface adsorbed species.

The TPD experimental results of TCE adsorbed over all probed bare iron oxides and oxyhydroxides tested are similar (results not shown). Vinyl chloride is observed as the main desorption product, besides TCE, in all cases. The similarity in the production of VC by all the probed iron surfaces serve as a corroboration of the in situ FTIR experiments, where similar surface adsorbed species were observed in all the iron species tested. This, together with the behaviour of the hydroxyl infrared bands strongly suggests the need of a common adsorption mechanism where the participation of the surface hydroxyl species in the adsorption/reaction mechanism plays a critical role.

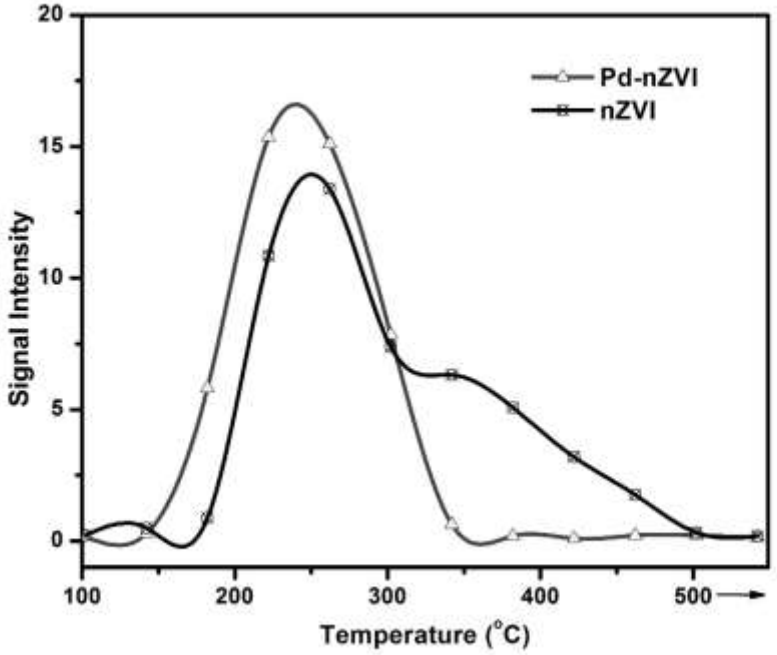

Figure 3.9. Normalized Temperature program desorption profile of desorbed vinyl chloride in TCE interaction over nZVI (black) and Pd – nZVI (grey).

Since the previous results indicated clear differences in reactivity and surface processes taking place upon desorption of TCE in the presence of palladium, we decided to evaluate the possible surface mechanisms involved in 1,2-DCA desorption. However, since 1,2-DCA lacks a double bond adsorption is limited in comparison to TCE.[58] Moreover, dechlorination of 1,2-DCA has a very high activation energy when compared to that of TCE.[59] Therefore, to overcome these limitations temperature program reaction (TPR) experiments were conducted instead of TPD allowing us to increase the production of the surface species.

Fig. 3.10 shows the 1,2-DCA-TPR profiles over nZVI and Pd/nZVI. For the case of the Pd-free nZVI surface (top) a maximum for the 1,2-DCA signal is observed at 150 ^{o}C while evolution of dechlorinated products is not observed below 150^{o}C. Above 150^{o}C, however, vinyl chloride and ethylene are observed. The peak corresponding to 1,2-DCA, with a maximum at 150 ^{o}C, can be rationalized in terms of a desorption profile peak where desorption from the saturated surface occurs as a continuous flow of 1,2-DCA is injected and the temperature increases, this desorption

phenomena continues until the activation energy barrier for the production of vinyl chloride and ethylene is overcome. This result provides further evidence dechlorination is a surface mediated reaction, where adsorption is required and precedes the dechlorination step, which takes places as the energy barriers are overcome. Since hydrodechlorination through β-elimination requires a Brönsted base capable of withdrawing a proton from the chlorinated organic molecule, resulting in the formation of a C-C π bond and the removal of the chlorine atom, the fact vinyl chloride is observed suggest the surface capacity to provide the required sites to promote the β-elimination reaction . This observation further confirms the important role of the hydroxyl groups present in the nZVI surface in adsorption/reaction mechanisms towards chlorinated hydrocarbons.

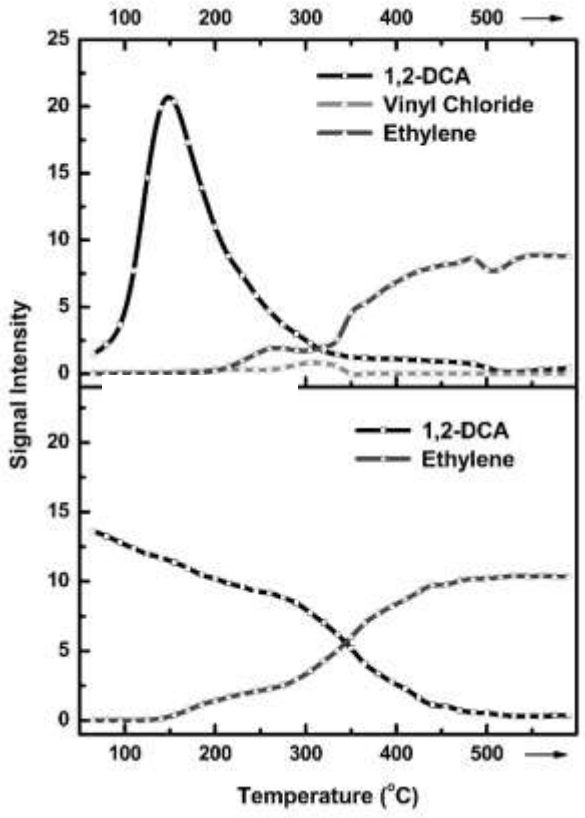

Figure 3.10. Temperature program reaction profile of 1,2-DCA (black) over nZVI (top). TPR profile of 1,2DCA with Pd / nZVI (Bottom).

In contrast, the 1,2-DCA-TPR experiments for Pd doped nZVI (bottom profile on Fig. 3.10) there is no peak observed for the 1,2-DCA profile and ethylene is the only dechlorination product observed, indicating that as Pd is added, vinyl chloride evolution does not take place. This observations suggest that 1,2-DCA undergoes rapid and full catalytic dechlorination in the presence of Pd.

These experiments were carried for all studied iron oxide species. For α–Fe_2O_3, γ–Fe_2O_3 and Fe_3O_4, the formation of ethylene was observed only when Pd was doped on the surface (results not shown). In contrast, for the case of α-FeOOH, ethylene was observed also for the Pd-free sample. When comparing the product speciation, the production of ethylene is also observed even in absence of Pd for the bare nZVI particles. The presence of ethylene in the experiments with α-FeOOH and nZVI is not completely surprising since previous surface studies have suggested the predominance of α-FeOOH in ZVI surfaces.[39] The presence of these type of hydroxylated species has also been confirmed under anoxic conditions by means of Mössbauer spectroscopy and computational simulations.[40] This would suggest that heavily hydroxylated surfaces such as α-FeOOH contain more actives sites required for the dechlorination of 1,2-DCA and TCE, once again indicating the importance of hydroxyl groups for the adsorption step, and as a proton source in the dechlorination process. Because of the heterogeneity of the surface composition of the nZVI particles, the availability of these actives sites may be limited in some cases. Other factors such as the pH, oxidation reduction potential (ORP), zeta potential, temperature and water chemistry have also been linked to the modification of the shell composition of iron nanoparticles.[41] As the surface is modified by all these previously mentionned parameters the composition and accessibility to the active sites can be modified, affecting the availability of hydroxyl groups on the surface and hence the dechlorination mechanism.

A second phenomenon was observed in the presence of γ-Fe_2O_3. VC and CO_2 were observed as reaction products. The formation of CO_2 as a product suggests oxidation of 1,2-DCA over the iron surface. The use of UV-Vis thus can potentially provide evidence of a reduction process taking place in the iron oxide species resulting in oxidation of 1,2-DCA. In terms of electronic structure, γ-Fe_2O_3 contains Fe^{+3} ions located in octahedral and tetrahedral coordination sites.[43] In contrast, α-Fe_2O_3 which also possess only fully oxidized Fe^{+3} species, has these ions located only

in octahedral sites.[44] In contrast, Fe_3O_4 has iron ions in both +2 and +3 states. In this case the Fe^{+3} are coordinated in tetrahedral and octahedral sites and Fe^{+2} in octahedral ones.[45]

In situ UV-Vis spectra were recorded at room temperature, under similar conditions as the in situ DRIFTS experiments. Spectra were obtained before and after interaction of 1,2-DCA and TCE with γ-Fe_2O_3, α-Fe_2O_3 , α-FeOOH (results not shown). From these experimental results no change in the bulk electronic structure of the probe surfaces after adsorption is observed. These results suggest that the adsorption process that occurs at room temperature is a surface phenomenon and that the iron species do not undergo changes in oxidation state after adsorption at this conditions. In order to better understand the formation of CO_2 during TPR and to further explore the reaction phenomena taking place over γ-Fe_2O_3, TPR experiments were conducted on an in situ UV-Vis set up. As previously mentioned, in situ UV-Vis has been used in the study of reactive surfaces to probe changes in oxidation state of the solid as gas phase reaction takes place.[42]

In Fig. 3.11 the in situ UV Visible spectra of γ-Fe_2O_3 before and after TPR with 1,2-DCA is presented. The spectrum corresponding to the bare γ-Fe_2O_3 surface is characterized by two bands.[46] Fig. 3.11 shows a band in the region near 630 nm for the sample before the TPR process, this band has been assigned to a Fe^{+3} ligand field electronic transition and is observed for other iron species with Fe^{+3} in octahedral coordination sites. However for γ-Fe_2O_3 the band is less resolved due to transitions of Fe^{+3} ions present in tetrahedral sites.[46] As the TPR process takes place, the disappearance of the band at 630 nm is evident. This cannot simply be explained by proposing a thermal phase transition (known to occur around 500^{o}C in γ-Fe_2O_3)[9], since this would lead to transformation to stable α-Fe_2O_3 which also has a band around 630nm.[46] In order to address this question a blank experiment was carried on γ-Fe_2O_3 without the injection of 1,2-DCA, with the aim to isolate the effect of the thermal treatment in the TPR experiment. The result is shown in Fig. 3.11 where a clear redshift in the peak at 750nm is observed, indicating formation of γ-Fe_2O_3. Thus, as the TPR ramp proceeds without the addition of 1,2-DCA the expected phase transition to γ-Fe_2O_3 occurs. This phase transition takes place below 500^{o}C since as particle size decreases (γ-Fe_2O_3 nanoparticles were used for the TPR experiments) phase transformation temperatures also decrease.[46]

In contrast, in the presence of 1,2-DCA, the UV spectra shows a further red shift on the peak at 750nm and the disappearance of the band at 630nm. The disappearance of this band suggests that either octahedral Fe^{+3} sites are lost or that a change in electronic structure of the iron has taken place during reaction with 1,2-DCA. Monitoring of the desorption products by GC/MS during this process identified CO_2 as one of the reaction products, indicating that oxidation of 1,2-DCA takes place, suggesting that iron is thus being reduced and pointing to a change on the electronic structure of the iron ions in the solid during this process.

To verify that reduction of γ-Fe_2O_3 takes place during TPR, X-ray difractograms were obtained for pristine γ-Fe_2O_3 and the γ-Fe_2O_3 sample after 1,2-DCA TPR. Figure 3.12 shows the patterns obtained, the difractogram located in the middle depicts the pattern obtained for pristine γ-Fe_2O_3, and the bottom profile corresponds to the XRD of Fe_3O_4 nanoparticles. Although both of these patterns are similar, they can be differentiated by the diffraction peaks of γ-Fe_2O_3 at $2\theta = 15^o$, 23.75^o and 26.08^o similarly a more subtle change can be detected in the 57.18^o and 53.57^o peaks, with a 0.35^o shift for the 57.18^o peak between γ-Fe_2O_3 and Fe_3O_4 and a 0.30^o shift for the 53.57^o peak are observed. These shifts lie well above the resolution capacity of the instrument (0.02^o).

Consistent with the UV/Vis observations, the γ-Fe_2O_3 sample obtained after the 1,2-DCA TPR experiment showed an obvious color change from the characteristic red-brown color of γ-Fe_2O_3, to a distinctive black color similar to the one of Fe_3O_4. The XRD pattern obtained for the spent sample after TPR displayed a shift to lower 2θ values of the 57.18^o and 53.57^o peaks characteristic of γ-Fe_2O_3. These shifts can be attributed to a convolution of γ-Fe_2O_3 and newly formed Fe_3O_4 diffraction peaks, confirming a change in electronic structure in the iron ions since, as opposed to Fe_2O_3, Fe_3O_4 contains divalent iron. Another feature confirming a modification in the crystalline structure after TPR is the change in the relative intensity of the diffraction peaks in comparison with the pure phase before reaction. We carried a similar in situ TPR UV/Vis experiment as well as XRD analysis before and after TPR (CO_2 not observed in this case, results not shown). No changes in the UV-Vis spectra, or X-ray diffraction patterns were observed regardless of the generation of VC in the bare iron oxide species and ethylene when Pd was impregnated. Thus we propose that the reactivity of Fe_2O_3 strongly depends on its crystalline structure, suggesting that as temperatures near the phase transition from γ–Fe_2O_3 to α–Fe_2O_3 are reached in the presence of

1,2-DCA, the tetrahedrally coordinated Fe^{+3} sites present in γ–Fe_2O_3 become more accessible and susceptible to reduction by the surface species present as result of chemisorption of the chlorinated hydrocarbon. The lack of change in the XRD diffractogram related to the crystalline structure of stable structures, such as α-Fe_2O_3, corroborate the results observe in the in situ UV-Vis experiments where phases like γ-Fe_2O_3,that are susceptible to phase transition, can promote the oxidation of the target contaminants as crystalline structure reconstruction takes place.

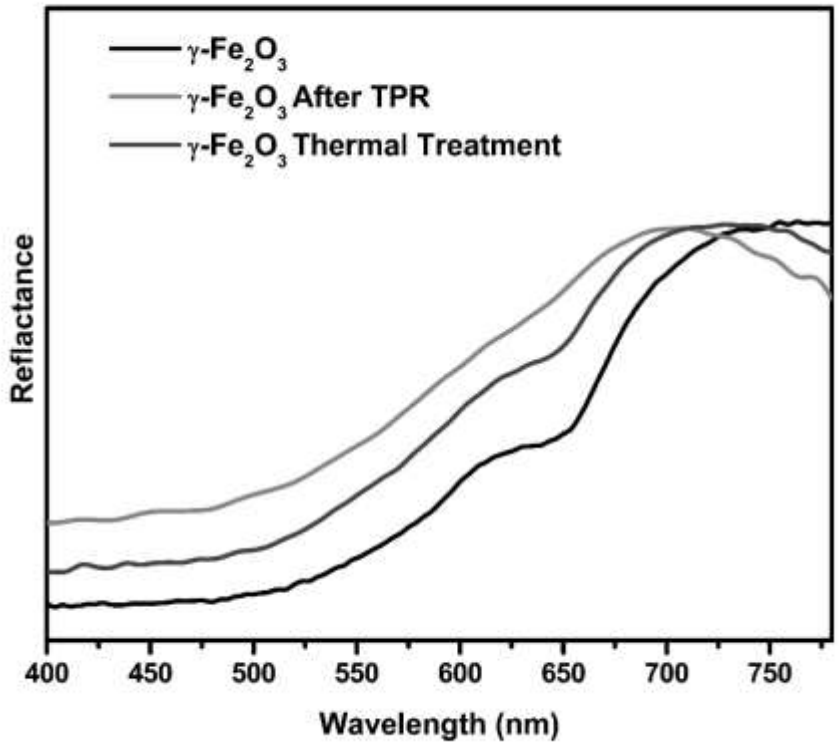

Figure 3.11. UV-Vis spectra of γ-Fe2O3 (black), γ-Fe2O3 after TPR with 1,2-DCA (grey) and γ-Fe2O3 after thermal treatment (dark grey).

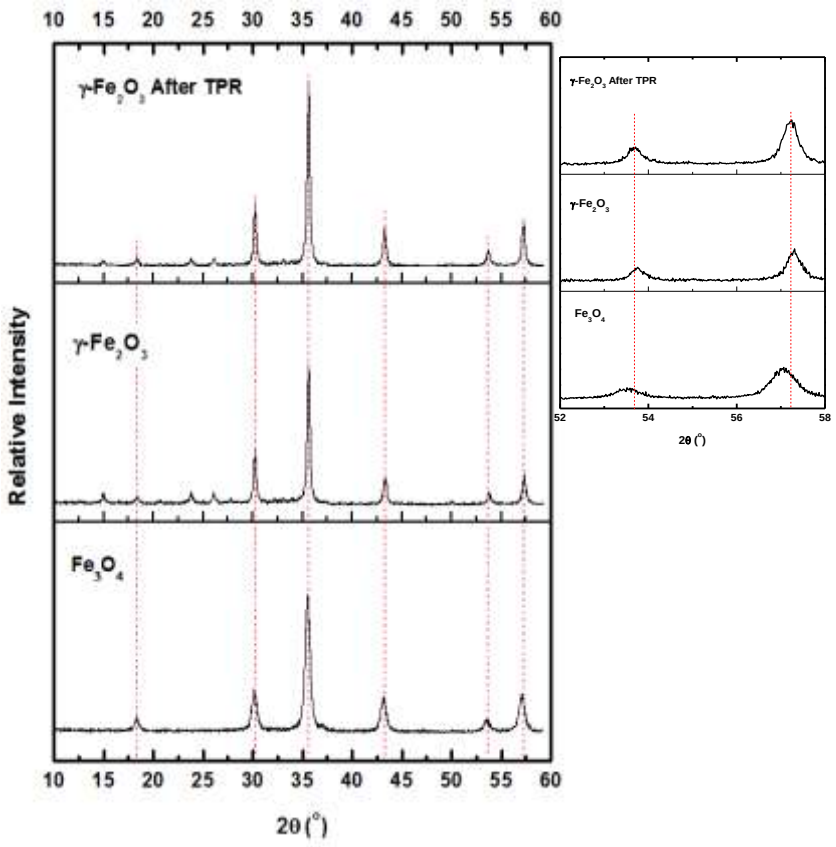

Figure 3.12. XRD spectra of as synthesized Fe_3O_4 (bottom), γ-Fe_2O_3 (middle), and γ-Fe_2O_3 after TPR with 1,2-DCA. Insert corresponds to a zoomed region of the spectra.

3.6.1 Surface mechanisms

Previous work has linked rates of decomposition of chlorinated hydrocarbons by iron surfaces to their surface composition, adsorption capacity and electron mobility. From our in situ FTIR experiments (Fig. 3.3 and 3.4), the interaction processes taking place on iron oxides surfaces appear to be regulated by the interaction between the hydroxylated species present in the surface and the chlorinated molecule. Spectroscopic observations show that the interaction with the O-H groups results in the formation of a carbon-oxygen bond, the disappearance of the C=C bond in TCE, and the weakening of the C-H bond. This suggests the formation of aliphatic non saturated (C-C) adsorbed species. In situ UV-Vis experiments confirmed the nature of these interactions as surface phenomena, since no changes on the solid electronic structure were observed at room temperature. TPD and TPR experiments provided complementary information on the identity of

the adsorbed species that are formed in the iron oxide surfaces. This information gathered through in situ FTIR and UV experiments can be assembled into a proposed surface mechanism. As similar type of interactions and desorption products were observed within all probed surface species, the adsorption mechanism can be suggested to occur through a similar mechanism. Differentiation within dechlorination capacity may thus be related to availability of adsorption sites, and the surface capacity to provide the required electrons for continuous dechlorination of the adsorbate. Fig. 3.13 depicts a proposed general mechanism, for the dechlorination process over the iron surfaces. The formation of the surface intermediary occurs as the nucleophilic π bond from the chlorinated hydrocarbon attacks the electrophilic region of the surface hydroxyl group (Brønsted acid site), the proton is released, the electrons that were originally bonding the proton to the surface withdraw to the oxygen atom which now bonds to the carbon atom (Fig 3.13a). The original surface proton now becomes bonded through a σ bond to the carbon atom, by the electrons that originally formed the π system (Fig 3.13b). As oxygen becomes richer in electrons from the removal of the surface proton, the formation of a carbocation, resulting from the destruction of the π system, is avoided by allowing the donation of the free pair of electrons from oxygen to the carbon atom (Fig 3.13b). The resulting adsorbed species agrees with our spectroscopic observations, where a carbon-oxygen bond is observed (Fig. 3.3 and 3.4), this species also explains the formation of the saturated hydrocarbon C-H vibration and both the disappearance of the C-C π system and O-H vibrational stretchings. As the surface of the iron species is populated with Lewis acid sites (Fe^{+3}), interaction between these acid sites and the Lewis base site of the chlorinated hydrocarbon (Cl) can take place adding additional stability to the adsorbed molecule (Fig.3.13c). The formation of this Lewis adduct would also result in the depletion of the electronic cloud of the Cl-C bond causing a weakening of this bond and explaining the observed red shift in the C-Cl stretching frequency. As the Cl-C bond is weakened by the formation of the Lewis adduct, the dechlorination of the surface adsorbed species can take place after electron transfer (Fig.3.13d). From this step, a dichlorinated species is produced (as observed by TPD in Fig 3.7) which can be re-adsorbed to the surface following a similar mechanism. This re-adsorption takes place in a second Brønsted acid site and dechlorination to vinyl chloride occurs through a similar mechanism where the formation of a C-O surface bonded species takes place again and electron transfer from the lattice results in the formation of vinyl chloride (Fig 3.4). An additional step resulting in the further formation of ethylene was observed on the surface of nZVI and α-FeOOH. As previously suggested the capacity

of nZVI to generate ethylene can be linked to the larger availability of highly hydroxylated surface species and their capacity to provide electrons. In contrast no ethylene was desorbed from the surfaces of α-Fe_2O_3, γ-Fe_2O_3 and Fe_3O_4. The inability of these surfaces to achieve full dechlorination to ethylene can be rationalized in terms of the insufficient availability of protons and electrons needed to trigger the hydrogenation process. The reduction capacity of the fully oxidized iron species can be thus attributed to the native defects of interstitial Fe^{+2} that are normally found in the crystal structure of these oxides.[47] The increase of the production of VC as temperature increases in the temperature program experiments (Fig.3.7 and Fig.3.10) can also be linked to the increase in the electron transfer capacity that arises from the increase of temperature.[48]

As the inclusion of Pd in our iron species surfaces to form a bimetallic systems was also tested, the catalytic effect of Pd in the dechlorination of TCE and 1,2-DCA under our experimental conditions needs to be rationalized. This will be done in the context of the widely reported interaction of noble metal surfaces with linear π systems, and the dissociative adsorption capacity of Pd towards chlorinated hydrocarbons[49] As part of our experimental observations, the catalytic effect of Pd in the adsorption process was clearly observed as evolution of ethylene in the reaction products was observed. In contrast to the Pd-free surfaces, the interaction with hydroxyl groups is affected when Pd is incorporated (Fig. 3.5 and Fig.3.6). As mentioned above, for the case of the Pd-free surfaces the formation of the adsorbate species is linked to the availability of the hydroxyl grounds on the surface, thus the addition of Pd results in the modification of this mechanism. Firstly, in contrast to the Pd-free surfaces, desorption of ethylene as a desorption/reaction product in the TPD and TPR experiments was observed as Pd was present in the system (Fig.3.10) in all cases: α-Fe_2O_3, γ-Fe_2O_3, Fe_3O_4 and FeOOH. Formation of ethylene from the reaction process of 1,2-DCA and TCE with nZVI was also observed and expected as it has been reported as one of the dechlorination products observed for Pd-doped nZVI.[1,23,27] The observation of ethylene in the presence of Pd over our iron surfaces is hypothesized to occur under the surface mechanisms depicted in Fig. 3.14. Pd has been reported to have dissociative adsorption capacities towards TCE and other chlorinated hydrocarbons.[50,51,52] As discussed in section 3.6, dissociative adsorption occurs readily in the Pd surface, and dechlorination takes places before the hydrogenation steps occurs.[37] In light of these previously reported results, the proposed dechlorination mechanisms in the presence of Pd was considered to be initiated from a mono dechlorinated adsorbed species as

this was reported to be present at highest concentration on the Pd surface. This is likely formed through dissociative adsorption, as it has been previously reported π planar bearing systems are adsorbed on Pd surfaces in a mono, bi, and tridentate manner (Fig 3.14a).[53] This adsorbed molecule can then undergo an attack by a nearby hydroxyl group resulting in the formation of a C-O bond as observed in the FTIR results. This will also result in the breakage of the molecule bond with the metal surface and the regeneration of the π system (Fig 3.14b). This is consistent with both the observation of a C-O bond in the FTIR (Fig. 3.5) and also the shift observed in the position of the O-H stretching band in the presence of Pd after halocarbon adsorption (Fig 3.5). As this takes place, the release of the proton from the Brønsted site occurs. The proton can thus be added to the double bond and re–adsorption to the Pd surface takes place (Fig 3.14c). This is followed by a β elimination of HCl to regenerate the π system. The continued reattachment of the molecule after each dechlorination step would also explain the reason for which no intermediate dichlorinated species were observed in the gas phase during the TPR and TPD experiments.

Availability of protons on the surface can allow the nucleophilic attack of the π bond towards a proton. Reattachment to the Pd surface takes place again and the elimination of proton will provide the electrons to the surface to reduce the anchoring iron, and the oxidation the adsorbed species resulting in the generation of a C=O bond (Fig 3.14g). The formation of these surface adsorbed carbonyl-like moiety would provide an explanation to the C=O vibration band observed in the in situ FTIR experiments (Fig. 3.5). As the full hydrogenation of the adsorbed molecule requires a higher availability of electrons from the surface, the formation of a reduced form of iron resulting from the formation of the carbonyl like species could serve as a source of electrons for the hydrogenation process taking place on another site as the iron is reoxidized. These conceptual mechanisms provide a concrete hypothesis for the capacity of the fully oxidized iron surfaces to allow a complete dechlorination process in the presence of Pd. In order to corroborate the proposed mechanism however, a comprehensive in situ study of the bare Pd surface under reaction conditions would be necessary.

As the nZVI surface is composed of a heterogeneous and complex mixture of iron oxides and oxyhydroxides, the surface morphology and speciation can lead to a distribution of non-equivalent adsorption sites, these sites due to steric inhibition, morphology and difference in adsorption strength can lead to the inability of the adsorbed contaminant to undergo dechlorination through

the proposed mechanisms. As Pd coverage in the surface is limited, the existence of Pd free areas would allow the simultaneous occurrence of both of our proposed mechanisms, nevertheless the lack of observed dichlorinated intermediaries in the presence of Pd could be related to a re-adsorption of the dichlorinated intermediaries on to the Pd surface, to undergo a further dechlorination. The scope of our research intended to understand at a fundamental level the interaction mechanisms of the groundwater contaminants TCE and 1,2-DCA, with iron oxide surfaces, therefore our experimental conditions address only the interactions between our contaminants and our iron surfaces. The inclusion of water or hydrogen would provide a source protons or atomic hydrogen that could result in an enhancement of the dechlorinated products.

Nevertheless, further works needs to be conducted in order to obtain information that can allow us to complement our in situ FTIR and UV-Vis observations, in order to fully understand the role, the optimal conditions and quantify the effect of the presence of hydroxyl groups on the dechlorination mechanism. Also additional experimental evidence needs to be provided with regards to the role of Pd through the use of in situ spectroscopic techniques suitable to probe the interaction of this bimetallic systems under interaction with the target contaminants.

However, from the performed experimental work, the use of surface probing techniques such as TPD, TPR in combination with in situ spectroscopic techniques have provided insightful information towards the elucidation of the surface interaction mechanisms regulating dechlorination processes. The importance of the surface hydroxylation has been clearly identified and the role of surface Lewis acid sites was also established. Implications of the obtained experimental results can be exploited in terms of the capacity to use surface chemistry techniques to engineer surface modified nZVI nanoparticles, where adsorption/reaction sites can be promoted to enhance the adsorption/dechlorination mechanisms. Engineering of an nZVI enhanced reactive surface can be achieved by different methods such as controlled grow of the oxide shell layer after nZVI synthesis, hydroxylation of the nZVI surface through chemical treatment, and injection of the nZVI particles under controlled water chemistry conditions to promote the formation of specific surface iron oxides/ oxyhydroxides species. Other implications involve the capacity to understand the importance of the surface composition of nZVI. This will enable researchers to achieve a better understanding of the reactive sites, and the conditions required for an enhanced reactivity of these materials.

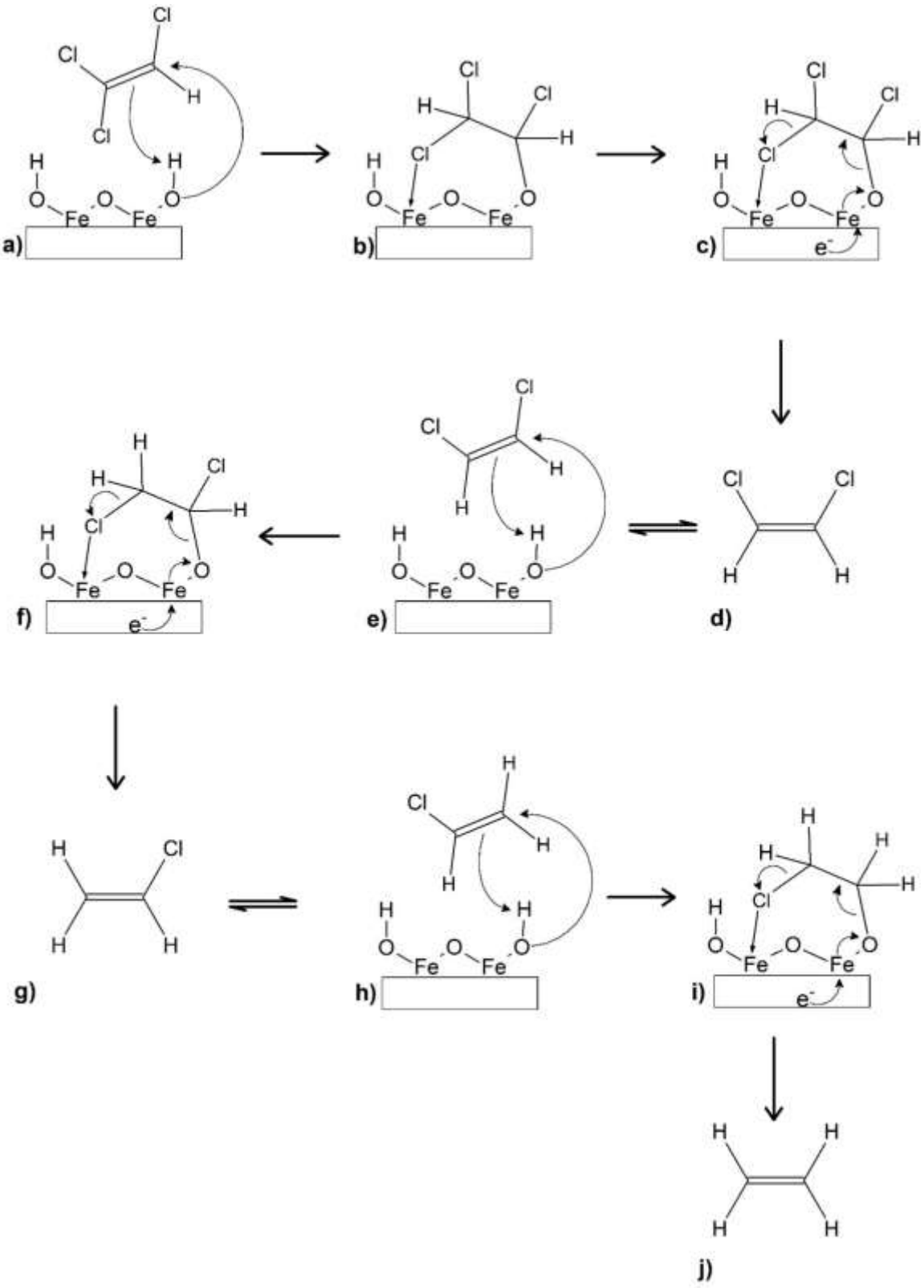

Figure 3.13. General surface dechlorination reaction mechanism over iron surfaces

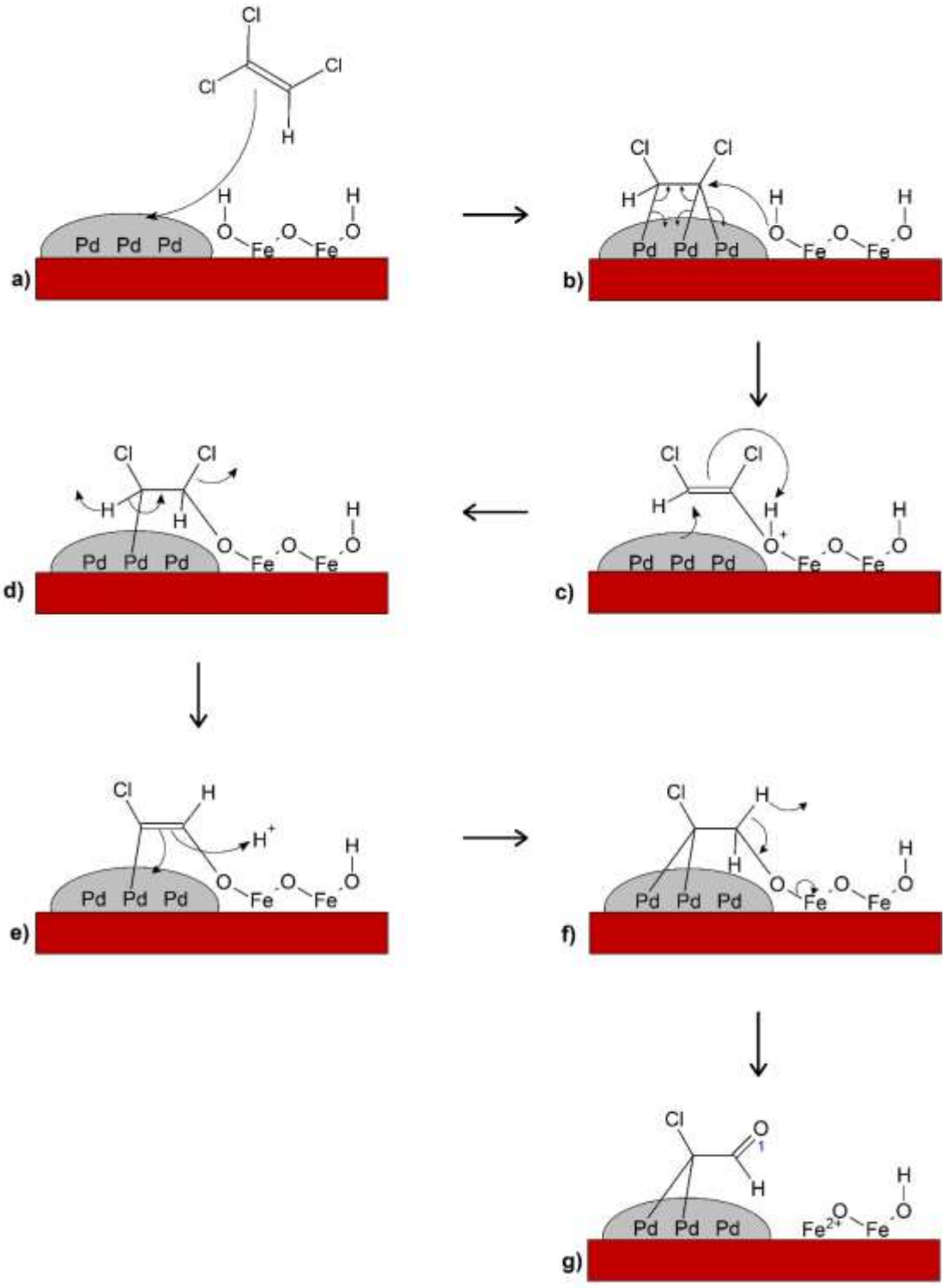

Figure 3.14. General surface dechlorination reaction mechanism over Pd doped iron surfaces

3.7 References

1. Zhang, W. X.; Wang, C. B.; Lien, H. L., Treatment of chlorinated organic contaminants with nanoscale bimetallic particles. *Catalysis Today* **1998,** *40* (4), 387-395.

2. Yan, W.; Lien, H.-L.; Koel, B. E.; Zhang, W.-x., Iron nanoparticles for environmental clean-up: recent developments and future outlook. *Environmental Science-Processes & Impacts* **2013,** *15* (1), 63-77.

3. Bennett, P.; He, F.; Zhao, D.; Aiken, B.; Feldman, L., In situ testing of metallic iron nanoparticle mobility and reactivity in a shallow granular aquifer. *Journal of contaminant hydrology* **2010,** *116* (1-4), 35-46.

4. Gillham, R. W.; Ohannesin, S. F., Enhanced Degradation of Halogenated Aliphatics by Zero-Valent Iron. *Ground Water* **1994,** *32* (6), 958-967.

5. Song, H.; Carraway, E. R., Reduction of Chlorinated Ethanes by Nanosized Zero-Valent Iron: Kinetics, Pathways, and Effects of Reaction Conditions. *Environmental Science & Technology* **2005,** *39* (16), 6237-6245.

6. Arnold, W. A.; Roberts, A. L., Pathways and kinetics of chlorinated ethylene and chlorinated acetylene reaction with Fe(O) particles. *Environmental Science & Technology* **2000,** *34* (9), 1794-1805.

7. Lopez A. Javier; Gonzalez, J. B. A. F. Z., Gustavo; Gomez, Maria E., Synthesis and characterization of Fe3O4 magnetic nanofluid. *Revista Latinoamericana de Metalurgia y Materiales* **2010,** *30* (1), 60-66.

8. Poedji Loekitowati Haiani, M. F., Ridwan, Marsi, and Dedi Setiabudidaya, Synthesis and Properties of Fe3O4 Nanoparticles by Co-precipitation Method to Removal Procion Dye *Iternational Journal of Envronmental Science and Development* **2013,** *4* (3).

9. Li, Y.-S.; Church, J. S.; Woodhead, A. L., Infrared and Raman spectroscopic studies on iron oxide magnetic nano-particles and their surface modifications. *Journal of Magnetism and Magnetic Materials* **2012,** *324* (8), 1543-1550.

10. Nunez, N. O.; Morales, M. P.; Tartaj, P.; Serna, C. J., Preparation of high acicular and uniform goethite particles by a modified-carbonate route. *J Mater Chem* **2000,** *10* (11), 2561-2565.

11. Cao, J. S.; Elliott, D.; Zhang, W. X., Perchlorate reduction by nanoscale iron particles. *Journal of Nanoparticle Research* **2005,** *7* (4-5), 499-506.

12. Wang, C.-B.; Zhang, W.-x., Synthesizing Nanoscale Iron Particles for Rapid and Complete Dechlorination of TCE and PCBs. *Environmental Science & Technology* **1997,** *31* (7), 2154-2156.

13. Chen, Y. H., Thermal properties of nanocrystalline goethite, magnetite, and maghemite. *Journal of Alloys and Compounds* **2013,** *553* (0), 194-198.

14. Ferretto, L.; Glisenti, A., Study of the surface acidity of an hematite powder. *Journal of Molecular Catalysis A: Chemical* **2002,** *187* (1), 119-128.

15. Scaranto, J.; Giorgianni, S., Adsorbate–substrate interaction between chlorodifluoromethane and titanium dioxide: Infrared spectroscopy and density functional theory studies. *Vibrational Spectroscopy* **2011,** *56* (2), 161-165.

16. Coloma, F.; Bachiller-Baeza, B.; Rochester, C. H.; Anderson, J. A., Infrared study of competitive crotonaldehyde and CO adsorption on Cu/TiO2. *Phys Chem Chem Phys* **2001,** *3* (21), 4817-4825.

17. Scaranto, J.; Charmet, A. P.; Stoppa, P.; Giorgianni, S., Vinyl halides adsorbed on TiO2 surface: FTIR spectroscopy studies and ab initio calculations. *Journal of Molecular Structure* **2005,** *741* (1-3), 213-219.

18. Dubicki, L.; Kakos, G. A.; Winter, G., Magnetism electronic spectra and structure of transition metal alkoxides .6. chromium (3) chloro alkoxides. *Aust. J. Chem.* **1968,** *21* (6), 1461-1472.

19. Kirkwood, D. A.; Stace, A. J., Infrared and collision-induced fragmentation of iron ethoxide cations. *International Journal of Mass Spectrometry and Ion Processes* **1997,** *171* (1–3), 39-49.

20. Adib, K.; Camillone, N.; Fitts, J. P.; Rim, K. T.; Flynn, G. W.; Joyce, S. A.; Osgood, R. M., CCl4 chemistry on the magnetite selvedge of single-crystal hematite: competitive surface reactions. *Surface Science* **2002,** *497* (1-3), 127-138.

21. Al-Baitai, Asmaa. H. de Leeuw, Nora., Computational Studies of the Interaction of Pollutants with Iron Oxide Surfaces. Thesis submited for the degree of Doctor of Philosophy, Univesity College London 2011.

22. van den Brink, R. W.; Mulder, P.; Louw, R.; Sinquin, G.; Petit, C.; Hindermann, J.-P., Catalytic Oxidation of Dichloromethane on γ-Al2O3: A Combined Flow and Infrared Spectroscopic Study. *Journal of Catalysis* **1998,** *180* (2), 153-160.

23. Lien, H. L.; Zhang, W. X., Hydrodechlorination of chlorinated ethanes by nanoscale Pd/Fe bimetallic particles. *J Environ Eng-Asce* **2005,** *131* (1), 4-10.

24. Feijen-Jeurissen, M. M. R.; Jorna, J. J.; Nieuwenhuys, B. E.; Sinquin, G.; Petit, C.; Hindermann, J.-P., Mechanism of catalytic destruction of 1,2-dichloroethane and trichloroethylene over γ-Al2O3 and γ-Al2O3 supported chromium and palladium catalysts. *Catalysis Today* **1999,** *54* (1), 65-79.

25. Nyberg, C.; Tengstål, C. G., Adsorption and reaction of water, oxygen, and hydrogen on Pd(100): Identification of adsorbed hydroxyl and implications for the catalytic H2–O2 reaction. *The Journal of Chemical Physics* **1984,** *80* (7), 3463-3468.

26. Papas, B. N.; Whitten, J. L., Dissociation of water on a palladium nanoparticle. *International Journal of Quantum Chemistry* **2010,** *110* (15), 3072-3079.

27. Lien, H.-L.; Zhang, W.-X., Nanoscale Pd/Fe bimetallic particles: Catalytic effects of palladium on hydrodechlorination. *Applied Catalysis B: Environmental* **2007,** *77* (1–2), 110-116.

28. Gorte, R. J., Temperature-programmed desorption for the characterization of oxide catalysts. *Catalysis Today* **1996,** *28* (4), 405-414.

29. Stevens, R. W.; Chuang, S. S. C.; Davis, B. H., Temperature-programmed desorption/decomposition with simultaneous DRIFTS analysis: adsorbed pyridine on sulfated ZrO2 and Pt-promoted sulfated ZrO2. *Thermochimica Acta* **2003,** *407* (1-2), 61-71.

30. Uludag-Demirer, S.; Bowers, A. R., Gas phase reduction of chlorinated vocs by zero valent iron. *Journal of Environmental Science and Health, Part A* **2001,** *36* (8), 1535-1547.

31. Liu, Y. Q.; Majetich, S. A.; Tilton, R. D.; Sholl, D. S.; Lowry, G. V., TCE dechlorination rates, pathways, and efficiency of nanoscale iron particles with different properties. *Environmental Science & Technology* **2005,** *39* (5), 1338-1345.

32. Uludag-Demirer, S.; Bowers, A. R., Adsorption/Reduction Reactions of Trichloroethylene by Elemental Iron in the Gas Phase: The Role of Water. *Environmental Science & Technology* **2000,** *34* (20), 4407-4412.

33. Yurkanis B., Paula. Organic Chemistry. Sixth Edition. Prentice Hall,1941. Pag.375-377.

34. Su, C.; Puls, R. W., Kinetics of Trichloroethene Reduction by Zerovalent Iron and Tin: Pretreatment Effect, Apparent Activation Energy, and Intermediate Products. *Environmental Science & Technology* **1999,** *33* (1), 163-168.

35. O'Carroll, D.; Sleep, B.; Krol, M.; Boparai, H.; Kocur, C., Nanoscale zero valent iron and bimetallic particles for contaminated site remediation. *Advances in Water Resources* **2013,** *51*, 104-122.

36. Plummer, L. N.; Busenberg, E.; Eberts, S. M.; Bexfield, L. M.; Brown, C. J.; Fahlquist, L. S.; Katz, B. G.; Landon, M. K., Low-Level Detections of Halogenated Volatile Organic Compounds in Groundwater: Use in Vulnerability Assessments. *J Hydrol Eng* **2008,** *13* (11), 1049-1068.

37. Kausamo, A.; Andersin, J.; Honkala, K., Mechanism of Trichloroethene Hydrodehalogenation: A First-Principles Kinetic Monte Carlo Study. *The Journal of Physical Chemistry C* **2014,** *118* (34), 19759-19767.

38. Zhang, N.; Luo, J.; Blowers, P.; Farrell, J., Understanding Trichloroethylene Chemisorption to Iron Surfaces Using Density Functional Theory. *Environmental Science & Technology* **2008,** *42* (6), 2015-2020.

39. Liu, C.-C.; Tseng, D.-H.; Wang, C.-Y., Effects of ferrous ions on the reductive dechlorination of trichloroethylene by zero-valent iron. *Journal of hazardous materials* **2006,** *136* (3), 706-713.

40. Filip, J.; Karlický, F.; Marušák, Z.; Lazar, P.; Černík, M.; Otyepka, M.; Zbořil, R., Anaerobic Reaction of Nanoscale Zerovalent Iron with Water: Mechanism and Kinetics. *The Journal of Physical Chemistry C* **2014,** *118* (25), 13817-13825.

41. Ritter, K.; Odziemkowski, M. S.; Gillham, R. W., An in situ study of the role of surface films on granular iron in the permeable iron wall technology. *Journal of contaminant hydrology* **2002,** *55* (1–2), 87-111.

42. Weckhuysen, B. M., Determining the active site in a catalytic process: Operando spectroscopy is more than a buzzword. *Phys Chem Chem Phys* **2003,** *5* (20), 4351-4360.

43. Grau-Crespo, R.; Al-Baitai, A. Y.; Saadoune, I.; De Leeuw, N. H., Vacancy ordering and electronic structure of gamma-Fe2O3 (maghemite): a theoretical investigation. *J. Phys.-Condes. Matter* **2010,** *22* (25).

44. Wu, C.; Yin, P.; Zhu, X.; OuYang, C.; Xie, Y., Synthesis of Hematite (α-Fe2O3) Nanorods: Diameter-Size and Shape Effects on Their Applications in Magnetism, Lithium Ion Battery, and Gas Sensors. *The Journal of Physical Chemistry B* **2006,** *110* (36), 17806-17812.

45. Yu, X. H.; Huo, C. F.; Li, Y. W.; Wang, J. G.; Jiao, H. J., Fe3O4 surface electronic structures and stability from GGA plus U. *Surface Science* **2012,** *606* (9-10), 872-879.

46. Sherman, D. M.; Waite, T. D., Electronic-spectra of fe-3+ oxides and oxide hydroxides in the near ir to near UV. *Am Mineral* **1985,** *70* (11-12), 1262-1269.

47. Lee, J.; Han, S., Thermodynamics of native point defects in [small alpha]-Fe2O3: an ab initio study. *Phys Chem Chem Phys* **2013,** *15* (43), 18906-18914.

48. Alexandrov, V.; Rosso, K. M., Electron transport in pure and substituted iron oxyhydroxides by small-polaron migration. *J. Chem. Phys.* **2014,** *140* (23).

49. Somarjai, Gabor A. Li, Yimin. Introduction to Surface Cemistry and Catalysis, 2nd Edition. Willey, 2010.

50. Schreier, C. G.; Reinhard, M., Catalytic Hydrodehalogenation of Chlorinated Ethylenes Using Palladium and Hydrogen for the Treatment of Contaminated Water. *Chemosphere* **1995,** *31* (6), 3475-3487.

51. Lowry, G. V.; Reinhard, M., Pd-Catalyzed TCE Dechlorination in Water: Effect of [H2](aq) and H2-Utilizing Competitive Solutes on the TCE Dechlorination Rate and Product Distribution. *Environmental Science & Technology* **2001,** *35* (4), 696-702.

52. Hildebrand, H.; Mackenzie, K.; Kopinke, F. D., Pd/Fe3O4 nano-catalysts for selective dehalogenation in wastewater treatment processes-Influence of water constituents. *Appl Catal B-Environ* **2009,** *91* (1-2), 389-396.

53. Somarjai, Gabor A. Li, Yimin. Introduction to Surface Cemistry and Catalysis, 2nd Edition. Willey, 2010.

54. Kakos, G.A.; Winter, G. C-O and Ti-O vibration frequencies in alkyltitanates. Aust. Journal of Chemistry **1968**, 21,793-795.

55. Condon, N. G.; Leibsle, F. M.; Lennie, A. R.; Murray, P. W.; Vaughan, D. J.; Thornton, G., Biphase Ordering of Iron-Oxide Surfaces. *Physical Review Letters* **1995,** *75* (10), 1961-1964.

56. Kiejna, A.; Pabisiak, T., Mixed Termination of Hematite (alpha-Fe(2)0(3))(0001) Surface. *Journal of Physical Chemistry C* **2013,** *117* (46), 24339-24344.

57. Hodgson, A.; Haq, S., Water adsorption and the wetting of metal surfaces. *Surface Science Reports* **2009,** *64* (9), 381-451.

58. Akonwie, L. N.; Kazachkin, D. V.; Luebke, D. R.; d'Itri, J. L., Effect of catalyst pre-reduction temperature on the reaction of 1,2-dichloroethane and H2 catalyzed by SiO2-supported PtCu bimetallics. *Applied Catalysis A: General* **2012,** *415-416*, 59-69.

59. Dolfing, J.; van Eekert, M.; Seech, A.; Vogan, J.; Mueller, J., In Situ Chemical Reduction (ISCR) Technologies: Significance of Low Eh Reactions. *Soil and Sediment Contamination: An International Journal* **2007,** *17* (1), 63-74.

60. Bernstein, H.J. The infrared spectra of trichloroethylene ($CHCl=CCl_2$ and $CDCl=CCl_2$) and asymmetrical tetrachloroethane (CH_2Cl-CCl_3, and CD_2Cl-CCl_3) from 2.5□ from 2. Canadian Journal of research,**1950**, 28 (B),132-139.

61. Su, C.; Puls, R. W., Kinetics of Trichloroethene Reduction by Zerovalent Iron and Tin: Pretreatment Effect, Apparent Activation Energy, and Intermediate Products. *Environmental Science & Technology* **1999,** *33* (1), 163-168.

62. Li, T.; Farrell, J., Electrochemical investigation of the rate-limiting mechanisms for trichloroethylene and carbon tetrachloride reduction at iron surfaces. *Environmental Science & Technology* **2001,** *35* (17), 3560-3565.

63. Phillips, L. A.; Raupp, G. B., Infrared spectroscopic investigation of gas—solid heterogeneous photocatalytic oxidation of trichloroethylene. *Journal of Molecular Catalysis* **1992,** *77* (3), 297-311.

64. Busca, G., Spectroscopic characterization of the acid properties of metal oxide catalysts. *Catalysis Today* **1998,** *41* (1-3), 191-206.

65. Lorenzelli, V.; Busca, G.; Sheppard, N., Infrared study of the surface reactivity of hematite. *Journal of Catalysis* **1980,** *66* (1), 28-35.

Chapter 4

4. Conclusions and recommendations

4.1 Conclusions

In the last 10 years, dechlorination of groundwater contaminants by nZVI particles has been subject of extensive research worldwide. The work reported has focused mainly on improving nZVI reactivity and its stability in drinking water suspensions. In terms of reactivity, state of the art knowledge suggests that dechlorination occurs as a surface mediated reaction. Regardless of the importance of this surface interaction, the role of the surface species in the adsorption/reaction mechanisms of chlorinated hydrocarbon with nZVI is still unknown.

In this work, in situ spectroscopic investigation and detailed surface characterization of the interactions between different iron bearing surfaces and 1,2 DCA and TCE lead us to conclude that hydroxylated species present on the iron bearing surfaces play a critical role in the adsorption process of 1,2-DCA and TCE over nZVI. Indeed, consumption of the surface hydroxyl groups is observed as result of the interaction of the chlorinated hydrocarbon and the iron bearing surfaces. At the same time, the formation of an ethoxy surface complex is observed with the concomitant weakening of the Cl-C bond. Results suggest this is linked to the formation of a Lewis adduct between Cl and the iron atoms present in the surface, further promoting dechlorination of the adsorbed molecule. The critical role of the hydroxyl groups present in the surface is therefore clearly stablished. This result can potentially provide field engineers with a protocol to engineer surface modified nZVI nanoparticles. In principle reactive sites can be generated to improve the dechlorination activity of the nZVI surface. Tailoring of the nZVI surface might take place using currently stablish protocols for modification of reactive surfaces, such as optimization of the oxide shell layer thickness through thermal treatment combined with aggressive hydroxylation of the reactive surface. Manipulation of water chemistry conditions can also offer a route for the generation of defined surface iron oxides/ oxyhydroxides phases.

The existence of a common adsorption mechanism for 1,2 DCA and TCE is also established by our work, as the formation of vinyl chloride was observed in all cases. TCE-TPR and TCE-TPD experiments showed formation of dichlorinated ethenes and vinyl chloride, likely resulting from the existence of nonequivalent adsorption sites. Although similar adsorption mechanisms were

observed between 1,2-DCA and TCE on all the probed iron bearing nanoparticles, recalcitrance of 1,2-DCA to dechlorination by nZVI particles, could be related to the ability of the adsorbed molecule to form the proposed surface intermediary. Since interaction through the hydroxylated surface and the formation of a saturated aliphatic compound (C-C), as TCE adsorbs in the iron oxides surfaces were observed by means of FTIR spectroscopy; these results suggest that the formation of the surface adsorbed intermediary is easier to achieve for unsaturated systems (C=C).

In addition, the effect of adding Pd resulted in the apparent decrease of hydroxyl groups in the surface, we propose that this could take place through dehydroxylation reactions on the iron oxide/hydroxides surface promoted by Pd. This observation suggest a modification on the iron bearing surface, triggered by the presence of Pd, supporting our hypothesis of the different dechlorination mechanism taking place in the presence of Pd. Indeed we observed disappearance of the dichlorinated intermediaries and the formation of ethylene as desorption products, further confirming the role of Pd as a dechlorination catalyst for this specific system.

4.2 Recommendations

From the experimental observations of this thesis a general surface adsorption mechanism has been proposed. This mechanism denotes the importance of the surface hydroxylation in the adsorption/reduction of the chlorinated contaminants. The adsorption/reduction phenomena seems to be linked to the ease with which the contaminant can form the surface intermediary required as first step for dechlorination. Therefore, a further analysis of the surface hydroxylation in nZVI, and the different capacities of the contaminants to form these types of surface intermediary, needs to be conducted.

The role of the surface hydroxylation in the adsorption and reaction mechanism can be further studied by manipulation of the population and activity of Brönsted acid sites. The generation of Brönsted and Lewis acid sites can be achieved by water vapor treatment under control conditions so surface oxidation is avoided. In contrast selective removal of Brönsted acid sites can be achieved by thermal treatment or annealing. As the surface of the different iron species evaluated in this work contain Lewis acid sites, and these sites can permit the formation of Lewis adducts, a better

understanding of the role, availability, distribution and strength of the Lewis acid sites, and their role in the desorption/reduction mechanisms can provide a further understanding of the adsorption phenomena.

Studying the surface sites strength, distribution and availability can be performed by means of different techniques widely utilized in the study of catalytic systems. Differentiation between Lewis and Brönsted acid sites can be conducted by titration with probe molecules which are known to adsorb over specific sites. Probe molecules like pyridine provide information about the amount of existing acid sites, and by combination with FTIR spectroscopy differentiation between Brönsted and Lewis acid sites. The use of molecules offering a larger degree of steric hindrance such as 2,6-dimethyl-pyridine allows to identify the existence of non-accessible adsorption sites.

Identification of surface reaction products was achieved by means of TPD and TPR experiments. Vinyl chloride was observed when TCE and 1,2-DCA interacted with the iron oxides / oxyhydroxides, suggesting the existence of a similar adsorption process, as observed by means of DRIFTS. 1,2-DCE and 1,1-DCE were also identified, this suggests the existence of non-equivalent reactive sites. In order to understand the importance and role of these different reactive sites, a quantification of the reaction products should be conducted as part of the TPD, TPR experiments.

The use of bimetallic systems for the dechlorination reaction has shown to be effective in the reduction of the production of dechlorinated intermediaries. Incorporation of Pd into the studied surfaces, demonstrated the capacity of the iron species to form ethylene as a product. The necessity of more concrete and direct evidence that could provide information about the catalytic process that takes place as Pd is added in to the surface, can permit the selection and design of better bimetallic nanoparticles systems. This could be carried out by using probe molecules such as hydrogen or CO, able to test the availability and accessibility of the noble metal species present in the surface. Techniques such in situ x-ray photoelectron spectroscopy (XPS) can be used to obtain valuable information about composition and chemical constitution of the surfaces as the adsorption/reaction process takes place. XPS analysis permits the differentiation between different elements, and the obtained binding energy is affected by chemical bonding, thus identification of the specific atom bonded to the Pd surface can be achieved, providing information that could be linked to the catalytic effect of Pd in the nZVI dechlorination reaction mechanism.

The limitation in the study in the context of the surface sensitiveness to aerobic conditions is clear, as the spectroscopic information obtained was collected under a very controlled environment. As nZVI particles are commonly utilized in groundwater systems where water quality parameters such as pH, ORP and dissolved ions among other parameters, can have a significant effect in the surface composition. The use of in situ techniques capable of probing systems under aqueous conditions can allow the study of the surface reaction and transformation mechanisms of the nZVI particles under more realistic conditions. In situ techniques such as ATR-FTIR, Raman spectroscopy and Mössbauer spectroscopy can be used for this purpose. The use of these spectroscopic techniques can provide complementary information that can allow a more robust understanding of the adsorption/reaction mechanism that takes place in the nZVI surface. In contrast to DRIFTS used in this work, ATR-FTIR spectroscopy can be utilized to study surface interactions in solution. This type of experiment is performed by flowing a solution over a film of the desired iron oxide or oxyhydroxides. Similarly in situ Raman spectroscopy can be used to monitor surface adsorption and interaction processes between the chlorinated hydrocarbons and the iron bearing nanoparticles. In contrast with infrared spectroscopy, Raman spectroscopy signal has the advantage to be non-responsive to the inclusion of water to the probed system. Also Raman spectroscopy allows the differentiation between different iron oxides or oxyhydroxides. Therefore, is possible to study the effect of TCE and 1,2-DCA aqueous solutions and groundwater chemistry in the surface composition of the iron bearing nanoparticles. These will allow the study of the effects of parameters such as pH, ORP, dissolved ions in the composition and reactivity of nZVI towards chlorinated hydrocarbons.

Mössbauer spectroscopy is also a technique able to provide a clear differentiation of the different iron oxides (oxyhydroxides) under in situ conditions. Since a limited amount of elements are suitable (iron being the most commonly used) for analysis by Mossbauer spectroscopy, in situ study of iron nanoparticles in reaction systems under controlled water chemistry conditions can be performed without the signal interference of parallel adsorption/reaction processes.

The proposed reaction mechanisms that are described in this work are formulated based on experimental observations of surface adsorbed intermediaries, and the identification of desorption/reaction products between nZVI and TCE or 1,2-DCA. In order to better understand the reaction process and provide theoretical evidence of the proposed surface adsorbed species and

reaction intermediaries, computational tools such as DFT can be utilized. DFT simulations can be used to calculate adsorption energies of different surface intermediaries, leading to the identification of the most thermodynamically feasible adsorbed species. DFT can also provide information of the expected spectroscopic response of the simulated interaction between chlorinated hydrocarbons and iron oxides (oxyhydroxides) surfaces, enabling a comparison with the experimental FTIR results obtained in this work.

The use of these in situ spectroscopic and surface characterization techniques, in combination with computational simulation tools, can thus provide sound evidence for a comprehensive understanding of the surface adsorption/reaction mechanisms that take place between iron bearing nanoparticles and chlorinated contaminants such as TCE and 1,2-DCA under groundwater condition, further advancing the understanding of these processes.

Curriculum Vitae

Name:	Jorge Luis Gabayet Dominguez
Post-secondary education and degrees:	Instituto Tecnológico de Tijuana. Baja California, México. 2006-2011
Related Work Experience	Research Assistant Western University 2013-2015 Teaching Assistant Western University 2013-2015